NASA
National Aeronautics and Space Administration

NASA CR-174703
CHAM H3605/16

ROCKET INJECTOR ANOMALIES STUDY

Volume II: Results of Parametric Studies

by
A.J. Przekwas, A.K. Singhal and L.T. Tam
CHAM of North America, Incorporated

August 1984

Prepared for
NATIONAL AERONAUTICS AND SPACE ADMINISTRATION
NASA-Lewis Research Center
Contract NAS3-23352

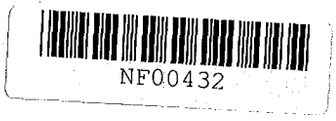

12 1 1 RN/NASA-CR-174703
DISPLAY 12/2/1
84N32429*# ISSUE 22 PAGE 3543 CATEGORY 20 RPT#: NASA-CR-174703 NAS 1.26:174703 CHAM-H3605/16-VOL-2 CNT#: NAS3-23352 84/07/00 2 VOLS 71 PAGES UNCLASSIFIED DOCUMENT

UTTL: Rocket injector anomalies study. Volume 2: Results of parametric studies TLSP: Final Report

AUTH: A/PRZEKWAS, A. J.; B/SINGHAL, A. K.; C/TAM, L. T.

CORP: CHAM of North America, Inc., Huntsville, Ala. AVAIL.NTIS SAP: HC A04/MF A01

MAJS: /*COMBUSTION CHAMBERS/*LIQUID PROPELLANT ROCKET ENGINES/*PROPULSION SYSTEM CONFIGURATIONS

MINS: / COMPUTER PROGRAMS/ COMPUTERIZED SIMULATION/ EULER-LAGRANGE EQUATION/ EVAPORATION/ FLOW DISTRIBUTION/ MATHEMATICAL MODELS/ SPRAYING

ABA: E.A.K.

ABS: The employment of a existing computer program to simulate three dimensional two phase gas spray flows in liquid propellant rocket engines. This was accomplished by modification of an existing three dimensional computer program (REFLAN3D) with Euler/Lagrange approach for simulating two phase spray flow, evaporation and combustion. The modified code is referred to as REFLAN3D-SPRAY. Computational studies of the model rocket engine combustion chamber are presented. The parametric studies of the two phase flow and combustion shows qualitatively correct response for variations in geometrical and physical parameters. The injection

ENTER:

1. Report No.	2. Government Accession No.	3. Recipient's Catalog No.
CR-174703		

4. Title and Subtitle	5. Report Date
Rocket Injector Anomalies Study, Results of Parametric Studies	July 1984
	6. Performing Organization Code
7. Author(s)	8. Performing Organization Report No.
A.J. Przekwas, A.K. Singhal and L.T. Tam	H3605/16
	10. Work Unit No.
9. Performing Organization Name and Address	11. Contract or Grant No.
CHAM of North America Incorporated 1525-A Sparkman Drive Huntsville, Alabama 35805	NAS3-23352
	13. Type of Report and Period Covered
12. Sponsoring Agency Name and Address	Final
NASA - Lewis Research Center	14. Sponsoring Agency Code

15. Supplementary Notes

Project Manager: Dr. Larry P. Cooper
NASA Lewis Research Center
21000 Brookpark Road
Cleveland, Ohio 44135

16. Abstract

The objective of the presented research project was to employ existing computer program for simulating three dimensional two-phase gas-spray flows in liquid propellant rocket engines. This has been accomplished by modifying an existing three-dimensional computer program (REFLAN3D) with Eulerian - Lagrangian approach for simulating two-phase spray flow, evaporation and combustion. The modified code is referred to as REFLAN3D-SPRAY. This report presents results of computational studies of the model rocket engine combustion chamber. The parametric studies of the two-phase flow and combustion showed qualitatively correct response for variations in geometrical and physical parameters. The injection nonuniformity test with blocked central fuel injector holes showed significant changes in the central flame **core** and minor influence on the wall heat transfer fluxes.

Mathematical background of the model is described in an accompanying report NASA CR 174702.

17. Key Words (Suggested by Author(s))	18. Distribution Statement
Rocket Engines, Propulsion, Combustor Models, Spray Combustion	

19. Security Classif. (of this report)	20. Security Classif. (of this page)	21. No. of pages	22. Price*
UNCLASSIFIED	UNCLASSIFIED	68	

*For sale by the National Technical Information Service, Springfield, Virginia 22161

N84-32429#

FOREWORD

CHAM of North America Incorporated has performed a Rocket Injector Anomaly Study under the NASA Contract NAS3-23352. The purpose of the study was to modify, test and demonstrate a computer code for predicting three-dimensional two-phase spray flow and combustion in rocket engines. The modified computer code REFLAN3D-SPRAY (REactive FLow ANalyzer 3-Dimensional, with two phase spray) and results of parametric studies have been described in the folloiwng two volumes:

Volume 1: Description of the Mathematical Model and Solution Procedure;
Volume 2: Results of Parametric Studies.

Transfer of the code to NASA LeRC computer center, and preparation of a user's manual are recommended as next steps of the study.

The authors wish to thank all those who have contributed to this work. In particular, thanks are due to Larry P. Cooper and Ken Davidian of the Communication and Propulsion Section of NASA LeRC; and to Laurence Keeton, Jack Keck, Kelli King, Janet Siersma, and Ronni Rossic of CHAM NA.

TABLE OF CONTENTS

SECTION 1
SUMMARY

The liquid fuelled rocket engine combustors consist of an injector plate and a thrust chamber. The injector plate consists of a number of propellant injectors which are designed to atomize the liquid jets of reactants and to promote intensive mixing between the vaporized components.

Figure 1.1 shows the schematic of the rocket engine and injector plate, with LOX-RP1-LOX unlike triplet injectors, considered. The purpose of the study was to demonstrate an analytical capability to predict the effects of reactant injection non-uniformities (injection anomalies) on heat transfer to the walls. For this purpose an existing three-dimensional single-phase flow and combustion computer code (REFLAN3D: - REactive FLow ANalyzer, 3-Dimensional) has been modified for simulating two-phase flows in liquid propellent rocket engines. The modified code is referred to as REFLAN3D-SPRAY.

Mathematical basis and solution procedure of REFLAN3D-SPRAY are described in Volume 1. This volume presents computational results to demonstrate the capability of the code. Reported results include numerical tests as well as several parametric test cases of the model rocket combustor (Figure 1.1).

The results of the effort undertaken in this program can be summarized as follows:

- The REFLAN3D computer code with Eulerian-Lagrangean technique has been adapted for three-dimensional, elliptic, two-phase flow with evaporation, heat transfer and combustion in liquid fuel rocket engines.

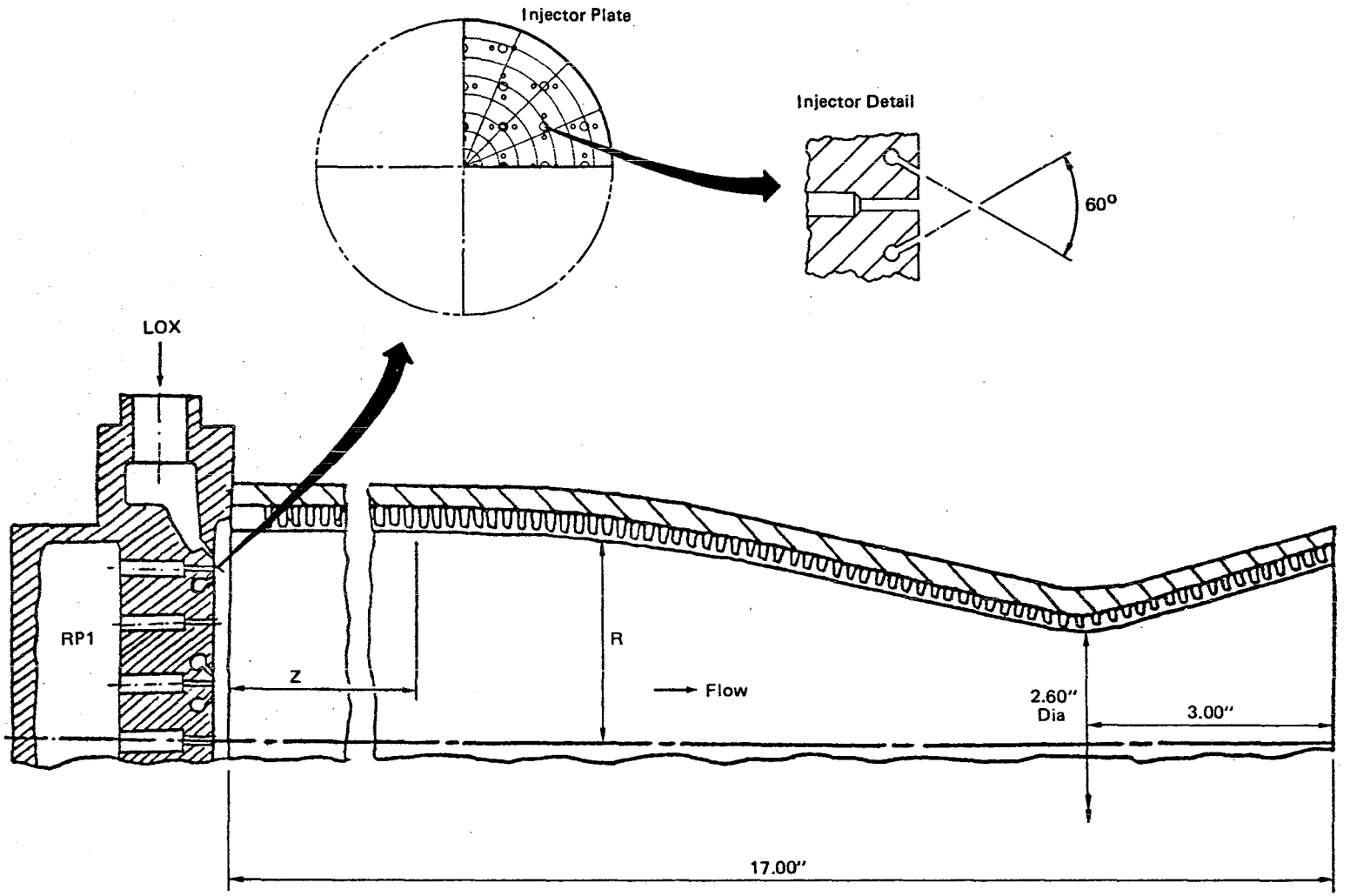

Figure 1.1 Rocket Engine Geometry and Injector Plate Configuration

- The code check-out calculations satisfied uniformity and symmetry requirements for both nonreactive and reactive turbulent flows.
- The parametric studies of the two-phase flow and combustion in rocket engine combustor showed qualitatively correct response for variations of geometrical and physical parameters.
- The injection nonuniformity test case, i.e. with blocked 25% fuel injector holes near the chamber, showed significant changes in the central flame core and minor influence on the wall heat transfer (Figure 1.2).
- The areas for model improvements, in both physical and computational aspects, have been identified and recommended for further studies.

The recommendations for further studies include:

a) preparation of a user's manual and code transfer to NASA LeRC;

b) improvements in the physical models of evaporation, turbulent diffusion of droplets, and chemical reaction;

c) numerical improvements to increase the accuracy of solution method; and

d) verification studies with and without comparisons with experimental data.

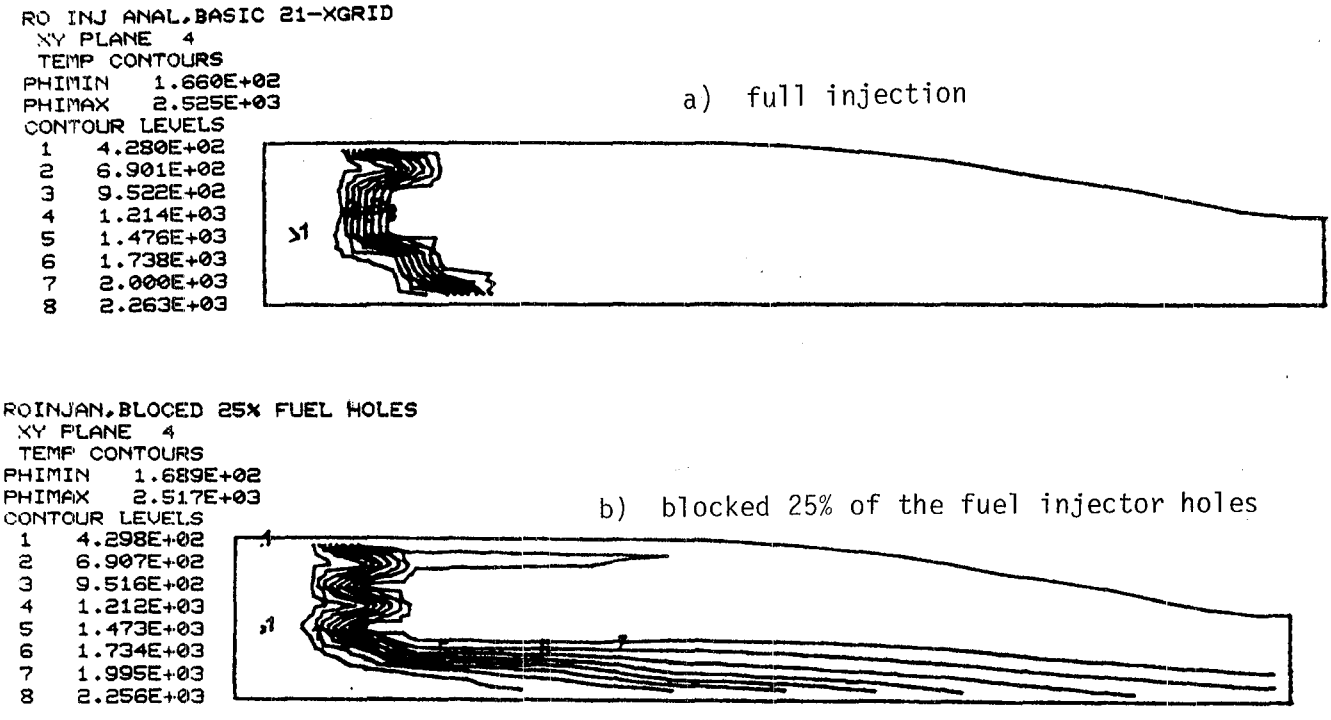

Figure 1.2 Temperature contours within the rocket engine

SECTION 2
INTRODUCTION

The objective of the present study was to demonstrate an analytical capability to predict the effects of reactant injection-nonuniformity (injection anomalies) upon local and overall heat transfer in a liquid propelled rocket engine combustion chamber. For this purpose the REFLAN3D (REactive FLow ANalyzer 3-Dimensional) computer code has been modified for the two-phase spray calculations and applied in this study. The modified code is referred to as REFLAN3D-SPRAY.

Detailed description of the mathematical model is provided in Volume 1, entitled "Description of the Mathematical Model and Solution Procedure".

This report constitutes the second volume of the documentation and describes the computational results and analysis of:

a) code check-out test cases (section 3), and

b) five parametric test cases (section 4).

Based on the analysis of these results further model refinements are identified and described in section 5. The need for model varification against experimental data is also discussed in section 5.

SECTION 3
CODE CHECK-OUT CALCULATIONS

In order to predict the effects of injection nonuniformity on the fluid flow and heat transfer pattern the numerical model has to be capable of responding to small changes in injection pattern. Therefore, in addition to common checks of computational stability, convergence rate etc, a model accuracy for handling cyclic boundary conditions must be checked before it can be used for injection anomaly studies. For this purpose two test cases were selected to check solution symmetry and uniformity characteristics.

3.1 SYMMETRY TESTS

Figure 3.1 presents the geometry configuration and computational grid used for the symmetry test calculation. The fluid enters the cylindrical duct through a partially blocked front plane. Two jets:

- the inner jet with smaller velocity, and
- the outer jet with larger velocity,

enter through a V-shaped opening in the front plane. The fluid leaves the duct through fully open exit plane.

A 180^0 sector of the duct has been used as the solution domain for the calculations with uniformly distributed grid (NX: NY: NZ - 21: 10:. 4). Due to the symmetry of the combustor geometry and symmetrical boundary conditions, the results of the computations should be symmetric about the $\Theta=90^0$ plane.

Results of the following two test cases are presented in this section:

A) A constant temperature (300^0K), constant viscosity (.001 kg/ms) flow with fixed inlet velocities (10 and 20 $\frac{m}{s}$) and fixed exit pressure (relative pressure, $P_{exit} = 0$), specified as a boundary condition.

B) All conditions same as is case A, except that the larger inlet velocity is changed from 20 to 50 m/s.

The k-ε turbulence model has been used for both test cases. Figure 3.2 presents calculated velocity vectors in all four axial planes for test case A. Note that the minimum (VELMIN) and maximum (VELMAX) velocity vectors at symmetric planes (1 and 4) and (2 and 3) are identical. The shape and size of the recirculation zones on plane 1 and 4 are also the same.

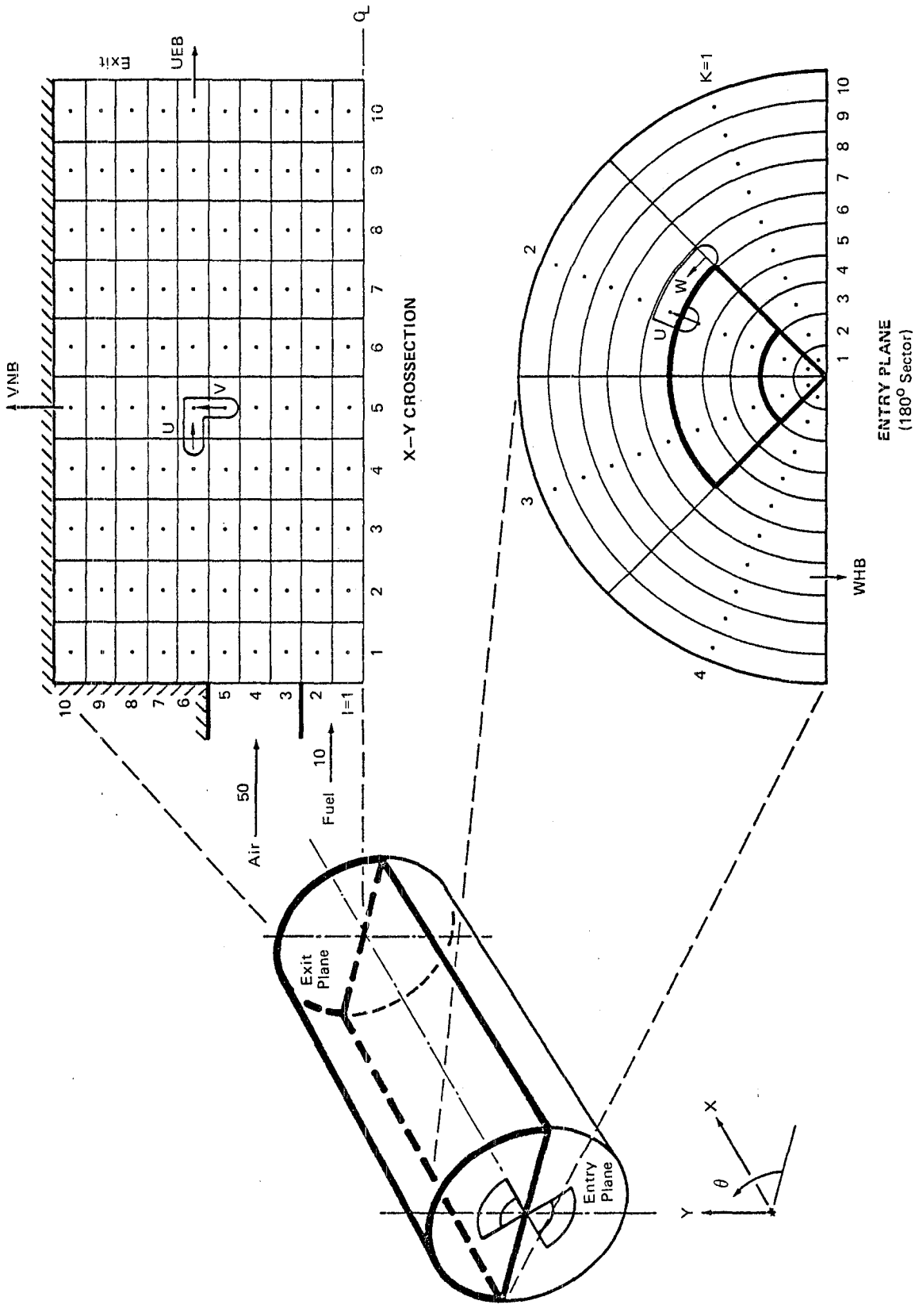

Figure 3.1 Chamber Geometry

XY PLANE 1
VELOCITY PLOTS
VELMIN 3.160E-02
VELMAX 9.825E+00

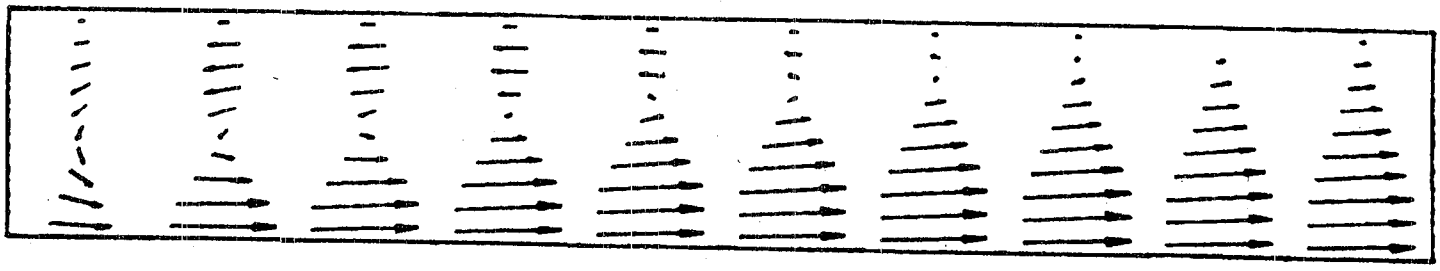

XY PLANE 2
VELOCITY PLOTS
VELMIN 8.245E-03
VELMAX 1.908E+01

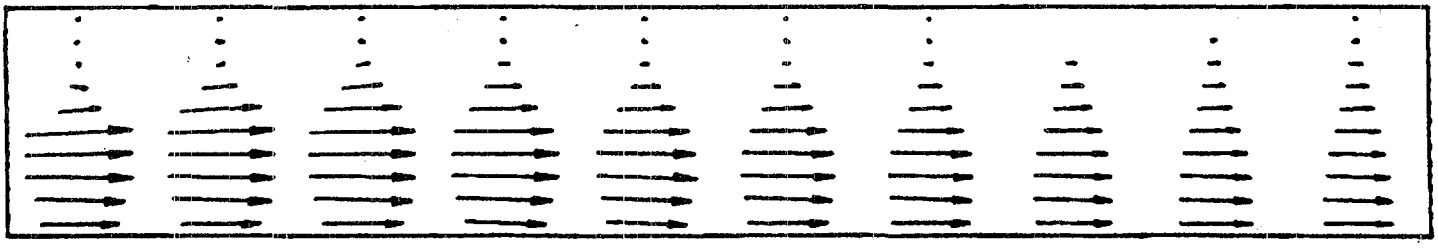

XY PLANE 3
VELOCITY PLOTS
VELMIN 8.245E-03
VELMAX 1.908E+01

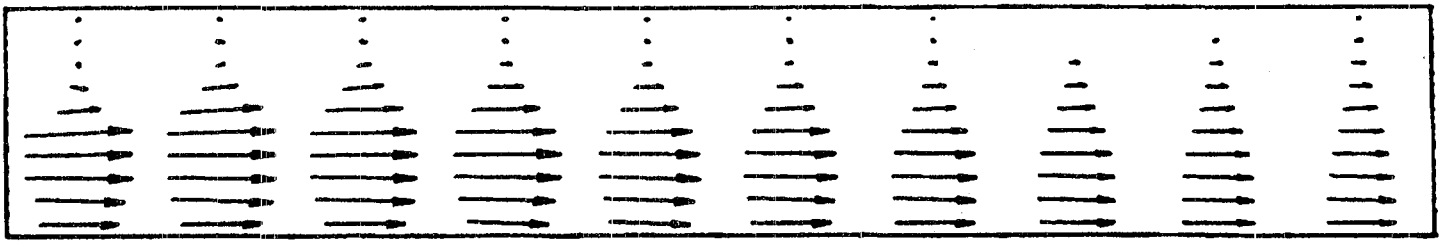

XY PLANE 4
VELOCITY PLOTS
VELMIN 3.161E-02
VELMAX 9.825E+00

Figure 3.2 Velocity vectors for the symmetry test case.

To enable a thorough examination, results of test case B are presented in the form of the following tables:

Table 3.1 - u-axial velocity (m/s) for each θ_k plane

Table 3.2 - v-radial velocity (m/s)

Table 3.3 - rw-angular momentum (m^2/s)

Table 3.4 - k-kinetic energy of turbulence (m^2/s^2)

Table 3.5 - global convective fluxes through the chamber cross section (kg/s)

Tables 3.1 to 3.4 indicate perfect symmetry about $\theta=90^o$. Results are symmetric at θ_1 and θ_4, and θ_2 and θ_3. Another symmetry verification is almost zero (10^{-9}) angular velocity at k=3 plane ($\theta=90^o$). Note that "backward boomerang" for velocity staggering is employed. Further guidance on interpretation of the computer output is provided in Appendix A of the present report.

Calculations were performed on a CRAY1 computer and total execution time for 100 iterations was 5.6 seconds. Figure 3.3 presents the convergence rate for test case B in the form of residual error variation with number of iterations. The residual error ε is calculated as the total mass inbalance for the entire calculation domain i.e.

$$\varepsilon \equiv \sum_{ijk} \left(\sum_{d} C_d \right)$$

where ijk denote grid indices, and d = N, S, E, W, H, and L signifies grid cells boundary at which the convective flux C_d is calculated.

The numerical convergence can also be verified from table 2.5 where global or total convective fluxes across various sections are presented. The notations used are:

Global net convective flux

$$FX_i \equiv \sum_k \sum_j (\rho u A) \qquad k=1 \ldots N=4;\ j=1 \ldots M=10$$

Global positive flux

$$FXP_i \equiv \sum_k \sum_j \max (0., \rho u A)$$

Global negative (recirculating) flux

$$FXM_i \equiv \sum_k \sum_j \min (0., \rho u A)$$

where u - axial velocity, ρ - density and, A - grid cell face area, and

i - axial, j - radial, k - circumferential coordinate indices.

Table 3.1 Axial Velocity

U-VELOCITY

*** K = 1 ***

J I=	1	2	3	4	5	6	7	8	9	10
10	0.00E+00	-8.77E+00	-1.02E+01	-6.89E+00	-2.51E+00	1.43E+00	3.48E+00	4.47E+00	4.91E+00	5.25E+00
9	0.00E+00	-7.75E+00	-7.90E+00	-4.57E+00	-5.88E-01	2.43E+00	4.16E+00	4.98E+00	5.32E+00	5.55E+00
8	0.00E+00	-6.38E+00	-5.71E+00	-2.36E+00	1.16E+00	3.47E+00	4.82E+00	5.42E+00	5.62E+00	5.72E+00
7	0.00E+00	-4.44E+00	-3.02E+00	3.08E-01	3.14E+00	4.76E+00	5.64E+00	5.93E+00	5.95E+00	5.88E+00
6	0.00E+00	-1.88E+00	3.29E-01	3.35E+00	5.37E+00	6.26E+00	6.57E+00	6.50E+00	6.28E+00	6.03E+00
5	0.00E+00	1.33E+00	4.31E+00	6.71E+00	7.81E+00	7.88E+00	7.55E+00	7.06E+00	6.60E+00	6.16E+00
4	0.00E+00	5.49E+00	8.84E+00	1.03E+01	1.03E+01	9.49E+00	8.48E+00	7.57E+00	6.86E+00	6.25E+00
3	0.00E+00	1.07E+01	1.36E+01	1.38E+01	1.26E+01	1.09E+01	9.27E+00	7.97E+00	7.05E+00	6.30E+00
2	0.00E+00	1.58E+01	1.78E+01	1.66E+01	1.44E+01	1.19E+01	9.79E+00	8.22E+00	7.15E+00	6.32E+00
1	0.00E+00	1.95E+01	2.05E+01	1.84E+01	1.54E+01	1.24E+01	1.00E+01	8.30E+00	7.17E+00	6.31E+00

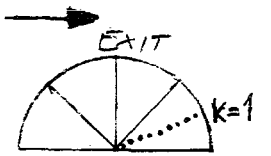

*** K = 2 ***

J I=	1	2	3	4	5	6	7	8	9	10
10	0.00E+00	-4.40E+00	-1.03E+00	7.37E-01	1.16E+00	1.64E+00	2.42E+00	3.18E+00	3.81E+00	4.35E+00
9	0.00E+00	2.31E-01	3.63E+00	3.88E+00	3.44E+00	3.22E+00	3.45E+00	3.88E+00	4.32E+00	4.71E+00
8	0.00E+00	6.48E+00	8.25E+00	7.02E+00	5.56E+00	4.63E+00	4.34E+00	4.45E+00	4.70E+00	4.94E+00
7	0.00E+00	1.50E+01	1.41E+01	1.09E+01	8.09E+00	6.24E+00	5.34E+00	5.07E+00	5.09E+00	5.15E+00
6	0.00E+00	2.48E+01	2.08E+01	1.53E+01	1.09E+01	7.97E+00	6.40E+00	5.73E+00	5.50E+00	5.37E+00
5	5.00E+01	3.60E+01	2.74E+01	1.95E+01	1.35E+01	9.63E+00	7.45E+00	6.39E+00	5.91E+00	5.59E+00
4	5.00E+01	4.01E+01	3.13E+01	2.23E+01	1.55E+01	1.10E+01	8.37E+00	7.00E+00	6.30E+00	5.81E+00
3	5.00E+01	3.91E+01	3.07E+01	2.26E+01	1.63E+01	1.19E+01	9.11E+00	7.53E+00	6.65E+00	6.01E+00
2	1.00E+01	2.74E+01	2.55E+01	2.08E+01	1.61E+01	1.23E+01	9.62E+00	7.95E+00	6.93E+00	6.17E+00
1	1.00E+01	2.12E+01	2.18E+01	1.91E+01	1.57E+01	1.24E+01	9.95E+00	8.22E+00	7.12E+00	6.28E+00

50 → 4

10 → 2

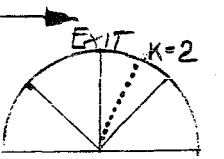

*** K = 3 ***

J I=	1	2	3	4	5	6	7	8	9	10
10	0.00E+00	-4.40E+00	-1.03E+00	7.37E-01	1.16E+00	1.64E+00	2.42E+00	3.18E+00	3.81E+00	4.35E+00
9	0.00E+00	2.31E-01	3.63E+00	3.88E+00	3.44E+00	3.22E+00	3.45E+00	3.88E+00	4.32E+00	4.71E+00
8	0.00E+00	6.48E+00	8.25E+00	7.02E+00	5.56E+00	4.63E+00	4.34E+00	4.45E+00	4.70E+00	4.94E+00
7	0.00E+00	1.50E+01	1.41E+01	1.09E+01	8.09E+00	6.24E+00	5.34E+00	5.07E+00	5.09E+00	5.15E+00
6	0.00E+00	2.48E+01	2.08E+01	1.53E+01	1.09E+01	7.97E+00	6.40E+00	5.73E+00	5.50E+00	5.37E+00
5	5.00E+01	3.60E+01	2.74E+01	1.95E+01	1.35E+01	9.63E+00	7.45E+00	6.39E+00	5.91E+00	5.59E+00
4	5.00E+01	4.01E+01	3.13E+01	2.23E+01	1.55E+01	1.10E+01	8.37E+00	7.00E+00	6.30E+00	5.81E+00
3	5.00E+01	3.91E+01	3.07E+01	2.26E+01	1.63E+01	1.19E+01	9.11E+00	7.53E+00	6.65E+00	6.01E+00
2	1.00E+01	2.74E+01	2.55E+01	2.08E+01	1.61E+01	1.23E+01	9.62E+00	7.95E+00	6.93E+00	6.17E+00
1	1.00E+01	2.12E+01	2.18E+01	1.91E+01	1.57E+01	1.24E+01	9.95E+00	8.22E+00	7.12E+00	6.28E+00

50 → 4

10 → 2

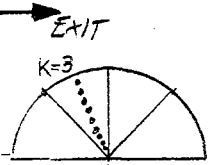

*** K = 4 ***

J I=	1	2	3	4	5	6	7	8	9	10
10	0.00E+00	-8.77E+00	-1.02E+01	-6.89E+00	-2.51E+00	1.43E+00	3.48E+00	4.47E+00	4.91E+00	5.25E+00
9	0.00E+00	-7.75E+00	-7.90E+00	-4.57E+00	-5.88E-01	2.43E+00	4.16E+00	4.98E+00	5.32E+00	5.55E+00
8	0.00E+00	-6.38E+00	-5.71E+00	-2.36E+00	1.16E+00	3.47E+00	4.82E+00	5.42E+00	5.62E+00	5.72E+00
7	0.00E+00	-4.44E+00	-3.02E+00	3.08E-01	3.14E+00	4.76E+00	5.64E+00	5.93E+00	5.95E+00	5.88E+00
6	0.00E+00	-1.88E+00	3.29E-01	3.35E+00	5.37E+00	6.26E+00	6.57E+00	6.50E+00	6.28E+00	6.03E+00
5	0.00E+00	1.33E+00	4.31E+00	6.71E+00	7.81E+00	7.88E+00	7.55E+00	7.06E+00	6.60E+00	6.16E+00
4	0.00E+00	5.49E+00	8.84E+00	1.03E+01	1.03E+01	9.49E+00	8.48E+00	7.57E+00	6.86E+00	6.25E+00
3	0.00E+00	1.07E+01	1.36E+01	1.38E+01	1.26E+01	1.09E+01	9.27E+00	7.97E+00	7.05E+00	6.30E+00
2	0.00E+00	1.58E+01	1.78E+01	1.66E+01	1.44E+01	1.19E+01	9.79E+00	8.22E+00	7.15E+00	6.32E+00
1	0.00E+00	1.95E+01	2.05E+01	1.84E+01	1.54E+01	1.24E+01	1.00E+01	8.30E+00	7.17E+00	6.31E+00

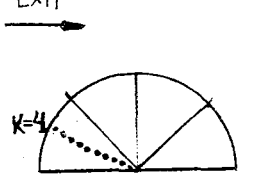

**** CHECK2 PRINT OF UEB I1= 1 IL=10 J1= 1 JL= 4

K J=	1	2	3	4	5	6	7	8	9	10
4	5.77E+00	5.92E+00	5.92E+00	5.85E+00	5.78E+00	5.71E+00	5.67E+00	5.70E+00	5.84E+00	6.27E+00
K= 3	5.32E+00	5.06E+00	4.96E+00	4.94E+00	4.93E+00	4.92E+00	4.93E+00	4.96E+00	5.02E+00	5.19E+00
2	5.32E+00	5.06E+00	4.96E+00	4.94E+00	4.93E+00	4.92E+00	4.93E+00	4.96E+00	5.02E+00	5.19E+00
1	5.77E+00	5.92E+00	5.92E+00	5.85E+00	5.78E+00	5.71E+00	5.67E+00	5.70E+00	5.84E+00	6.27E+00

Table 3.2 Radial Velocity

V=VELOCITY

*** K = 1 ***

J \ I=	1	2	3	4	5	6	7	8	9	10
10	-1.62E+00	-6.41E-01	3.00E-01	7.29E-01	8.79E-01	6.48E-01	4.82E-01	3.78E-01	3.51E-01	4.60E-01
9	-3.06E+00	-1.02E+00	6.22E-01	1.40E+00	1.59E+00	1.23E+00	9.31E-01	7.38E-01	6.84E-01	7.87E-01
8	-4.25E+00	-1.20E+00	9.89E-01	2.01E+00	2.20E+00	1.77E+00	1.35E+00	1.08E+00	9.98E-01	1.06E+00
7	-5.00E+00	-1.15E+00	1.41E+00	2.55E+00	2.70E+00	2.22E+00	1.72E+00	1.39E+00	1.29E+00	1.30E+00
6	-5.22E+00	-8.49E-01	1.86E+00	2.99E+00	3.10E+00	2.59E+00	2.03E+00	1.66E+00	1.54E+00	1.52E+00
5	-5.08E+00	-2.58E-01	2.31E+00	3.31E+00	3.37E+00	2.86E+00	2.27E+00	1.88E+00	1.76E+00	1.71E+00
4	-4.52E+00	5.28E-01	2.68E+00	3.49E+00	3.50E+00	2.99E+00	2.41E+00	2.03E+00	1.91E+00	1.88E+00
3	-3.54E+00	1.20E+00	2.84E+00	3.43E+00	3.40E+00	2.93E+00	2.39E+00	2.05E+00	1.96E+00	1.96E+00
2	-1.77E+00	1.35E+00	2.46E+00	2.85E+00	2.80E+00	2.41E+00	1.99E+00	1.74E+00	1.68E+00	1.73E+00
1	0.00E+00	0.00E+00	0.00E+00	0.00E+00	0.00E+00	0.00E+00	0.00E+00	0.00E+00	0.00E+00	0.00E+00

EXIT

*** K = 2 ***

J \ I=	1	2	3	4	5	6	7	8	9	10
10	-1.06E+00	1.03E+00	7.28E-01	2.42E-01	1.84E-02	-7.44E-02	-1.26E-01	-1.61E-01	-1.73E-01	-8.23E-02
9	-1.48E+00	2.13E+00	1.26E+00	4.21E-01	-1.25E-02	-1.90E-01	-2.76E-01	-3.34E-01	-3.57E-01	-2.40E-01
8	-9.24E-01	2.96E+00	1.60E+00	4.90E-01	-1.08E-01	-3.52E-01	-4.54E-01	-5.23E-01	-5.55E-01	-4.36E-01
7	1.17E+00	3.31E+00	1.64E+00	3.76E-01	-3.08E-01	-5.79E-01	-6.70E-01	-7.35E-01	-7.72E-01	-6.63E-01
6	5.45E+00	3.06E+00	1.28E+00	1.99E-02	-6.49E-01	-8.84E-01	-9.30E-01	-9.70E-01	-1.01E+00	-9.15E-01
5	2.65E+00	1.81E+00	4.36E-01	-6.13E-01	-1.14E+00	-1.26E+00	-1.22E+00	-1.22E+00	-1.25E+00	-1.19E+00
4	3.46E-01	2.95E-01	-6.99E-01	-1.42E+00	-1.71E+00	-1.67E+00	-1.53E+00	-1.47E+00	-1.48E+00	-1.46E+00
3	-2.71E+00	-1.31E+00	-1.76E+00	-2.13E+00	-2.19E+00	-2.00E+00	-1.76E+00	-1.65E+00	-1.65E+00	-1.67E+00
2	-1.19E+00	-1.51E+00	-1.99E+00	-2.25E+00	-2.20E+00	-1.94E+00	-1.66E+00	-1.52E+00	-1.52E+00	-1.59E+00
1	0.00E+00	0.00E+00	0.00E+00	0.00E+00	0.00E+00	0.00E+00	0.00E+00	0.00E+00	0.00E+00	0.00E+00

EXIT

INLET

*** K = 3 ***

J \ I=	1	2	3	4	5	6	7	8	9	10
10	-1.06E+00	1.03E+00	7.28E-01	2.42E-01	1.84E-02	-7.44E-02	-1.26E-01	-1.61E-01	-1.73E-01	-8.23E-02
9	-1.48E+00	2.13E+00	1.26E+00	4.21E-01	-1.25E-02	-1.90E-01	-2.76E-01	-3.34E-01	-3.57E-01	-2.40E-01
8	-9.24E-01	2.96E+00	1.60E+00	4.90E-01	-1.08E-01	-3.52E-01	-4.54E-01	-5.23E-01	-5.55E-01	-4.36E-01
7	1.17E+00	3.31E+00	1.64E+00	3.76E-01	-3.08E-01	-5.79E-01	-6.70E-01	-7.35E-01	-7.72E-01	-6.63E-01
6	5.45E+00	3.06E+00	1.28E+00	1.99E-02	-6.49E-01	-8.84E-01	-9.30E-01	-9.70E-01	-1.01E+00	-9.15E-01
5	2.65E+00	1.81E+00	4.36E-01	-6.13E-01	-1.14E+00	-1.26E+00	-1.22E+00	-1.22E+00	-1.25E+00	-1.19E+00
4	3.46E-01	2.95E-01	-6.99E-01	-1.42E+00	-1.71E+00	-1.67E+00	-1.53E+00	-1.47E+00	-1.48E+00	-1.46E+00
3	-2.71E+00	-1.31E+00	-1.76E+00	-2.13E+00	-2.19E+00	-2.00E+00	-1.76E+00	-1.65E+00	-1.65E+00	-1.67E+00
2	-1.19E+00	-1.51E+00	-1.99E+00	-2.25E+00	-2.20E+00	-1.94E+00	-1.66E+00	-1.52E+00	-1.52E+00	-1.59E+00
1	0.00E+00	0.00E+00	0.00E+00	0.00E+00	0.00E+00	0.00E+00	0.00E+00	0.00E+00	0.00E+00	0.00E+00

EXIT

INLET

*** K = 4 ***

J \ I=	1	2	3	4	5	6	7	8	9	10
10	-1.62E+00	-6.41E-01	3.00E-01	7.29E-01	8.79E-01	6.48E-01	4.82E-01	3.78E-01	3.51E-01	4.60E-01
9	-3.06E+00	-1.02E+00	6.22E-01	1.40E+00	1.59E+00	1.23E+00	9.31E-01	7.38E-01	6.84E-01	7.87E-01
8	-4.25E+00	-1.20E+00	9.89E-01	2.01E+00	2.20E+00	1.77E+00	1.35E+00	1.08E+00	9.98E-01	1.06E+00
7	-5.00E+00	-1.15E+00	1.41E+00	2.55E+00	2.70E+00	2.22E+00	1.72E+00	1.39E+00	1.29E+00	1.30E+00
6	-5.22E+00	-8.49E-01	1.86E+00	2.99E+00	3.10E+00	2.59E+00	2.03E+00	1.66E+00	1.54E+00	1.52E+00
5	-5.08E+00	-2.58E-01	2.31E+00	3.31E+00	3.37E+00	2.86E+00	2.27E+00	1.88E+00	1.76E+00	1.71E+00
4	-4.52E+00	5.28E-01	2.68E+00	3.49E+00	3.50E+00	2.99E+00	2.41E+00	2.03E+00	1.91E+00	1.88E+00
3	-3.54E+00	1.20E+00	2.84E+00	3.43E+00	3.40E+00	2.93E+00	2.39E+00	2.05E+00	1.96E+00	1.96E+00
2	-1.77E+00	1.35E+00	2.46E+00	2.85E+00	2.80E+00	2.41E+00	1.99E+00	1.74E+00	1.68E+00	1.73E+00
1	0.00E+00	0.00E+00	0.00E+00	0.00E+00	0.00E+00	0.00E+00	0.00E+00	0.00E+00	0.00E+00	0.00E+00

EXIT

**** CHECK2 PRINT OF VNB I1= 1 IL=10 J1= 1 JL= 4

J \ I=	1	2	3	4	5	6	7	8	9	10
4	0.00E+00	0.00E+00	0.00E+00	0.00E+00	0.00E+00	0.00E+00	0.00E+00	0.00E+00	0.00E+00	0.00E+00
3	0.00E+00	0.00E+00	0.00E+00	0.00E+00	0.00E+00	0.00E+00	0.00E+00	0.00E+00	0.00E+00	0.00E+00
2	0.00E+00	0.00E+00	0.00E+00	0.00E+00	0.00E+00	0.00E+00	0.00E+00	0.00E+00	0.00E+00	0.00E+00
1	0.00E+00	0.00E+00	0.00E+00	0.00E+00	0.00E+00	0.00E+00	0.00E+00	0.00E+00	0.00E+00	0.00E+00

Table 3.3 Angular Momentum

************************************ SWIRL VELOCITY ************************************

*** K = 1 ***

I=	1	2	3	4	5	6	7	8	9	10
10	0.00E+00	0.00E+00	0.00E+00	0.00E+00	0.00E+00	0.00E+00	0.00E+00	0.00E+00	0.00E+00	0.00E+00
9	0.00E+00	0.00E+00	0.00E+00	0.00E+00	0.00E+00	0.00E+00	0.00E+00	0.00E+00	0.00E+00	0.00E+00
8	0.00E+00	0.00E+00	0.00E+00	0.00E+00	0.00E+00	0.00E+00	0.00E+00	0.00E+00	0.00E+00	0.00E+00
7	0.00E+00	0.00E+00	0.00E+00	0.00E+00	0.00E+00	0.00E+00	0.00E+00	0.00E+00	0.00E+00	0.00E+00
6	0.00E+00	0.00E+00	0.00E+00	0.00E+00	0.00E+00	0.00E+00	0.00E+00	0.00E+00	0.00E+00	0.00E+00
5	0.00E+00	0.00E+00	0.00E+00	0.00E+00	0.00E+00	0.00E+00	0.00E+00	0.00E+00	0.00E+00	0.00E+00
4	0.00E+00	0.00E+00	0.00E+00	0.00E+00	0.00E+00	0.00E+00	0.00E+00	0.00E+00	0.00E+00	0.00E+00
3	0.00E+00	0.00E+00	0.00E+00	0.00E+00	0.00E+00	0.00E+00	0.00E+00	0.00E+00	0.00E+00	0.00E+00
2	0.00E+00	0.00E+00	0.00E+00	0.00E+00	0.00E+00	0.00E+00	0.00E+00	0.00E+00	0.00E+00	0.00E+00
1	0.00E+00	0.00E+00	0.00E+00	0.00E+00	0.00E+00	0.00E+00	0.00E+00	0.00E+00	0.00E+00	0.00E+00

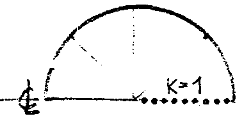

*** K = 2 ***

I=	1	2	3	4	5	6	7	8	9	10
	1.34E+00	-2.88E+00	-3.02E+00	-1.29E+00	6.46E-01	1.91E+00	2.30E+00	2.36E+00	2.32E+00	2.07E+00
	2.19E+00	-1.76E+00	-2.57E+00	-1.55E+00	-7.21E-02	1.00E+00	1.45E+00	1.58E+00	1.58E+00	1.37E+00
	2.86E+00	-8.34E-01	-2.07E+00	-1.55E+00	-4.93E-01	3.82E-01	8.13E-01	9.69E-01	9.91E-01	8.31E-01
	3.28E+00	-1.81E-01	-1.62E+00	-1.46E+00	-7.53E-01	-6.96E-02	3.19E-01	4.80E-01	5.12E-01	4.02E-01
	3.11E+00	1.67E-01	-1.24E+00	-1.32E+00	-8.77E-01	-3.71E-01	-4.46E-02	1.04E-01	1.39E-01	6.82E-02
	2.01E+00	2.73E-01	-9.28E-01	-1.13E+00	-8.92E-01	-5.42E-01	-2.87E-01	-1.62E-01	-1.31E-01	-1.73E-01
	1.03E+00	1.20E-01	-7.23E-01	-9.38E-01	-8.24E-01	-6.00E-01	-4.16E-01	-3.20E-01	-2.95E-01	-3.20E-01
	3.17E-01	-1.37E-01	-5.88E-01	-7.32E-01	-6.87E-01	-5.57E-01	-4.35E-01	-3.68E-01	-3.51E-01	-3.66E-01
INLET	1.10E-01	-2.35E-01	-4.15E-01	-4.85E-01	-4.72E-01	-4.07E-01	-3.37E-01	-2.97E-01	-2.87E-01	-2.98E-01
	5.18E-03	-6.97E-02	-1.08E-01	-1.23E-01	-1.21E-01	-1.04E-01	-8.74E-02	-7.81E-02	-7.67E-02	-8.07E-02

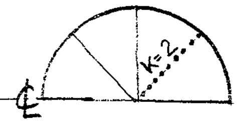

*** K = 3 ***

I=	1	2	3	4	5	6	7	8	9	10
	-8.61E-08	-5.26E-08	-3.34E-08	-2.03E-08	-1.74E-08	-2.70E-08	-4.32E-08	-5.61E-08	-5.84E-08	-4.55E-08
	8.12E-08	-4.03E-08	-2.58E-08	-1.58E-08	-1.27E-08	-1.81E-08	-2.88E-08	-3.78E-08	-3.93E-08	-2.96E-08
	6.86E-08	-3.43E-08	-2.12E-08	-1.27E-08	-9.74E-09	-1.29E-08	-2.06E-08	-2.74E-08	-2.84E-08	-2.08E-08
	4.88E-08	-2.98E-08	-1.86E-08	-1.09E-08	-7.79E-09	-9.77E-09	-1.59E-08	-2.15E-08	-2.21E-08	-1.58E-08
	3.04E-08	-2.51E-08	-1.67E-08	-9.58E-09	-6.37E-09	-7.81E-09	-1.31E-08	-1.78E-08	-1.81E-08	-1.27E-08
	-1.73E-08	-2.18E-08	-1.52E-08	-8.36E-09	-5.13E-09	-6.24E-09	-1.09E-08	-1.50E-08	-1.52E-08	-1.03E-08
	-1.92E-08	-2.17E-08	-1.37E-08	-6.78E-09	-3.83E-09	-4.55E-09	-7.88E-09	-1.09E-08	-1.12E-08	-7.03E-09
INLET	-1.68E-08	-1.69E-08	-9.59E-09	-4.34E-09	-2.36E-09	-2.38E-09	-2.33E-09	-2.98E-09	-3.92E-09	-8.83E-10
	1.87E-09	-1.61E-09	-1.73E-09	-1.22E-09	-9.43E-10	3.86E-10	6.80E-09	1.06E-08	8.20E-09	9.60E-09
	5.13E-08	1.57E-08	4.25E-09	7.12E-10	-1.47E-10	2.27E-09	1.34E-08	2.03E-08	1.68E-08	1.71E-08

SYMMETRY PLANE

θ=90°

*** K = 4 ***

I=	1	2	3	4	5	6	7	8	9	10
	1.34E+00	2.88E+00	3.02E+00	1.29E+00	-6.46E-01	-1.91E+00	-2.30E+00	-2.36E+00	-2.32E+00	-2.07E+00
	2.19E+00	1.76E+00	2.57E+00	1.55E+00	7.21E-02	-1.00E+00	-1.45E+00	-1.58E+00	-1.58E+00	-1.37E+00
	2.86E+00	8.34E-01	2.07E+00	1.55E+00	4.93E-01	-3.82E-01	-8.13E-01	-9.69E-01	-9.91E-01	-8.31E-01
	3.28E+00	1.81E-01	1.62E+00	1.46E+00	7.53E-01	6.96E-02	-3.19E-01	-4.80E-01	-5.12E-01	-4.02E-01
	1.11E+00	-1.67E-01	1.24E+00	1.32E+00	8.77E-01	3.71E-01	4.46E-02	-1.04E-01	-1.39E-01	-6.82E-02
	2.01E+00	-2.73E-01	9.28E-01	1.13E+00	8.92E-01	5.42E-01	2.87E-01	1.62E-01	1.31E-01	1.73E-01
	1.03E+00	-1.20E-01	7.23E-01	9.38E-01	8.24E-01	6.00E-01	4.16E-01	3.20E-01	2.95E-01	3.20E-01
INLET	1.17E-01	1.37E-01	5.88E-01	7.32E-01	6.87E-01	5.57E-01	4.35E-01	3.68E-01	3.51E-01	3.66E-01
	.10E-01	2.35E-01	4.15E-01	4.85E-01	4.72E-01	4.07E-01	3.37E-01	2.97E-01	2.87E-01	2.98E-01
	[illegible]	[illegible]	[illegible]	[illegible]	[illegible]	[illegible]	[illegible]	[illegible]	[illegible]	[illegible]

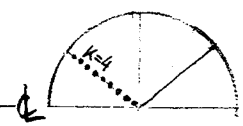

**** CHECK2 PRINT OF WHB I1= 1 IL=10 J1= 1 JL=10

I=	1	2	3	4	5	6	7	8	9	10
	.00E+00	0.00E+00	0.00E+00	0.00E+00	0.00E+00	0.00E+00	0.00E+00	0.00E+00	0.00E+00	0.00E+00
	.00E+00	0.00E+00	0.00E+00	0.00E+00	0.00E+00	0.00E+00	0.00E+00	0.00E+00	0.00E+00	0.00E+00
	.00E+00	0.00E+00	0.00E+00	0.00E+00	0.00E+00	0.00E+00	0.00E+00	0.00E+00	0.00E+00	0.00E+00
	.00E+00	0.00E+00	0.00E+00	0.00E+00	0.00E+00	0.00E+00	0.00E+00	0.00E+00	0.00E+00	0.00E+00
	.00E+00	0.00E+00	0.00E+00	0.00E+00	0.00E+00	0.00E+00	0.00E+00	0.00E+00	0.00E+00	0.00E+00
	.00E+00	0.00E+00	0.00E+00	0.00E+00	0.00E+00	0.00E+00	0.00E+00	0.00E+00	0.00E+00	0.00E+00
	.00E+00	0.00E+00	0.00E+00	0.00E+00	0.00E+00	0.00E+00	0.00E+00	0.00E+00	0.00E+00	0.00E+00
	.00E+00	0.00E+00	0.00E+00	0.00E+00	0.00E+00	0.00E+00	0.00E+00	0.00E+00	0.00E+00	0.00E+00
	.00E+00	0.00E+00	0.00E+00	0.00E+00	0.00E+00	0.00E+00	0.00E+00	0.00E+00	0.00E+00	0.00E+00
	.00E+00	0.00E+00	0.00E+00	0.00E+00	0.00E+00	0.00E+00	0.00E+00	0.00E+00	0.00E+00	0.00E+00

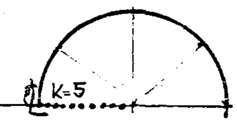

Table 3.4 Kinetic Energy of Turbulence

K.E. OF TURBULENCE

*** K = 1 ***

1	2	3	4	5	6	7	8	9	10
3.71E+00	1.17E+01	1.22E+01	1.07E+01	6.55E+00	4.96E+00	3.89E+00	3.04E+00	2.47E+00	2.23E+00
.85E+01	7.87E+01	7.47E+01	5.70E+01	4.06E+01	2.96E+01	2.20E+01	1.65E+01	1.28E+01	1.05E+01
.11E+01	1.15E+02	1.04E+02	7.79E+01	5.58E+01	4.05E+01	2.98E+01	2.23E+01	1.71E+01	1.39E+01
5.75E+01	1.45E+02	1.26E+02	9.32E+01	6.74E+01	4.88E+01	3.57E+01	2.65E+01	2.02E+01	1.62E+01
.29E+02	1.64E+02	1.37E+02	1.03E+02	7.59E+01	5.53E+01	4.04E+01	2.98E+01	2.25E+01	1.79E+01
.13E+02	1.58E+02	1.35E+02	1.07E+02	8.12E+01	6.01E+01	4.40E+01	3.24E+01	2.42E+01	1.91E+01
7.95E+01	1.38E+02	1.26E+02	1.06E+02	8.35E+01	6.33E+01	4.67E+01	3.42E+01	2.55E+01	2.00E+01
.87E+01	1.25E+02	1.18E+02	1.03E+02	8.44E+01	6.54E+01	4.86E+01	3.56E+01	2.64E+01	2.07E+01
.99E+01	1.16E+02	1.12E+02	1.00E+02	8.48E+01	6.70E+01	5.00E+01	3.66E+01	2.72E+01	2.13E+01
6.42E+01	1.09E+02	1.08E+02	9.86E+01	8.49E+01	6.76E+01	5.06E+01	3.70E+01	2.74E+01	2.15E+01

*** K = 2 ***

1	2	3	4	5	6	7	8	9	10
3.27E+00	1.19E+01	7.43E+00	5.09E+00	4.37E+00	3.30E+00	2.52E+00	1.97E+00	1.60E+00	1.43E+00
.48E+00	7.71E+01	7.34E+01	5.48E+01	3.74E+01	2.50E+01	1.72E+01	1.24E+01	9.33E+00	7.68E+00
.75E+01	1.01E+02	1.01E+02	7.77E+01	5.38E+01	3.59E+01	2.46E+01	1.76E+01	1.31E+01	1.06E+01
4.71E+01	1.19E+02	1.20E+02	9.49E+01	6.69E+01	4.50E+01	3.07E+01	2.17E+01	1.61E+01	1.28E+01
.17E+02	1.33E+02	1.28E+02	1.05E+02	7.66E+01	5.25E+01	3.60E+01	2.54E+01	1.86E+01	1.48E+01
9.14E+01	1.14E+02	1.21E+02	1.07E+02	8.21E+01	5.82E+01	4.05E+01	2.86E+01	2.10E+01	1.65E+01
.32E+01	8.31E+01	1.05E+02	1.03E+02	8.40E+01	6.20E+01	4.41E+01	3.14E+01	2.30E+01	1.80E+01
.15E+01	8.82E+01	1.01E+02	9.93E+01	8.44E+01	6.46E+01	4.70E+01	3.38E+01	2.48E+01	1.94E+01
7.63E+01	1.05E+02	1.05E+02	9.84E+01	8.47E+01	6.65E+01	4.92E+01	3.58E+01	2.64E+01	2.07E+01
.26E+01	1.08E+02	1.07E+02	9.84E+01	8.49E+01	6.75E+01	5.05E+01	3.69E+01	2.73E+01	2.14E+01

*** K = 3 ***

1	2	3	4	5	6	7	8	9	10
3.27E+00	1.19E+01	7.43E+00	5.09E+00	4.37E+00	3.30E+00	2.52E+00	1.97E+00	1.60E+00	1.43E+00
.48E+00	7.71E+01	7.34E+01	5.48E+01	3.74E+01	2.50E+01	1.72E+01	1.24E+01	9.33E+00	7.68E+00
.75E+01	1.01E+02	1.01E+02	7.77E+01	5.38E+01	3.59E+01	2.46E+01	1.76E+01	1.31E+01	1.06E+01
4.71E+01	1.19E+02	1.20E+02	9.49E+01	6.69E+01	4.50E+01	3.07E+01	2.17E+01	1.61E+01	1.28E+01
.17E+02	1.33E+02	1.28E+02	1.05E+02	7.66E+01	5.25E+01	3.60E+01	2.54E+01	1.86E+01	1.48E+01
9.14E+01	1.14E+02	1.21E+02	1.07E+02	8.21E+01	5.82E+01	4.05E+01	2.86E+01	2.10E+01	1.65E+01
.32E+01	8.31E+01	1.05E+02	1.03E+02	8.40E+01	6.20E+01	4.41E+01	3.14E+01	2.30E+01	1.80E+01
.15E+01	8.82E+01	1.01E+02	9.93E+01	8.44E+01	6.46E+01	4.70E+01	3.38E+01	2.48E+01	1.94E+01
7.63E+01	1.05E+02	1.05E+02	9.84E+01	8.47E+01	6.65E+01	4.92E+01	3.58E+01	2.64E+01	2.07E+01
.26E+01	1.08E+02	1.07E+02	9.84E+01	8.49E+01	6.75E+01	5.05E+01	3.69E+01	2.73E+01	2.14E+01

*** K = 4 ***

1	2	3	4	5	6	7	8	9	10
3.71E+00	1.17E+01	1.22E+01	1.07E+01	6.55E+00	4.96E+00	3.89E+00	3.04E+00	2.47E+00	2.23E+00
.85E+01	7.87E+01	7.47E+01	5.70E+01	4.06E+01	2.96E+01	2.20E+01	1.65E+01	1.28E+01	1.05E+01
5.11E+01	1.15E+02	1.04E+02	7.79E+01	5.58E+01	4.05E+01	2.98E+01	2.23E+01	1.71E+01	1.39E+01
5.75E+01	1.45E+02	1.26E+02	9.32E+01	6.74E+01	4.88E+01	3.57E+01	2.65E+01	2.02E+01	1.62E+01
1.29E+02	1.64E+02	1.37E+02	1.03E+02	7.59E+01	5.53E+01	4.04E+01	2.98E+01	2.25E+01	1.79E+01
1.13E+02	1.58E+02	1.35E+02	1.07E+02	8.12E+01	6.01E+01	4.40E+01	3.24E+01	2.42E+01	1.91E+01
7.95E+01	1.38E+02	1.26E+02	1.06E+02	8.35E+01	6.33E+01	4.67E+01	3.42E+01	2.55E+01	2.00E+01
7.87E+01	1.25E+02	1.18E+02	1.03E+02	8.44E+01	6.54E+01	4.86E+01	3.56E+01	2.64E+01	2.07E+01
7.99E+01	1.16E+02	1.12E+02	1.00E+02	8.48E+01	6.70E+01	5.00E+01	3.66E+01	2.72E+01	2.13E+01
6.42E+01	1.09E+02	1.08E+02	9.86E+01	8.49E+01	6.76E+01	5.06E+01	3.70E+01	2.74E+01	2.15E+01

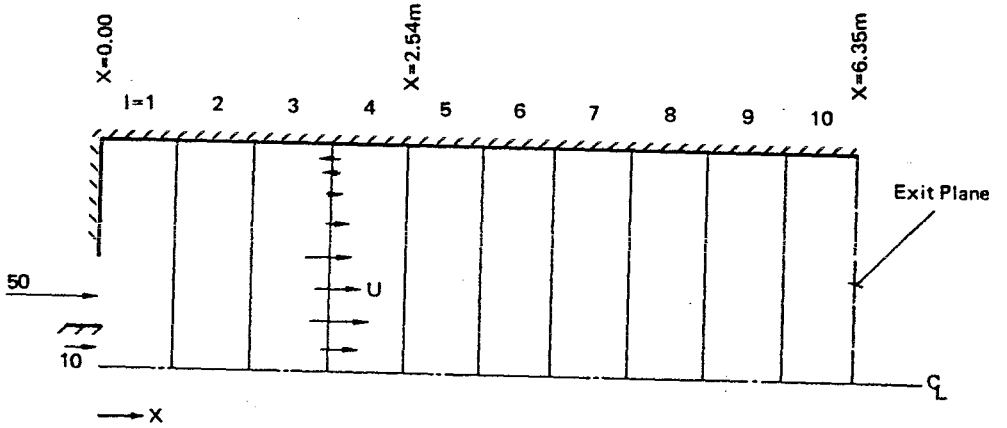

CONVECTIVE FLUXES THROUGH THE CHAMBER CROSSECTIONS

I=	1	XM=	0.000E+00	FX=	1.473138E+01	FXP=	1.473138E+01	FXN=	0.000000E+00	FULFLX=	0.000000E+0
I=	2	XM=	6.350E-01	FX=	1.473135E+01	FXP=	2.224907E+01	FXN=	-7.517717E+00	FULFLX=	0.000000E+0
I=	3	XM=	1.270E+00	FX=	1.473133E+01	FXP=	2.112332E+01	FXN=	-6.391988E+00	FULFLX=	0.000000E+0
I=	4	XM=	1.905E+00	FX=	1.473132E+01	FXP=	1.803385E+01	FXN=	-3.302532E+00	FULFLX=	0.000000E+0
I=	5	XM=	2.540E+00	FX=	1.473132E+01	FXP=	1.551363E+01	FXN=	-7.823103E-01	FULFLX=	0.000000E+0
I=	6	XM=	3.175E+00	FX=	1.473134E+01	FXP=	1.473134E+01	FXN=	0.000000E+00	FULFLX=	0.000000E+0
I=	7	XM=	3.810E+00	FX=	1.473139E+01	FXP=	1.473139E+01	FXN=	0.000000E+00	FULFLX=	0.000000E+0
I=	8	XM=	4.445E+00	FX=	1.473146E+01	FXP=	1.473146E+01	FXN=	0.000000E+00	FULFLX=	0.000000E+0
I=	9	XM=	5.080E+00	FX=	1.473153E+01	FXP=	1.473153E+01	FXN=	0.000000E+00	FULFLX=	0.000000E+0
I=	10	XM=	5.715E+00	FX=	1.473157E+01	FXP=	1.473157E+01	FXN=	0.000000E+00	FULFLX=	0.000000E+0
I=	11	XM=	6.350E+00	FX=	1.473159E+01	FXP=	1.473159E+01	FXN=	0.000000E+00	FULFLX=	0.000000E+0

Table 3.5 Convective Fluxes Through the Chamber Crossections

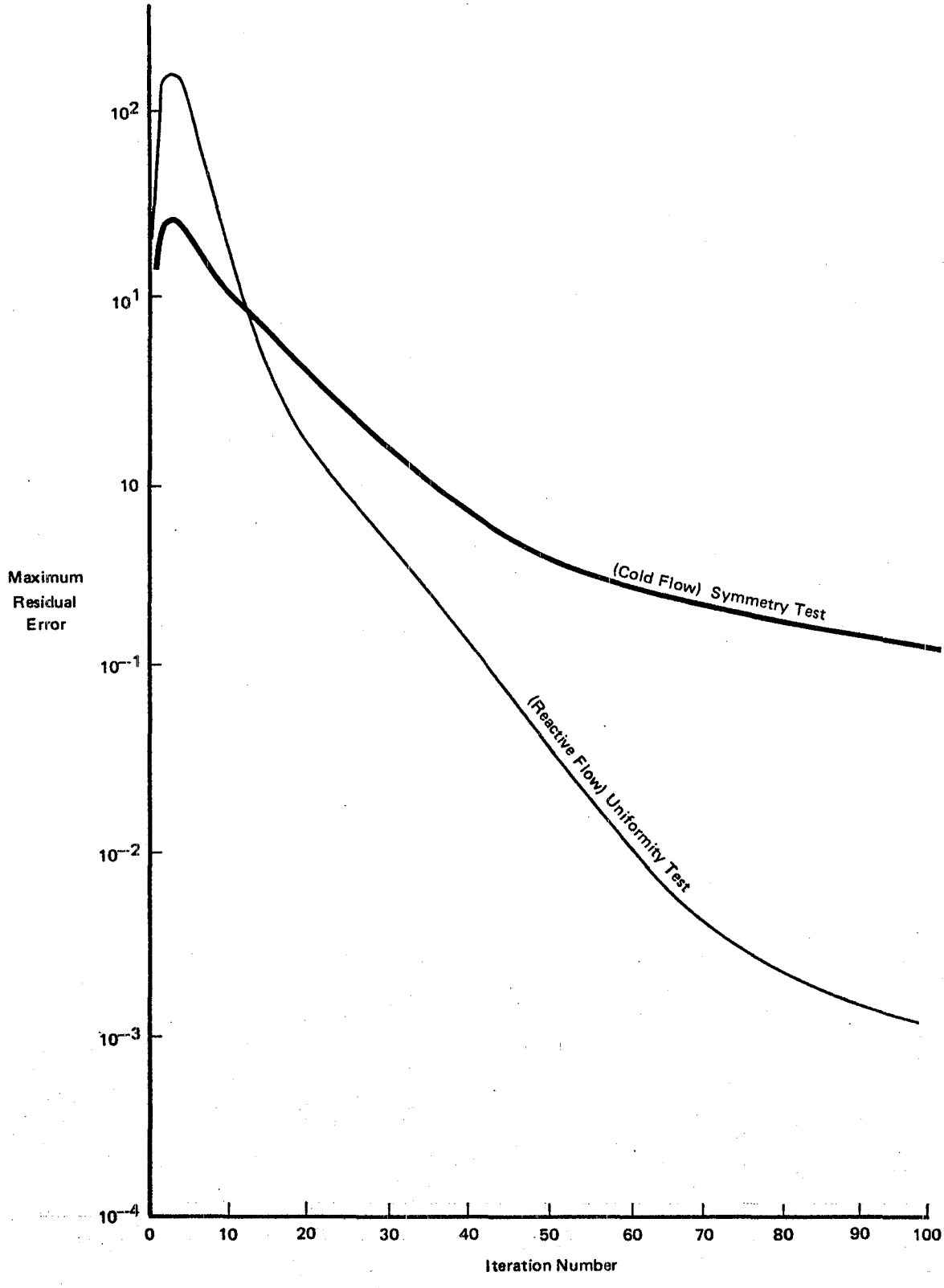

Figure 3.3 Convergence rate for the symmetry and uniformity test.

The global mass flux FX = 14.73138 should be, and is preserved, at each axial location I = 1 . . . . . 10.

3.2 UNIFORMITY TESTS

The uniformity tests have been performed on similar chamber geometry with axi-symmetric fluid entry (figure 3.4). A turbulent flow with propane-air combustion in a chamber with sudden enlargment has been considered. Figure 3.4 presents the geometry and inlet conditions. Fuel enters the chamber through the axial slot at x=0 with $u=10\frac{m}{s}$, v=0, w=0, and air through the annular inlet with $u=50\frac{m}{s}$, v=0, w=0 (see table 3.6). Results are presented by the following tables:

- 3.6 - u -axial velocity (m/s)
- 3.7 - v -radial velocity (m/s)
- 3.8 - rw-angular velocity (m^2/s)
- 3.9 - k -kinetic enerty of turbulence (m^2/s^2)
- 3.10- T-absolute temperature (^oK)
- 3.11- m_{fu}-fuel mass fraction (-)
- 3.12- FX, FXP, FXN and FULFLX fluxes (kg/s).

Calculated results are uniform on all θ_k (k = 1, 2, 3, 4,) planes. Note that the recirculation zone extends up to the middle of the chamber. The angular momentum rw should be zero throughout the chamber. It was predicted as 10^{-8} - 10^{-12} at $\theta=90^o$ and as 10^{-4} - 10^{-6} at $\theta = 45^o$ and $\theta = 135^o$ respectively. These values are within acceptable error limits.

The values k, T and m_{fu} also indicate good uniformity. Table 3.12, in addition to global mass fluxes (FX, FXP, FXN), also provides total cross-section unburned fuel flow rate, which is defined as:

$$FULFLX = \sum_k \sum_j (\rho u A \cdot m_{fu})_{j,k}$$

The convergence and conservativity of the numerical algorithm can be verified by FX distribution. Note - the FX = 17.79037 kg/s value is exactly preserved at each axial i-plane (table 3.12).

The convergence rate for the uniformity test case is presented in figure 3.3. The residual error for test case B indicates better convergence for the flow with uniform inflow. Intensive recirculation zones in case A (symmetry test) are responsible for relatively slower convergence rate.

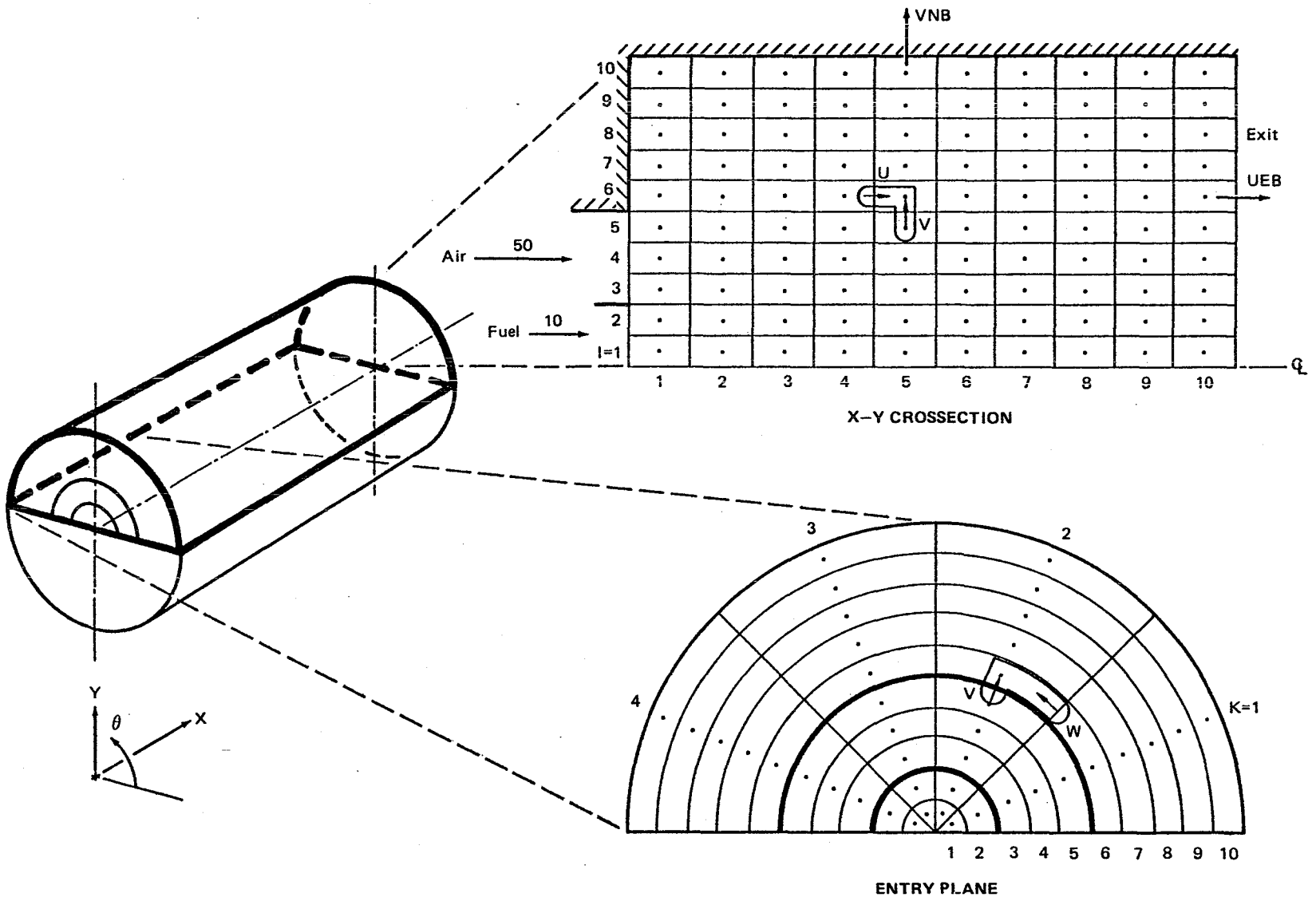

Figure 3.4 Combustion Chamber Geometry

Table 3.6 Axial Velocity

U-VELOCITY

*** K = 1 ***

J	I= 1	2	3	4	5	6	7	8	9	10
10	0.00E+00	-8.49E+00	-8.59E+00	-4.97E+00	-1.89E+00	3.96E+00	2.83E+01	3.26E+01	3.34E+01	3.37E+01
9	0.00E+00	-5.31E+00	-2.86E+00	4.57E-02	2.75E+00	7.45E+00	2.92E+01	3.37E+01	3.49E+01	3.57E+01
8	0.00E+00	-3.73E-01	3.13E+00	5.01E+00	6.91E+00	1.05E+01	3.09E+01	3.46E+01	3.58E+01	3.67E+01
7	0.00E+00	8.16E+00	1.08E+01	1.12E+01	1.19E+01	1.38E+01	3.37E+01	3.59E+01	3.69E+01	3.76E+01
6	0.00E+00	2.13E+01	2.08E+01	1.88E+01	1.76E+01	1.74E+01	3.74E+01	3.77E+01	3.81E+01	3.86E+01
5	5.00E+01	3.97E+01	3.29E+01	2.75E+01	2.39E+01	2.09E+01	4.16E+01	3.97E+01	3.95E+01	3.97E+01
AIR 4	5.00E+01	4.62E+01	4.12E+01	3.50E+01	2.95E+01	2.38E+01	4.55E+01	4.15E+01	4.09E+01	4.08E+01
3	5.00E+01	4.61E+01	4.27E+01	3.78E+01	3.22E+01	2.51E+01	4.78E+01	4.29E+01	4.20E+01	4.17E+01
2	1.00E+01	3.18E+01	3.28E+01	3.20E+01	2.96E+01	2.34E+01	4.81E+01	4.35E+01	4.26E+01	4.23E+01
FU 1	1.00E+01	2.17E+01	2.57E+01	2.69E+01	2.65E+01	2.13E+01	4.76E+01	4.34E+01	4.27E+01	4.26E+01

*** K = 2 ***

J	I= 1	2	3	4	5	6	7	8	9	10
10	0.00E+00	-8.49E+00	-8.60E+00	-4.97E+00	-1.90E+00	3.96E+00	2.83E+01	3.26E+01	3.34E+01	3.37E+01
9	0.00E+00	-5.31E+00	-2.86E+00	4.21E-02	2.75E+00	7.45E+00	2.92E+01	3.37E+01	3.49E+01	3.57E+01
8	0.00E+00	-3.75E-01	3.13E+00	5.00E+00	6.91E+00	1.05E+01	3.09E+01	3.46E+01	3.58E+01	3.67E+01
7	0.00E+00	8.16E+00	1.08E+01	1.12E+01	1.19E+01	1.38E+01	3.37E+01	3.59E+01	3.69E+01	3.76E+01
6	0.00E+00	2.13E+01	2.08E+01	1.88E+01	1.76E+01	1.74E+01	3.74E+01	3.77E+01	3.81E+01	3.86E+01
5	5.00E+01	3.97E+01	3.29E+01	2.75E+01	2.39E+01	2.09E+01	4.16E+01	3.97E+01	3.95E+01	3.97E+01
AIR 4	5.00E+01	4.62E+01	4.12E+01	3.50E+01	2.95E+01	2.38E+01	4.55E+01	4.15E+01	4.09E+01	4.08E+01
3	5.00E+01	4.61E+01	4.27E+01	3.78E+01	3.22E+01	2.51E+01	4.78E+01	4.29E+01	4.20E+01	4.17E+01
2	1.00E+01	3.18E+01	3.28E+01	3.20E+01	2.96E+01	2.34E+01	4.81E+01	4.35E+01	4.26E+01	4.23E+01
FU 1	1.00E+01	2.17E+01	2.57E+01	2.69E+01	2.65E+01	2.13E+01	4.76E+01	4.34E+01	4.27E+01	4.26E+01

*** K = 3 ***

J	I= 1	2	3	4	5	6	7	8	9	10
10	0.00E+00	-8.49E+00	-8.60E+00	-4.97E+00	-1.90E+00	3.96E+00	2.83E+01	3.26E+01	3.34E+01	3.37E+01
9	0.00E+00	-5.31E+00	-2.86E+00	4.21E-02	2.75E+00	7.45E+00	2.92E+01	3.37E+01	3.49E+01	3.57E+01
8	0.00E+00	-3.75E-01	3.13E+00	5.00E+00	6.91E+00	1.05E+01	3.09E+01	3.46E+01	3.58E+01	3.67E+01
7	0.00E+00	8.16E+00	1.08E+01	1.12E+01	1.19E+01	1.38E+01	3.37E+01	3.59E+01	3.69E+01	3.76E+01
6	0.00E+00	2.13E+01	2.08E+01	1.88E+01	1.76E+01	1.74E+01	3.74E+01	3.77E+01	3.81E+01	3.86E+01
5	5.00E+01	3.97E+01	3.29E+01	2.75E+01	2.39E+01	2.09E+01	4.16E+01	3.97E+01	3.95E+01	3.97E+01
AIR 4	5.00E+01	4.62E+01	4.12E+01	3.50E+01	2.95E+01	2.38E+01	4.55E+01	4.15E+01	4.09E+01	4.08E+01
3	5.00E+01	4.61E+01	4.27E+01	3.78E+01	3.22E+01	2.51E+01	4.78E+01	4.29E+01	4.20E+01	4.17E+01
2	1.00E+01	3.18E+01	3.28E+01	3.20E+01	2.96E+01	2.34E+01	4.81E+01	4.35E+01	4.26E+01	4.23E+01
FU 1	1.00E+01	2.17E+01	2.57E+01	2.69E+01	2.65E+01	2.13E+01	4.76E+01	4.34E+01	4.27E+01	4.26E+01

*** K = 4 ***

J	I= 1	2	3	4	5	6	7	8	9	10
10	0.00E+00	-8.49E+00	-8.59E+00	-4.97E+00	-1.89E+00	3.96E+00	2.83E+01	3.26E+01	3.34E+01	3.37E+01
9	0.00E+00	-5.31E+00	-2.86E+00	4.57E-02	2.75E+00	7.45E+00	2.92E+01	3.37E+01	3.49E+01	3.57E+01
8	0.00E+00	-3.73E-01	3.13E+00	5.01E+00	6.91E+00	1.05E+01	3.09E+01	3.46E+01	3.58E+01	3.67E+01
7	0.00E+00	8.16E+00	1.08E+01	1.12E+01	1.19E+01	1.38E+01	3.37E+01	3.59E+01	3.69E+01	3.76E+01
6	0.00E+00	2.13E+01	2.08E+01	1.88E+01	1.76E+01	1.74E+01	3.74E+01	3.77E+01	3.81E+01	3.86E+01
5	5.00E+01	3.97E+01	3.29E+01	2.75E+01	2.39E+01	2.09E+01	4.16E+01	3.97E+01	3.95E+01	3.97E+01
AIR 4	5.00E+01	4.62E+01	4.12E+01	3.50E+01	2.95E+01	2.38E+01	4.55E+01	4.15E+01	4.09E+01	4.08E+01
3	5.00E+01	4.61E+01	4.27E+01	3.78E+01	3.22E+01	2.51E+01	4.78E+01	4.29E+01	4.20E+01	4.17E+01
2	1.00E+01	3.18E+01	3.28E+01	3.20E+01	2.96E+01	2.34E+01	4.81E+01	4.35E+01	4.26E+01	4.23E+01
FU 1	1.00E+01	2.17E+01	2.57E+01	2.69E+01	2.65E+01	2.13E+01	4.76E+01	4.34E+01	4.27E+01	4.26E+01

**** CHECK2 PRINT OF UER II= 1 IL=10 JI= 1 JL= 4

J	I= 1	2	3	4	5	6	7	8	9	10
4	4.2260E+01	4.1981E+01	4.1388E+01	4.0525E+01	3.9491E+01	3.8466E+01	3.7594E+01	3.6926E+01	3.6409E+01	3.5306E+01
3	4.2260E+01	4.1982E+01	4.1389E+01	4.0527E+01	3.9493E+01	3.8470E+01	3.7599E+01	3.6931E+01	3.6415E+01	3.5313E+01
2	4.2260E+01	4.1982E+01	4.1389E+01	4.0527E+01	3.9493E+01	3.8470E+01	3.7599E+01	3.6931E+01	3.6415E+01	3.5313E+01
1	4.2260E+01	4.1981E+01	4.1388E+01	4.0525E+01	3.9491E+01	3.8466E+01	3.7594E+01	3.6926E+01	3.6409E+01	3.5306E+01

Table 3.7 Radial Velocity

V-VELOCITY

*** K = 1 ***

J I=	1	2	3	4	5	6	7	8	9	10
10	-1.74E+00	-2.18E-02	7.44E-01	6.49E-01	1.18E+00	4.03E+00	6.72E-01	5.31E-02	-3.66E-02	2.50E-01
9	-3.04E+00	4.69E-01	1.41E+00	1.26E+00	2.16E+00	7.32E+00	1.33E+00	1.73E-01	4.69E-04	3.19E-01
8	-3.53E+00	1.25E+00	1.98E+00	1.79E+00	2.95E+00	1.02E+01	1.90E+00	3.01E-01	5.66E-02	3.14E-01
7	-2.36E+00	2.01E+00	2.38E+00	2.16E+00	3.45E+00	1.24E+01	2.32E+00	4.08E-01	1.14E-01	2.79E-01
6	1.67E+00	2.29E+00	2.43E+00	2.26E+00	3.57E+00	1.35E+01	2.50E+00	4.77E-01	1.71E-01	2.50E-01
5	-2.73E-01	1.28E+00	1.81E+00	1.94E+00	3.23E+00	1.24E+01	2.28E+00	4.89E-01	2.27E-01	2.51E-01
4	-1.24E+00	4.87E-01	9.23E-01	1.21E+00	2.41E+00	8.58E+00	1.80E+00	4.77E-01	2.60E-01	2.43E-01
3	-3.10E+00	-2.62E-01	9.34E-02	3.80E-01	1.38E+00	4.12E+00	1.28E+00	3.97E-01	2.30E-01	2.00E-01
2	-1.00E+00	-3.10E-01	-7.24E-02	6.82E-02	6.06E-01	1.32E+00	6.69E-01	2.31E-01	1.37E-01	1.17E-01
1	0.00E+00	0.00E+00	0.00E+00	0.00E+00	0.00E+00	0.00E+00	0.00E+00	0.00E+00	0.00E+00	0.00E+00

*** K = 2 ***

J I=	1	2	3	4	5	6	7	8	9	10
10	-1.74E+00	-2.19E-02	7.44E-01	-6.49E-01	1.18E+00	4.03E+00	6.73E-01	5.34E-02	-3.63E-02	2.50E-01
9	-3.04E+00	4.69E-01	1.41E+00	1.26E+00	2.16E+00	7.33E+00	1.33E+00	1.74E-01	1.11E-03	3.20E-01
8	-3.53E+00	1.25E+00	1.98E+00	1.79E+00	2.95E+00	1.02E+01	1.90E+00	3.02E-01	5.76E-02	3.15E-01
7	-2.36E+00	2.01E+00	2.38E+00	2.16E+00	3.45E+00	1.24E+01	2.32E+00	4.09E-01	1.16E-01	2.80E-01
6	1.67E+00	2.29E+00	2.43E+00	2.26E+00	3.58E+00	1.35E+01	2.50E+00	4.79E-01	1.73E-01	2.51E-01
5	-2.73E-01	1.28E+00	1.81E+00	1.94E+00	3.23E+00	1.24E+01	2.28E+00	4.91E-01	2.30E-01	2.53E-01
4	-1.24E+00	4.87E-01	9.24E-01	1.21E+00	2.41E+00	8.58E+00	1.80E+00	4.80E-01	2.62E-01	2.45E-01
3	-3.10E+00	-2.62E-01	9.37E-02	3.81E-01	1.38E+00	4.12E+00	1.28E+00	4.00E-01	2.33E-01	2.03E-01
2	-1.00E+00	-3.10E-01	-7.22E-02	6.86E-02	6.07E-01	1.33E+00	6.72E-01	2.35E-01	1.40E-01	1.19E-01
1	0.00E+00	0.00E+00	0.00E+00	0.00E+00	0.00E+00	0.00E+00	0.00E+00	0.00E+00	0.00E+00	0.00E+00

*** K = 3 ***

J I=	1	2	3	4	5	6	7	8	9	10
10	-1.74E+00	-2.19E-02	7.44E-01	6.49E-01	1.18E+00	4.03E+00	6.73E-01	5.34E-02	-3.63E-02	2.50E-01
9	-3.04E+00	4.69E-01	1.41E+00	1.26E+00	2.16E+00	7.33E+00	1.33E+00	1.74E-01	1.11E-03	3.20E-01
8	-3.53E+00	1.25E+00	1.98E+00	1.79E+00	2.95E+00	1.02E+01	1.90E+00	3.02E-01	5.76E-02	3.15E-01
7	-2.36E+00	2.01E+00	2.38E+00	2.16E+00	3.45E+00	1.24E+01	2.32E+00	4.09E-01	1.16E-01	2.80E-01
6	1.67E+00	2.29E+00	2.43E+00	2.26E+00	3.58E+00	1.35E+01	2.50E+00	4.79E-01	1.73E-01	2.51E-01
5	-2.73E-01	1.28E+00	1.81E+00	1.94E+00	3.23E+00	1.24E+01	2.28E+00	4.91E-01	2.30E-01	2.53E-01
4	-1.24E+00	4.87E-01	9.24E-01	1.21E+00	2.41E+00	8.58E+00	1.80E+00	4.80E-01	2.62E-01	2.45E-01
3	-3.10E+00	-2.62E-01	9.37E-02	3.81E-01	1.38E+00	4.12E+00	1.28E+00	4.00E-01	2.33E-01	2.03E-01
2	-1.00E+00	-3.10E-01	-7.22E-02	6.86E-02	6.07E-01	1.33E+00	6.72E-01	2.35E-01	1.40E-01	1.19E-01
1	0.00E+00	0.00E+00	0.00E+00	0.00E+00	0.00E+00	0.00E+00	0.00E+00	0.00E+00	0.00E+00	0.00E+00

*** K = 4 ***

J I=	1	2	3	4	5	6	7	8	9	10
10	-1.74E+00	-2.18E-02	7.44E-01	6.49E-01	1.18E+00	4.03E+00	6.72E-01	5.31E-02	-3.66E-02	2.50E-01
9	-3.04E+00	4.69E-01	1.41E+00	1.26E+00	2.16E+00	7.32E+00	1.33E+00	1.73E-01	4.69E-04	3.19E-01
8	-3.53E+00	1.25E+00	1.98E+00	1.79E+00	2.95E+00	1.02E+01	1.90E+00	3.01E-01	5.66E-02	3.14E-01
7	-2.36E+00	2.01E+00	2.38E+00	2.16E+00	3.45E+00	1.24E+01	2.32E+00	4.08E-01	1.14E-01	2.79E-01
6	1.67E+00	2.29E+00	2.43E+00	2.26E+00	3.57E+00	1.35E+01	2.50E+00	4.77E-01	1.71E-01	2.50E-01
5	-2.73E-01	1.28E+00	1.81E+00	1.94E+00	3.23E+00	1.24E+01	2.28E+00	4.89E-01	2.27E-01	2.51E-01
4	-1.24E+00	4.87E-01	9.23E-01	1.21E+00	2.41E+00	8.58E+00	1.80E+00	4.77E-01	2.60E-01	2.43E-01
3	-3.10E+00	-2.62E-01	9.34E-02	3.80E-01	1.38E+00	4.12E+00	1.28E+00	3.97E-01	2.30E-01	2.00E-01
2	-1.00E+00	-3.10E-01	-7.24E-02	6.82E-02	6.06E-01	1.32E+00	6.69E-01	2.31E-01	1.37E-01	1.17E-01
1	0.00E+00	0.00E+00	0.00E+00	0.00E+00	0.00E+00	0.00E+00	0.00E+00	0.00E+00	0.00E+00	0.00E+00

*** CHECK2 PRINT OF VNB I1= 1 IL=10 J1= 1 JL= 4

I=	1	2	3	4	5	6	7	8	9	10	
4	0.0000E+00	0.0000E+00	0.0000E+00	0.0000E+00	0.0000E+00	0.0000E+00	0.0000E+00	0.0000E+00	0.0000E+00	0.0000E+00	0.0000E+00
3	0.0000E+00	0.0000E+00	0.0000E+00	0.0000E+00	0.0000E+00	0.0000E+00	0.0000E+00	0.0000E+00	0.0000E+00	0.0000E+00	0.0000E+00
2	0.0000E+00	0.0000E+00	0.0000E+00	0.0000E+00	0.0000E+00	0.0000E+00	0.0000E+00	0.0000E+00	0.0000E+00	0.0000E+00	0.0000E+00
1	0.0	0.0	0.0	0.0	0.0	0.0	0.0	0.0	0.0	0.0	0.0

Table 3.8
Angular Momentum

SWIRL VELOCITY

*** K = 1 ***

J \ I=	1	2	3	4	5	6	7	8	9	10
10	0,00E+00	0,00E+00	0,00E+00	0,00E+00	0,00E+00	0,00E+00	0,00E+00	0,00E+00	0,00E+00	0,00E+00
9	0,00E+00	0,00E+00	0,00E+00	0,00E+00	0,00E+00	0,00E+00	0,00E+00	0,00E+00	0,00E+00	0,00E+00
8	0,00E+00	0,00E+00	0,00E+00	0,00E+00	0,00E+00	0,00E+00	0,00E+00	0,00E+00	0,00E+00	0,00E+00
7	0,00E+00	0,00E+00	0,00E+00	0,00E+00	0,00E+00	0,00E+00	0,00E+00	0,00E+00	0,00E+00	0,00E+00
6	0,00E+00	0,00E+00	0,00E+00	0,00E+00	0,00E+00	0,00E+00	0,00E+00	0,00E+00	0,00E+00	0,00E+00
5	0,00E+00	0,00E+00	0,00E+00	0,00E+00	0,00E+00	0,00E+00	0,00E+00	0,00E+00	0,00E+00	0,00E+00
4	0,00E+00	0,00E+00	0,00E+00	0,00E+00	0,00E+00	0,00E+00	0,00E+00	0,00E+00	0,00E+00	0,00E+00
3	0,00E+00	0,00E+00	0,00E+00	0,00E+00	0,00E+00	0,00E+00	0,00E+00	0,00E+00	0,00E+00	0,00E+00
2	0,00E+00	0,00E+00	0,00E+00	0,00E+00	0,00E+00	0,00E+00	0,00E+00	0,00E+00	0,00E+00	0,00E+00
1	0,00E+00	0,00E+00	0,00E+00	0,00E+00	0,00E+00	0,00E+00	0,00E+00	0,00E+00	0,00E+00	0,00E+00

*** K = 2 ***

J \ I=	1	2	3	4	5	6	7	8	9	10
10	-8,77E-04	-2,45E-04	-7,18E-04	-6,62E-04	-1,77E-04	-3,76E-05	2,68E-05	-4,00E-04	-5,75E-04	-5,58E-04
9	-1,08E-03	-2,74E-04	-5,94E-04	-5,27E-04	-1,02E-06	3,43E-04	3,94E-04	-5,55E-05	-2,53E-04	-2,66E-04
8	-1,27E-03	-3,23E-04	-4,48E-04	-3,84E-04	8,00E-05	5,38E-04	5,80E-04	1,48E-04	-4,81E-05	-8,58E-05
7	-1,24E-03	-3,99E-04	-3,21E-04	-2,49E-04	1,20E-04	6,32E-04	6,49E-04	2,62E-04	7,90E-05	2,24E-05
6	-8,34E-04	-3,42E-04	-2,05E-04	-1,31E-04	1,41E-04	6,55E-04	6,20E-04	3,03E-04	1,50E-04	8,63E-05
5	-1,86E-04	-1,23E-04	-7,75E-05	-3,22E-05	1,51E-04	6,31E-04	5,27E-04	2,94E-04	1,85E-04	1,29E-04
4	-4,68E-05	-5,42E-06	9,93E-06	3,19E-05	1,48E-04	5,98E-04	4,34E-04	2,75E-04	2,13E-04	1,69E-04
3	-1,90E-05	1,10E-05	2,65E-05	4,70E-05	1,22E-04	4,92E-04	3,38E-04	2,66E-04	2,45E-04	2,10E-04
2	-8,35E-06	1,16E-05	2,29E-05	3,59E-05	7,91E-05	3,07E-04	2,43E-04	2,32E-04	2,33E-04	2,04E-04
1	-2,38E-06	2,05E-06	6,07E-06	1,03E-05	2,13E-05	8,04E-05	7,77E-05	7,76E-05	7,42E-05	5,95E-05

*** K = 3 ***

J \ I=	1	2	3	4	5	6	7	8	9	10
10	5,23E-11	9,63E-11	7,47E-11	-2,61E-10	-1,06E-09	-1,98E-09	-5,16E-09	-1,20E-08	-2,50E-08	-4,01E-08
9	4,01E-11	6,96E-11	1,04E-10	-1,40E-10	-7,30E-10	-1,49E-09	-4,80E-09	-1,18E-08	-2,47E-08	-3,82E-08
8	1,86E-11	2,97E-11	7,87E-11	-5,85E-11	-4,59E-10	-1,04E-09	-4,18E-09	-1,09E-08	-2,31E-08	-3,55E-08
7	-4,61E-12	-6,43E-12	3,88E-11	-1,32E-11	-2,55E-10	-6,72E-10	-3,52E-09	-9,72E-09	-2,14E-08	-3,35E-08
6	-2,11E-11	-2,86E-11	2,77E-12	7,83E-13	-1,26E-10	-4,04E-10	-2,88E-09	-8,43E-09	-1,97E-08	-3,22E-08
5	-2,28E-11	-3,65E-11	-1,97E-11	-1,90E-12	-5,61E-11	-2,27E-10	-2,26E-09	-6,99E-09	-1,74E-08	-3,03E-08
4	-1,65E-11	-3,06E-11	-2,53E-11	-6,86E-12	-2,48E-11	-1,40E-10	-1,70E-09	-5,30E-09	-1,34E-08	-2,47E-08
3	-7,35E-12	-1,66E-11	-1,68E-11	-7,36E-12	-1,44E-11	-1,01E-10	-1,18E-09	-3,41E-09	-6,55E-09	-1,07E-08
2	-6,54E-13	-1,21E-11	-1,48E-11	-1,35E-11	-2,15E-11	-8,48E-11	-8,40E-10	-1,66E-09	4,20E-09	1,62E-08
1	-5,10E-13	-1,37E-11	-2,70E-11	-3,52E-11	-3,74E-11	-8,62E-11	-7,33E-10	-5,47E-10	1,42E-08	4,17E-08

*** K = 4 ***

J \ I=	1	2	3	4	5	6	7	8	9	10
10	8,77E-04	2,45E-04	7,18E-04	6,62E-04	1,77E-04	3,76E-05	-2,68E-05	3,99E-04	5,75E-04	5,58E-04
9	1,08E-03	2,74E-04	5,94E-04	5,27E-04	1,02E-06	-3,43E-04	-3,94E-04	5,55E-05	2,53E-04	2,66E-04
8	1,27E-03	3,23E-04	4,48E-04	3,84E-04	-8,00E-05	-5,38E-04	-5,80E-04	-1,48E-04	4,80E-05	8,58E-05
7	1,24E-03	3,99E-04	3,21E-04	2,49E-04	-1,20E-04	-6,32E-04	-6,49E-04	-2,62E-04	-7,90E-05	-2,25E-05
6	8,34E-04	3,42E-04	2,05E-04	1,31E-04	-1,41E-04	-6,55E-04	-6,20E-04	-3,03E-04	-1,50E-04	-8,64E-05
5	1,86E-04	1,23E-04	7,75E-05	3,22E-05	-1,51E-04	-6,31E-04	-5,27E-04	-2,94E-04	-1,85E-04	-1,29E-04
4	4,68E-05	5,42E-06	-9,93E-06	-3,19E-05	-1,48E-04	-5,98E-04	-4,34E-04	-2,75E-04	-2,13E-04	-1,69E-04
3	1,90E-05	-1,10E-05	-2,65E-05	-4,70E-05	-1,22E-04	-4,92E-04	-3,38E-04	-2,66E-04	-2,45E-04	-2,10E-04
2	8,35E-06	-1,16E-05	-2,29E-05	-3,59E-05	-7,91E-05	-3,07E-04	-2,43E-04	-2,32E-04	-2,33E-04	-2,04E-04
1	2,38E-06	-2,05E-06	-6,07E-06	-1,03E-05	-2,13E-05	-8,04E-05	-7,77E-05	-7,76E-05	-7,42E-05	-5,94E-05

**** CHECK2 PRINT OF WHB I1= 1 IL=10 J1= 1 JL=10

J I=	1	2	3	4	5	6	7	8	9	10		
10	0,0000E+00	0,0000E+00	0,0000E+00	0,0000E+00	0,0000E+00	0,0000E+00	0,0000E+00	0,0000E+00	0,0000E+00	0,0000E+00	0,0000E+00	0,0000E+00
9	0,0000E+00	0,0000E+00	0,0000E+00	0,0000E+00	0,0000E+00	0,0000E+00	0,0000E+00	0,0000E+00	0,0000E+00	0,0000E+00	0,0000E+00	0,0000E+00
8	0,0000E+00	0,0000E+00	0,0000E+00	0,0000E+00	0,0000E+00	0,0000E+00	0,0000E+00	0,0000E+00	0,0000E+00	0,0000E+00	0,0000E+00	0,0000E+00
7	0,0000E+00	0,0000E+00	0,0000E+00	0,0000E+00	0,0000E+00	0,0000E+00	0,0000E+00	0,0000E+00	0,0000E+00	0,0000E+00	0,0000E+00	0,0000E+00
6	0,0000E+00	0,0000E+00	0,0000E+00	0,0000E+00	0,0000E+00	0,0000E+00	0,0000E+00	0,0000E+00	0,0000E+00	0,0000E+00	0,0000E+00	0,0000E+00
5	0,0000E+00	0,0000E+00	0,0000E+00	0,0000E+00	0,0000E+00	0,0000E+00	0,0000E+00	0,0000E+00	0,0000E+00	0,0000E+00	0,0000E+00	0,0000E+00
4	0,0000E+00	0,0000E+00	0,0000E+00	0,0000E+00	0,0000E+00	0,0000E+00	0,0000E+00	0,0000E+00	0,0000E+00	0,0000E+00	0,0000E+00	0,0000E+00
3	0,0000E+00	0,0000E+00	0,0000E+00	0,0000E+00	0,0000E+00	0,0000E+00	0,0000E+00	0,0000E+00	0,0000E+00	0,0000E+00	0,0000E+00	0,0000E+00
2	0,0000E+00	0,0000E+00	0,0000E+00	0,0000E+00	0,0000E+00	0,0000E+00	0,0000E+00	0,0000E+00	0,0000E+00	0,0000E+00	0,0000E+00	0,0000E+00

Table 3.9 Kinetic Energy of Turbulence

K.E. OF TURBULENCE

*** K = 1 ***

J I=	1	2	3	4	5	6	7	8	9	10
10	5.92E+00	1.32E+01	1.94E+01	1.61E+01	6.99E+00	2.58E+01	2.33E+01	2.19E+01	2.11E+01	2.09E+01
9	1.82E+01	7.90E+01	9.62E+01	8.39E+01	6.75E+01	1.03E+02	8.09E+01	6.50E+01	5.42E+01	4.71E+01
8	2.07E+01	1.13E+02	1.29E+02	1.12E+02	8.83E+01	1.19E+02	9.93E+01	8.13E+01	6.81E+01	5.89E+01
7	3.23E+01	1.34E+02	1.48E+02	1.30E+02	9.95E+01	1.21E+02	1.07E+02	8.95E+01	7.58E+01	6.60E+01
6	6.19E+01	1.38E+02	1.49E+02	1.34E+02	1.02E+02	1.15E+02	1.07E+02	9.19E+01	7.91E+01	6.96E+01
5	5.48E+01	9.20E+01	1.15E+02	1.15E+02	9.24E+01	1.05E+02	1.01E+02	8.90E+01	7.83E+01	7.00E+01
4	1.44E+01	3.24E+01	5.90E+01	7.64E+01	7.32E+01	9.22E+01	8.96E+01	8.17E+01	7.41E+01	6.77E+01
3	2.07E+01	2.49E+01	3.39E+01	4.68E+01	5.43E+01	7.70E+01	7.60E+01	7.23E+01	6.80E+01	6.38E+01
2	4.01E+01	4.29E+01	4.15E+01	4.20E+01	4.60E+01	6.53E+01	6.57E+01	6.44E+01	6.24E+01	6.00E+01
1	2.17E+01	4.08E+01	4.26E+01	4.10E+01	4.30E+01	6.19E+01	6.12E+01	6.03E+01	5.92E+01	5.78E+01

*** K = 2 ***

J I=	1	2	3	4	5	6	7	8	9	10
10	5.92E+00	1.32E+01	1.94E+01	1.61E+01	6.98E+00	2.58E+01	2.33E+01	2.19E+01	2.11E+01	2.10E+01
9	1.82E+01	7.90E+01	9.62E+01	8.39E+01	6.75E+01	1.03E+02	8.10E+01	6.50E+01	5.42E+01	4.71E+01
8	2.07E+01	1.13E+02	1.29E+02	1.12E+02	8.83E+01	1.19E+02	9.93E+01	8.13E+01	6.81E+01	5.89E+01
7	3.23E+01	1.34E+02	1.48E+02	1.30E+02	9.95E+01	1.21E+02	1.07E+02	8.95E+01	7.58E+01	6.60E+01
6	6.19E+01	1.38E+02	1.49E+02	1.34E+02	1.02E+02	1.15E+02	1.07E+02	9.19E+01	7.91E+01	6.96E+01
5	5.48E+01	9.20E+01	1.15E+02	1.15E+02	9.24E+01	1.05E+02	1.01E+02	8.90E+01	7.83E+01	7.00E+01
4	1.44E+01	3.24E+01	5.90E+01	7.64E+01	7.32E+01	9.22E+01	8.96E+01	8.17E+01	7.41E+01	6.77E+01
3	2.07E+01	2.49E+01	3.39E+01	4.68E+01	5.43E+01	7.70E+01	7.60E+01	7.23E+01	6.80E+01	6.38E+01
2	4.01E+01	4.29E+01	4.15E+01	4.20E+01	4.60E+01	6.53E+01	6.57E+01	6.44E+01	6.24E+01	6.00E+01
1	2.17E+01	4.08E+01	4.26E+01	4.10E+01	4.30E+01	6.19E+01	6.12E+01	6.03E+01	5.92E+01	5.78E+01

*** K = 3 ***

J I=	1	2	3	4	5	6	7	8	9	10
10	5.92E+00	1.32E+01	1.94E+01	1.61E+01	6.98E+00	2.58E+01	2.33E+01	2.19E+01	2.11E+01	2.10E+01
9	1.82E+01	7.90E+01	9.62E+01	8.39E+01	6.75E+01	1.03E+02	8.10E+01	6.50E+01	5.42E+01	4.71E+01
8	2.07E+01	1.13E+02	1.29E+02	1.12E+02	8.83E+01	1.19E+02	9.93E+01	8.13E+01	6.81E+01	5.89E+01
7	3.23E+01	1.34E+02	1.48E+02	1.30E+02	9.95E+01	1.21E+02	1.07E+02	8.95E+01	7.58E+01	6.60E+01
6	6.19E+01	1.38E+02	1.49E+02	1.34E+02	1.02E+02	1.15E+02	1.07E+02	9.19E+01	7.91E+01	6.96E+01
5	5.48E+01	9.20E+01	1.15E+02	1.15E+02	9.24E+01	1.05E+02	1.01E+02	8.90E+01	7.83E+01	7.00E+01
4	1.44E+01	3.24E+01	5.90E+01	7.64E+01	7.32E+01	9.22E+01	8.96E+01	8.17E+01	7.41E+01	6.77E+01
3	2.07E+01	2.49E+01	3.39E+01	4.68E+01	5.43E+01	7.70E+01	7.60E+01	7.23E+01	6.80E+01	6.38E+01
2	4.01E+01	4.29E+01	4.15E+01	4.20E+01	4.60E+01	6.53E+01	6.57E+01	6.44E+01	6.24E+01	6.00E+01
1	2.17E+01	4.08E+01	4.26E+01	4.10E+01	4.30E+01	6.19E+01	6.12E+01	6.03E+01	5.92E+01	5.78E+01

*** K = 4 ***

J I=	1	2	3	4	5	6	7	8	9	10
10	5.92E+00	1.32E+01	1.94E+01	1.61E+01	6.99E+00	2.58E+01	2.33E+01	2.19E+01	2.11E+01	2.09E+01
9	1.82E+01	7.90E+01	9.62E+01	8.39E+01	6.75E+01	1.03E+02	8.09E+01	6.50E+01	5.42E+01	4.71E+01
8	2.07E+01	1.13E+02	1.29E+02	1.12E+02	8.83E+01	1.19E+02	9.93E+01	8.13E+01	6.81E+01	5.89E+01
7	3.23E+01	1.34E+02	1.48E+02	1.30E+02	9.95E+01	1.21E+02	1.07E+02	8.95E+01	7.58E+01	6.60E+01
6	6.19E+01	1.38E+02	1.49E+02	1.34E+02	1.02E+02	1.15E+02	1.07E+02	9.19E+01	7.91E+01	6.96E+01
5	5.48E+01	9.20E+01	1.15E+02	1.15E+02	9.24E+01	1.05E+02	1.01E+02	8.90E+01	7.83E+01	7.00E+01
4	1.44E+01	3.24E+01	5.90E+01	7.64E+01	7.32E+01	9.22E+01	8.96E+01	8.17E+01	7.41E+01	6.77E+01
3	2.07E+01	2.49E+01	3.39E+01	4.68E+01	5.43E+01	7.70E+01	7.60E+01	7.23E+01	6.80E+01	6.38E+01
2	4.01E+01	4.29E+01	4.15E+01	4.20E+01	4.60E+01	6.53E+01	6.57E+01	6.44E+01	6.24E+01	6.00E+01
1	2.17E+01	4.08E+01	4.26E+01	4.10E+01	4.30E+01	6.19E+01	6.12E+01	6.03E+01	5.92E+01	5.78E+01

Table 3.10 Absolute Temperature

TEMPERATURE

*** K = 1 ***

J I=	1	2	3	4	5	6	7	8	9	10
10	5.56E+02	5.52E+02	5.52E+02	5.68E+02	6.39E+02	1.39E+03	1.44E+03	1.46E+03	1.48E+03	1.50E+03
9	5.51E+02	5.41E+02	5.40E+02	5.54E+02	6.33E+02	1.41E+03	1.50E+03	1.53E+03	1.56E+03	1.58E+03
8	5.47E+02	5.35E+02	5.34E+02	5.46E+02	6.22E+02	1.46E+03	1.56E+03	1.60E+03	1.62E+03	1.65E+03
7	5.40E+02	5.30E+02	5.29E+02	5.39E+02	6.09E+02	1.54E+03	1.65E+03	1.68E+03	1.71E+03	1.73E+03
6	5.27E+02	5.23E+02	5.24E+02	5.33E+02	5.97E+02	1.66E+03	1.76E+03	1.79E+03	1.80E+03	1.82E+03
5	5.07E+02	5.13E+02	5.18E+02	5.29E+02	5.87E+02	1.79E+03	1.88E+03	1.90E+03	1.91E+03	1.91E+03
4	5.02E+02	5.08E+02	5.18E+02	5.30E+02	5.82E+02	1.90E+03	1.95E+03	1.95E+03	1.95E+03	1.96E+03
3	5.15E+02	5.28E+02	5.37E+02	5.45E+02	5.84E+02	1.87E+03	1.89E+03	1.90E+03	1.92E+03	1.93E+03
2	6.07E+02	5.98E+02	5.89E+02	5.79E+02	5.96E+02	1.76E+03	1.81E+03	1.85E+03	1.88E+03	1.90E+03
1	6.31E+02	6.19E+02	6.08E+02	5.96E+02	6.05E+02	1.67E+03	1.75E+03	1.80E+03	1.85E+03	1.88E+03

*** K = 2 ***

J I=	1	2	3	4	5	6	7	8	9	10
10	5.56E+02	5.52E+02	5.52E+02	5.68E+02	6.39E+02	1.39E+03	1.44E+03	1.46E+03	1.48E+03	1.50E+03
9	5.51E+02	5.41E+02	5.40E+02	5.54E+02	6.33E+02	1.41E+03	1.50E+03	1.53E+03	1.56E+03	1.58E+03
8	5.47E+02	5.35E+02	5.34E+02	5.46E+02	6.22E+02	1.46E+03	1.56E+03	1.60E+03	1.62E+03	1.65E+03
7	5.40E+02	5.30E+02	5.29E+02	5.39E+02	6.09E+02	1.54E+03	1.65E+03	1.68E+03	1.71E+03	1.73E+03
6	5.27E+02	5.23E+02	5.24E+02	5.33E+02	5.97E+02	1.66E+03	1.76E+03	1.79E+03	1.80E+03	1.82E+03
5	5.07E+02	5.13E+02	5.18E+02	5.29E+02	5.87E+02	1.79E+03	1.88E+03	1.90E+03	1.91E+03	1.91E+03
4	5.02E+02	5.08E+02	5.18E+02	5.30E+02	5.82E+02	1.90E+03	1.95E+03	1.95E+03	1.95E+03	1.96E+03
3	5.15E+02	5.28E+02	5.37E+02	5.45E+02	5.84E+02	1.87E+03	1.89E+03	1.90E+03	1.92E+03	1.93E+03
2	6.07E+02	5.98E+02	5.89E+02	5.79E+02	5.96E+02	1.76E+03	1.81E+03	1.85E+03	1.88E+03	1.90E+03
1	6.31E+02	6.19E+02	6.08E+02	5.96E+02	6.05E+02	1.67E+03	1.75E+03	1.80E+03	1.85E+03	1.88E+03

*** K = 3 ***

J I=	1	2	3	4	5	6	7	8	9	10
10	5.56E+02	5.52E+02	5.52E+02	5.68E+02	6.39E+02	1.39E+03	1.44E+03	1.46E+03	1.48E+03	1.50E+03
9	5.51E+02	5.41E+02	5.40E+02	5.54E+02	6.33E+02	1.41E+03	1.50E+03	1.53E+03	1.56E+03	1.58E+03
8	5.47E+02	5.35E+02	5.34E+02	5.46E+02	6.22E+02	1.46E+03	1.56E+03	1.60E+03	1.62E+03	1.65E+03
7	5.40E+02	5.30E+02	5.29E+02	5.39E+02	6.09E+02	1.54E+03	1.65E+03	1.68E+03	1.71E+03	1.73E+03
6	5.27E+02	5.23E+02	5.24E+02	5.33E+02	5.97E+02	1.66E+03	1.76E+03	1.79E+03	1.80E+03	1.82E+03
5	5.07E+02	5.13E+02	5.18E+02	5.29E+02	5.87E+02	1.79E+03	1.88E+03	1.90E+03	1.91E+03	1.91E+03
4	5.02E+02	5.08E+02	5.18E+02	5.30E+02	5.82E+02	1.90E+03	1.95E+03	1.95E+03	1.95E+03	1.96E+03
3	5.15E+02	5.28E+02	5.37E+02	5.45E+02	5.84E+02	1.87E+03	1.89E+03	1.90E+03	1.92E+03	1.93E+03
2	6.07E+02	5.98E+02	5.89E+02	5.79E+02	5.96E+02	1.76E+03	1.81E+03	1.85E+03	1.88E+03	1.90E+03
1	6.31E+02	6.19E+02	6.08E+02	5.96E+02	6.05E+02	1.67E+03	1.75E+03	1.80E+03	1.85E+03	1.88E+03

*** K = 4 ***

J I=	1	2	3	4	5	6	7	8	9	10
10	5.56E+02	5.52E+02	5.52E+02	5.68E+02	6.39E+02	1.39E+03	1.44E+03	1.46E+03	1.48E+03	1.50E+03
9	5.51E+02	5.41E+02	5.40E+02	5.54E+02	6.33E+02	1.41E+03	1.50E+03	1.53E+03	1.56E+03	1.58E+03
8	5.47E+02	5.35E+02	5.34E+02	5.46E+02	6.22E+02	1.46E+03	1.56E+03	1.60E+03	1.62E+03	1.65E+03
7	5.40E+02	5.30E+02	5.29E+02	5.39E+02	6.09E+02	1.54E+03	1.65E+03	1.68E+03	1.71E+03	1.73E+03
6	5.27E+02	5.23E+02	5.24E+02	5.33E+02	5.97E+02	1.66E+03	1.76E+03	1.79E+03	1.80E+03	1.82E+03
5	5.07E+02	5.13E+02	5.18E+02	5.29E+02	5.87E+02	1.79E+03	1.88E+03	1.90E+03	1.91E+03	1.91E+03
4	5.02E+02	5.08E+02	5.18E+02	5.30E+02	5.82E+02	1.90E+03	1.95E+03	1.95E+03	1.95E+03	1.96E+03
3	5.15E+02	5.28E+02	5.37E+02	5.45E+02	5.84E+02	1.87E+03	1.89E+03	1.90E+03	1.92E+03	1.93E+03
2	6.07E+02	5.98E+02	5.89E+02	5.79E+02	5.96E+02	1.76E+03	1.81E+03	1.85E+03	1.88E+03	1.90E+03
1	6.31E+02	6.19E+02	6.08E+02	5.96E+02	6.05E+02	1.67E+03	1.75E+03	1.80E+03	1.85E+03	1.88E+03

Table 3.11 Fuel Mass Fraction

FUEL CONCENTRATION

*** K = 1 ***

J \ I=	1	2	3	4	5	6	7	8	9	10
10	7.19E-03	7.66E-03	9.41E-03	1.34E-02	1.77E-02	1.08E-03	1.25E-04	1.39E-05	1.41E-06	1.30E-07
9	6.80E-03	6.55E-03	8.43E-03	1.30E-02	1.78E-02	1.62E-03	1.40E-04	1.12E-05	8.21E-07	5.61E-08
8	6.31E-03	5.76E-03	7.92E-03	1.28E-02	1.86E-02	1.74E-03	1.18E-04	7.25E-06	4.33E-07	3.64E-08
7	5.35E-03	5.01E-03	7.58E-03	1.32E-02	2.06E-02	1.70E-03	8.92E-05	4.77E-06	6.19E-07	3.37E-07
6	3.65E-03	4.17E-03	7.74E-03	1.49E-02	2.45E-02	1.75E-03	9.22E-05	1.63E-05	1.11E-05	8.99E-06
AIR → 5	1.08E-03	3.50E-03	9.53E-03	1.95E-02	3.22E-02	2.60E-03	5.10E-04	3.76E-04	3.28E-04	2.67E-04
4	1.58E-03	7.36E-03	1.83E-02	3.24E-02	4.80E-02	8.93E-03	8.56E-03	8.28E-03	7.05E-03	5.50E-03
3	2.18E-02	4.36E-02	6.02E-02	7.19E-02	8.15E-02	3.48E-02	3.27E-02	2.80E-02	2.27E-02	1.79E-02
FUEL → 2	3.34E-01	2.74E-01	2.26E-01	1.78E-01	1.44E-01	8.01E-02	6.46E-02	5.07E-02	3.92E-02	3.01E-02
1	5.77E-01	4.32E-01	3.37E-01	2.57E-01	1.93E-01	1.16E-01	8.93E-02	6.73E-02	5.04E-02	3.79E-02

*** K = 2 ***

J \ I=	1	2	3	4	5	6	7	8	9	10
10	7.19E-03	7.67E-03	9.41E-03	1.34E-02	1.77E-02	1.08E-03	1.24E-04	1.38E-05	1.40E-06	1.29E-07
9	6.80E-03	6.56E-03	8.43E-03	1.30E-02	1.78E-02	1.62E-03	1.40E-04	1.11E-05	8.15E-07	5.56E-08
8	6.31E-03	5.76E-03	7.93E-03	1.28E-02	1.86E-02	1.74E-03	1.17E-04	7.22E-06	4.31E-07	3.63E-08
7	5.36E-03	5.01E-03	7.58E-03	1.33E-02	2.06E-02	1.70E-03	8.90E-05	4.76E-06	6.19E-07	3.38E-07
6	3.66E-03	4.17E-03	7.75E-03	1.49E-02	2.45E-02	1.75E-03	9.21E-05	1.63E-05	1.12E-05	9.03E-06
5	1.08E-03	3.50E-03	9.53E-03	1.95E-02	3.23E-02	2.60E-03	5.11E-04	3.77E-04	3.30E-04	2.69E-04
A 4	1.58E-03	7.36E-03	1.83E-02	3.24E-02	4.81E-02	8.94E-03	8.58E-03	8.30E-03	7.06E-03	5.52E-03
3	2.18E-02	4.36E-02	6.02E-02	7.19E-02	8.15E-02	3.48E-02	3.27E-02	2.80E-02	2.28E-02	1.79E-02
F 2	3.34E-01	2.74E-01	2.26E-01	1.78E-01	1.44E-01	8.01E-02	6.46E-02	5.07E-02	3.92E-02	3.01E-02
1	5.77E-01	4.32E-01	3.37E-01	2.57E-01	1.93E-01	1.16E-01	8.93E-02	6.73E-02	5.04E-02	3.79E-02

*** K = 3 ***

J \ I=	1	2	3	4	5	6	7	8	9	10
10	7.19E-03	7.67E-03	9.41E-03	1.34E-02	1.77E-02	1.08E-03	1.24E-04	1.38E-05	1.40E-06	1.29E-07
9	6.80E-03	6.56E-03	8.43E-03	1.30E-02	1.78E-02	1.62E-03	1.40E-04	1.11E-05	8.15E-07	5.56E-08
8	6.31E-03	5.76E-03	7.93E-03	1.28E-02	1.86E-02	1.74E-03	1.17E-04	7.22E-06	4.31E-07	3.63E-08
7	5.36E-03	5.01E-03	7.58E-03	1.33E-02	2.06E-02	1.70E-03	8.90E-05	4.76E-06	6.19E-07	3.38E-07
6	3.66E-03	4.17E-03	7.75E-03	1.49E-02	2.45E-02	1.75E-03	9.21E-05	1.63E-05	1.12E-05	9.03E-06
5	1.08E-03	3.50E-03	9.53E-03	1.95E-02	3.23E-02	2.60E-03	5.11E-04	3.77E-04	3.30E-04	2.69E-04
A 4	1.58E-03	7.36E-03	1.83E-02	3.24E-02	4.81E-02	8.94E-03	8.58E-03	8.30E-03	7.06E-03	5.52E-03
3	2.18E-02	4.36E-02	6.02E-02	7.19E-02	8.15E-02	3.48E-02	3.27E-02	2.80E-02	2.28E-02	1.79E-02
F 2	3.34E-01	2.74E-01	2.26E-01	1.78E-01	1.44E-01	8.01E-02	6.46E-02	5.07E-02	3.92E-02	3.01E-02
1	5.77E-01	4.32E-01	3.37E-01	2.57E-01	1.93E-01	1.16E-01	8.93E-02	6.73E-02	5.04E-02	3.79E-02

*** K = 4 ***

J \ I=	1	2	3	4	5	6	7	8	9	10
10	7.19E-03	7.66E-03	9.41E-03	1.34E-02	1.77E-02	1.08E-03	1.25E-04	1.39E-05	1.41E-06	1.30E-07
9	6.80E-03	6.55E-03	8.43E-03	1.30E-02	1.78E-02	1.62E-03	1.40E-04	1.12E-05	8.21E-07	5.61E-08
8	6.31E-03	5.76E-03	7.92E-03	1.28E-02	1.86E-02	1.74E-03	1.18E-04	7.25E-06	4.33E-07	3.64E-08
7	5.35E-03	5.01E-03	7.58E-03	1.32E-02	2.06E-02	1.70E-03	8.92E-05	4.77E-06	6.19E-07	3.37E-07
6	3.65E-03	4.17E-03	7.74E-03	1.49E-02	2.45E-02	1.75E-03	9.22E-05	1.63E-05	1.11E-05	8.99E-06
5	1.08E-03	3.50E-03	9.53E-03	1.95E-02	3.22E-02	2.60E-03	5.10E-04	3.76E-04	3.28E-04	2.67E-04
A 4	1.58E-03	7.36E-03	1.83E-02	3.24E-02	4.80E-02	8.93E-03	8.56E-03	8.28E-03	7.05E-03	5.50E-03
3	2.18E-02	4.36E-02	6.02E-02	7.19E-02	8.15E-02	3.48E-02	3.27E-02	2.80E-02	2.27E-02	1.79E-02
F 2	3.34E-01	2.74E-01	2.26E-01	1.78E-01	1.44E-01	8.01E-02	6.46E-02	5.07E-02	3.92E-02	3.01E-02
1	5.77E-01	4.32E-01	3.37E-01	2.57E-01	1.93E-01	1.16E-01	8.93E-02	6.73E-02	5.04E-02	3.79E-02

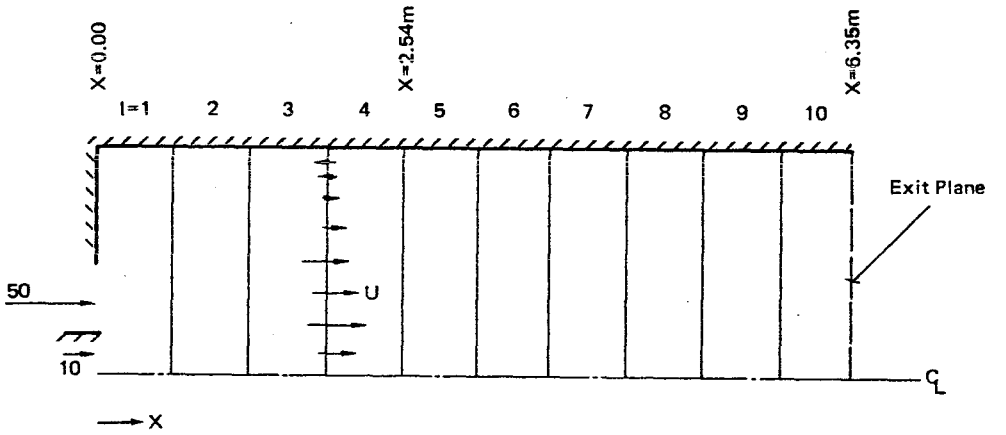

CONVECTIVE FLUXES THROUGH THE CHAMBER CROSSECTIONS

I=	1	XM=	0,000E+00	FX=	1,779037E+01	FXP=	1,779037E+01	FXN=	0,000000E+00	FULFLX=	7,614280E-01
I=	2	XM=	6,350E-01	FX=	1,779037E+01	FXP=	2,161037E+01	FXN=	-3,819999E+00	FULFLX=	7,687377E-01
I=	3	XM=	1,270E+00	FX=	1,779037E+01	FXP=	2,093192E+01	FXN=	-3,141554E+00	FULFLX=	7,726516E-01
I=	4	XM=	1,905E+00	FX=	1,779037E+01	FXP=	1,914738E+01	FXN=	-1,357011E+00	FULFLX=	7,778274E-01
I=	5	XM=	2,540E+00	FX=	1,779037E+01	FXP=	1,825102E+01	FXN=	-4,606514E-01	FULFLX=	7,796212E-01
I=	6	XM=	3,175E+00	FX=	1,779037E+01	FXP=	1,779037E+01	FXN=	0,000000E+00	FULFLX=	7,463765E-01
I=	7	XM=	3,810E+00	FX=	1,779037E+01	FXP=	1,779037E+01	FXN=	0,000000E+00	FULFLX=	1,537066E-01
I=	8	XM=	4,445E+00	FX=	1,779037E+01	FXP=	1,779037E+01	FXN=	0,000000E+00	FULFLX=	9,865331E-02
I=	9	XM=	5,080E+00	FX=	1,779037E+01	FXP=	1,779037E+01	FXN=	0,000000E+00	FULFLX=	7,675099E-02
I=	10	XM=	5,715E+00	FX=	1,779037E+01	FXP=	1,779037E+01	FXN=	0,000000E+00	FULFLX=	5,950782E-02
I=	11	XM=	6,350E+00	FX=	1,779037E+01	FXP=	1,779037E+01	FXN=	0,000000E+00	FULFLX=	4,519946E-02

Table 3.12 Convective Fluxes Through the Combustion Chamber Crossections

SECTION 4
PARAMETRIC STUDIES OF INJECTOR ANOMALIES

4.1 OBJECTIVE

The objective of the present study is to demonstrate a capability to simulate two-phase spray flow, heat transfer, evaporation and combustion within the rocket engines for predicting the effects of reactant injections nonuniformity upon local and overall heat transfer. For this purpose, six test cases have been considered. The basic test case has been set up based on the data specified by NASA. First, four model sensitivity tests were performed to examine the influence of physical and numerical parameters on the fluid flow and combustion. The final sixth test case considered an injection nonuniformity, in which 25% of the central part of the fuel injector had been blocked.

All results are presented in graphical form.

4.2 THE COMBUSTION CHAMBER AND INJECTOR GEOMETRY

The configuration of the model combustion chamber employed in the present calculations is shown in Figure 4.1. The combustion chamber is 0.33m long. Chamber diameter at the injection plane is d_o = 121.92mm and at the throat d_t = 66.04mm. Contraction ratio is approximately 4.

Figure 4.2 presents details of the fuel and oxidizer injector plane. Fuel is supplied to the injector through the fuel connector (marked FUL on figure 4.2) and axially enters the triplet injectors. Liquid oxygen enters radially (connector OX on Figure 4.2) and is distributed through the annular collector to all oxygen triplet inlets.

Detail C on Figure 4.2 presents the LOX-RP1-LOX triplet. The triplet arrangement within the injector plane is also shown in Figure 4.2. Note that due to the specific hole arrangement the injection plane has two symmetry lines. Therefore, a 90^o sector has been used for the numerical simulation studies.

The grid arrangement for the 90^o sector of the combustor is shown in Figure 4.3. A uniform nonorthogonal grid in x-axial, y-radial and $z(=\theta)$ circumferential directions with NX:NY:NZ - (21:8:4) is employed for all test cases. Figure 4.3 presents the injector hole distribution and the y-θ grid.

The calculation domain in the axial direction extends up to the throat section of the nozzle.

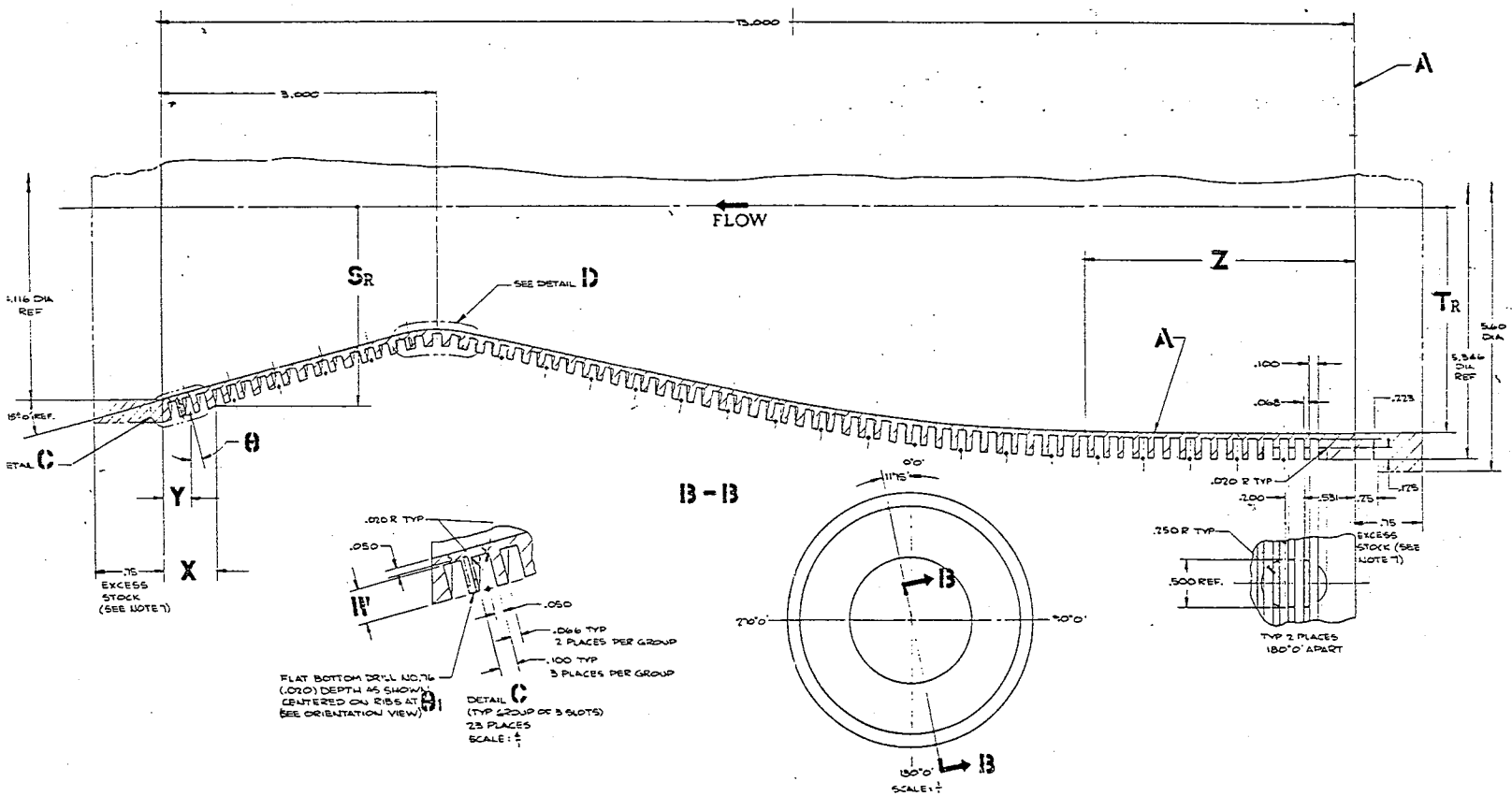

Figure 4.1 Nozzle Geometry

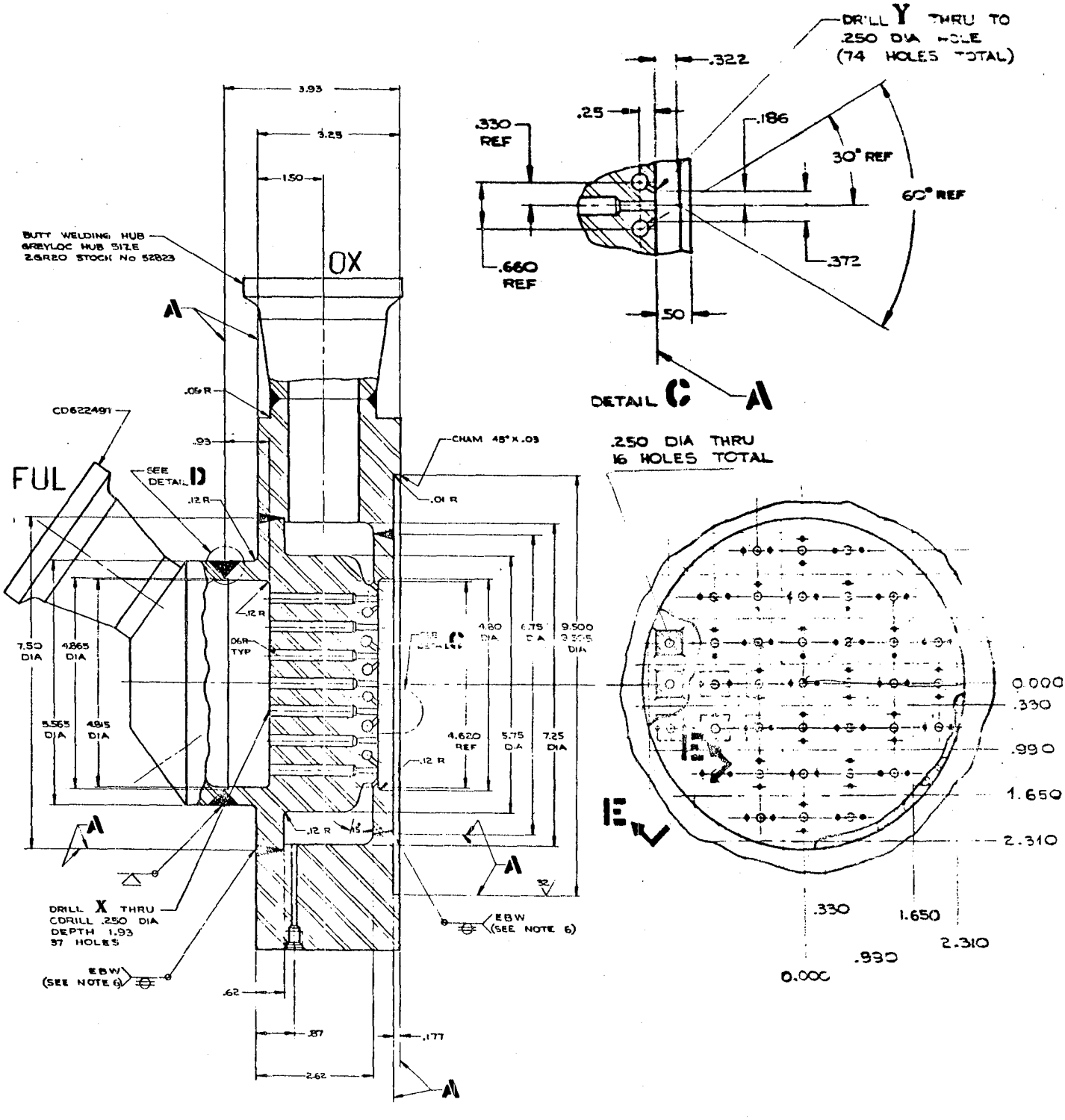

Figure 4.2 LOX-RP1-LOX Injector geometry and Injection triplet arrangement (X = 1.70 mm, Y = 1.85 mm)

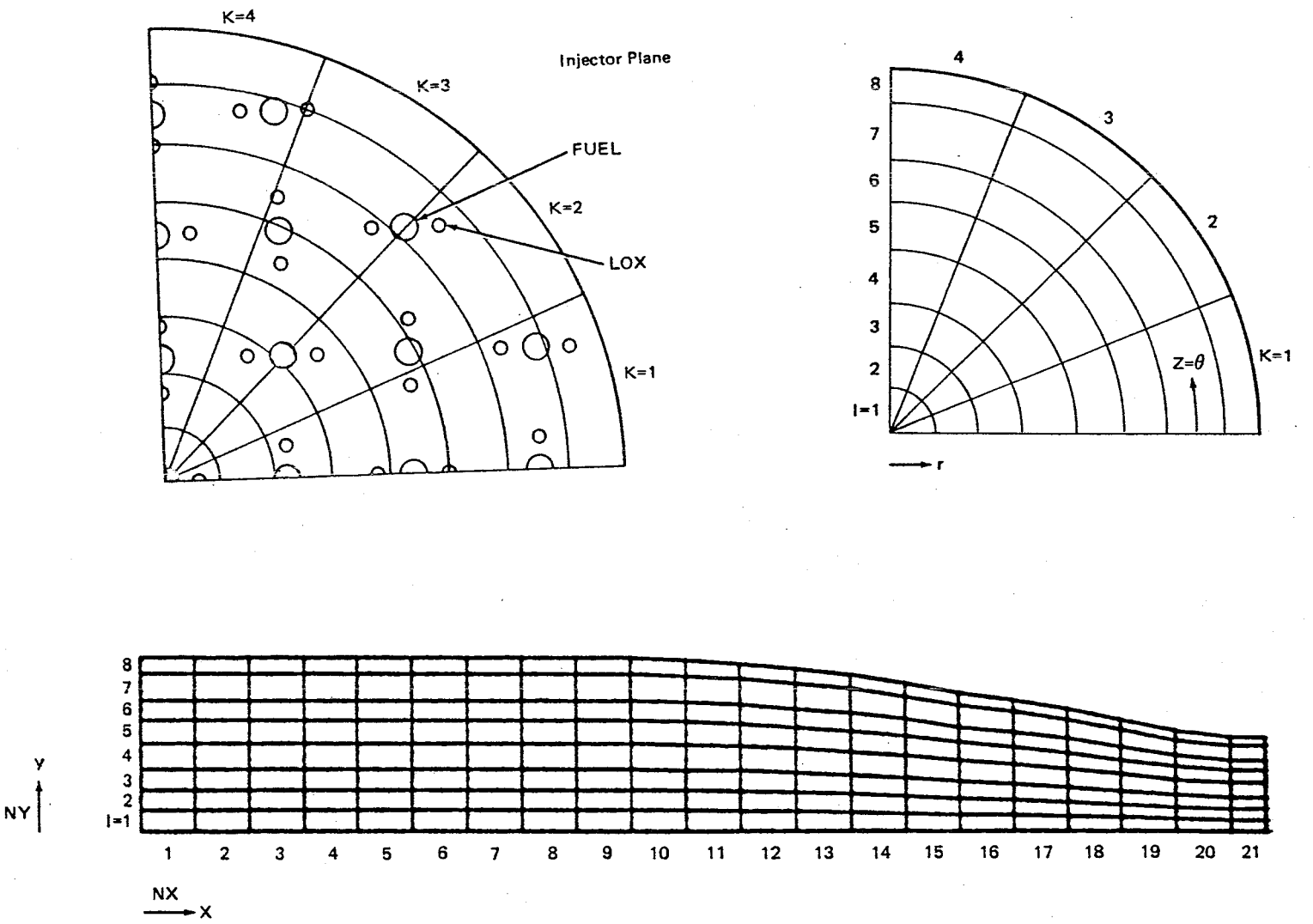

Figure 4.3 Grid Arrangement for the Rocket Injector Anomalies Study.

4.3 BASIC TEST CASE SPECIFICATION

A fully coupled two-phase spray flow, evaporation heat transfer and combustion with a uniform reactant injection distribution has been considered. Table 4.1 presents a summary of input data specifications for the basic test case. It includes:

- geometrical data,
- physical parameters, and
- injector data.

During the calculations it has been assumed that oxygen enters the combustion chamber in a fully vaporized form, while kerosene (RP1) enters in the form of discrete jets of the liquid fuel sprays. To describe the gas phase motion (oxygen + combustion products) Eulerian frame of coordinates has been used. The liquid phase (fuel) is described in Lagrangian coordinates. The spray is represented by 80 individual droplet parcels (16 slot and 5 droplet diameters). The liquid spray jet, at each injection slot, is represented by 5-initial droplet sizes D_0.

Figure 4.4 presents assumed droplet distribution function and selected droplet diameters ($D_\varnothing$ = 5, 10, 20, 30, 40 and 60μm).

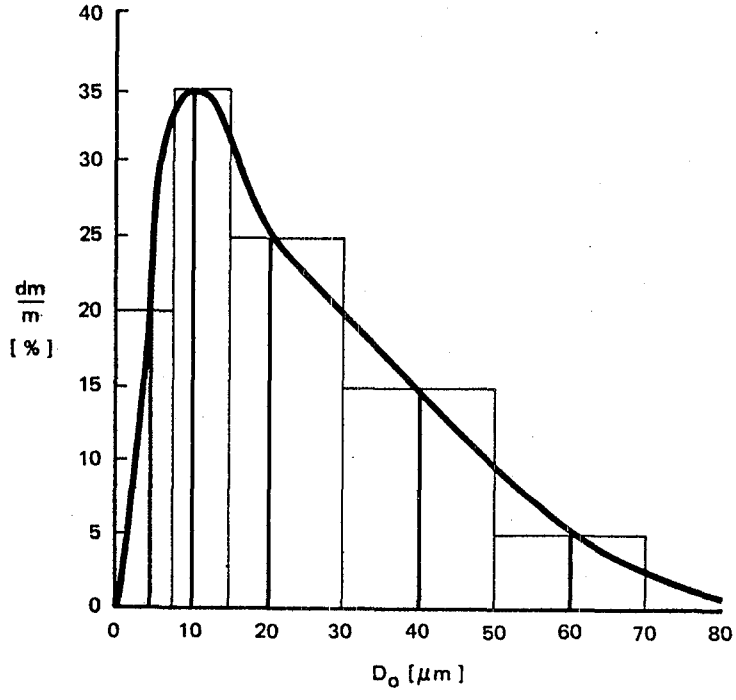

Figure 4.4 Droplet Distribution Function

Table 4.1 Basic Test Case Data Specification for Combustion in Rocket Engine Calculations

SPECIFICATION	DATA	UNIT
Chamber radius at injection plane	60.36	mm
Chamber radius at the throat	33.02	mm
Chamber length (to the throat)	330	mm
Injector type UNLIKE TRIPLET	284	--
Total number of triplets	37	--
Number of fuel holes in 90^0 sector	9.25	--
Number of oxygen holes in 90^0 sector	19.0	--
Number of grids (NX:NY:NZ)	21:8:4	--
Total fuel flow rate through 90^0 sector	4.632 (0.525)	lbm/sec kg/sec
Total oxygen flow rate through 90^0 sector	13.924 (1.578)	lbm/sec kg/sec
Fuel type ($C_{11.96}H_{23.23}$)	RP1	--
Fuel molecular weight	167	g/mol
Fuel boiling temperature (RP1)	487	^0K
Heat of Vaporization (RP1)	56.5	kcal/kg
Heat of Combustion (RP1)	236700 (10457)	J/kg (kcal/kg)
Liquid Fuel Inlet Temperature	60 (288.6)	^0F (^0K)
Density of Liquid Fuel at 300 ^0K	800	kg/m^3
Laminar Vapor Diffusion Coefficient	$1.5 \cdot 10^{-4}$	kg/ms
Vapor Specific Heat	2000	J/kg K
Oxygen Inlet Temperature (assumed vapor oxygen temperature)	150(83) 150	R (K) K
Operating Pressure	$41.37 \cdot 10^5$ (600)	N/m^2 (psia)
Droplet Median Diameter (for distribution function see Figure 4.5)	27	μm

The mass-median droplet diameter of the droplet distribution function ($D_{pm} \cong 20\text{-}30\mu m$) for the triplet injector has been selected based on experimental data of FANG (Reference 1.). For jet diameter 1.85 mm the approximate D_{pm} is 27μm (See Figure 4.5). All droplets are assumed to be injected axailly from the liquid fuel nozzle.

4.4 TEST CASES FOR THE PARAMETRIC EVALUATION.

The intent of the model sensitivity study was to asses the behavior of the model when flow conditions, empirical factors and numerical parameters were altered about selected mean values: Under the current contract this task was limited to five test cases. The selected five test cases included variation in:

- droplet evaporation rate formula,
- vapor fuel reaction rate formula,
- droplet diameter distribution function, and
- liquid fuel injection distribution.

Table 4.2 presents the basic test case (T0) default parameters and five test cases (T1 to T5) parameter specification summary. Note that in test cases T1 - T5 only one parameter at a time has been altered; the remaining parameters were specified as in the basic test T0. In all cases a 21: 8: 4 grid has been used.

Table 4.2 Test Cases for Parametric Evaluation

TEST NUMBER	TEST CASE DESCRIPTION	DIFF. COEF $(\frac{kg}{ms})$	REACTION RATE CONST. P_{FU}	% OF FUEL HOLES BLOCKAGE
T0	Base case	$1.5 \cdot 10^{-4}$	10^{10}	0
T1	Doubled evaporation rate	$3.0 \cdot 10^{-4}$	10^{10}	0
T2	Halved evaporation rate	$0.75 \cdot 10^{-4}$	10^{10}	0
T3	Increased reaction rate	$1.5 \cdot 10^{-4}$	10^{12}	0
T4	Altered droplet distribution	$1.5 \cdot 10^{-4}$	10^{10}	0
T5	Blocked fuel holes near axis	$1.5 \cdot 10^{-4}$	10^{10}	~25

Further details of the test cases are described below:

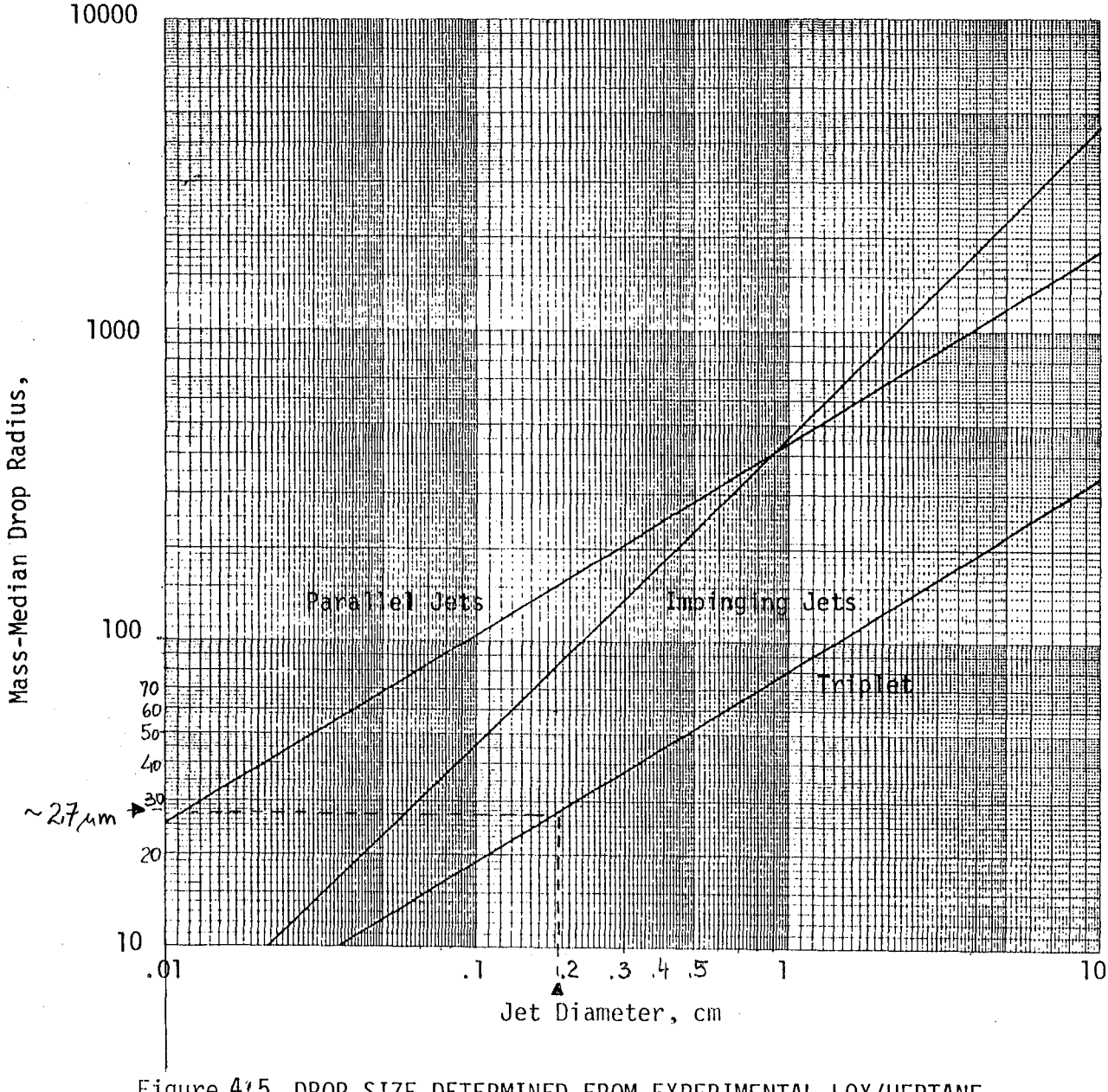

Figure 4.5 DROP SIZE DETERMINED FROM EXPERIMENTAL LOX/HEPTANE ENGINE PERFORMANCE (REFERENCE 1)

Influence of Diffusion Coefficient in the Evaporation Rate Formula

First two test cases T1 and T2 were designed to investigate the influence of the vapor diffusion coefficient of $\mathcal{D}$ on the rate of evaporation of the liquid droplets. The evaporation rate formula is exressed as:

$$\frac{dD}{dt} = -\frac{4\rho\mathcal{D}}{\rho_d C_p D} \text{ in } (1+B) \qquad \text{where} \quad B = \frac{C_d (T-Tsat)}{L} \tag{4.1}$$

and in the basic test case, the diffusion coefficients $\mathcal{D}$ has been estimated to be: 10^{-6} m^2/s (see reference 2 page 204). The $\rho\mathcal{D}$ is obtained as:

$$\rho\mathcal{D} = \frac{P \cdot M}{8314 \cdot T_{sat}} \cdot \mathcal{D} \cong \frac{41. \times 10^5 \cdot 196}{8314 \cdot 600} \cdot 10^{-6} \cong (1. \div 2.) \times 10^{-4} \frac{kg}{ms} \tag{4.2}$$

In the basic test case (T0) value of $\rho\mathcal{D}$ equal to $1.5 \cdot 10^{-4} \frac{kg}{ms}$ has been used.

For model sensitivity studies, this value has been respectively doubled (Test Case T1) and reduced to half (Test Case T2).

Influence of the Reaction Rate Constant

The two step combustion reaction rate scheme employed in the model assumes Arrhenius reaction rate expressions in the following form:

$$R_{fu} = R_{fu}(m_{fu})^{a_{fu}}(m_{ox})^{b_{fu}} \cdot \exp(-E_{fu}/RT) \tag{4.3}$$

$$R_{co} = R_{co}(m_{co})^{a_{co}}(m_{ox})^{b_{co}}(m_{co_2})^{c_{co}} \exp(-E_{co}/RT) \tag{4.4}$$

where $a_{fu}, b_{fu}, a_{co}, b_{co}, c_{co} = 1$ and

$P_{fu} = 1.10^{10}$ $(kg/m^3 s)$ $\qquad E_{fu} = 18000$ (cal/g)

$P_{co} = 7.10^{10}$ $\qquad E_{co} = 1860$

The fuel reaction constant P_{fu} in the reaction mechanism is less reliable. At the same time this reaction provides most of the hear release. In the present study a test case with P_{fu} increased to 1.10^{12} (two order increment) has been considered to study changes in the flame structur.

Influence of the Droplet Distribution Function

Liquid fuel injected into the combustion chamber through the axial hole of the "triplet LOX-RP1-LOX" injector is atomized and sprayed in the form of droplets of different diameters. Exact specification of the spray characteristics for the chamber operating conditions is very difficult. Approximate specification of the droplet diameter distribution function at the injection location requires knowledge of median droplet diameter (D_m), and minimum and maximun diameters (D_{min}, D_{max}). Experimental data by Fang [1] indicate that the median droplet diameter for the triplet injector and RP1 fuel can be taken equal to 27 μm. The maximum droplet diameter is estimated as 80 -120 μm.

Figure 4.6 presents two assumed droplet distribution functions at the injection point for basic test case T0 (solid line) and for test case T4 (dotted line). In both cases median droplet diameter is similar. In the test case T4 maximum droplet diameter has been reduced and number of smaller diameter droplets (15 to 30μm) increased.

Table 4.3 presents discrete droplet distribution function (D_o - droplet diameter and P-droplet population number) for both test cases.

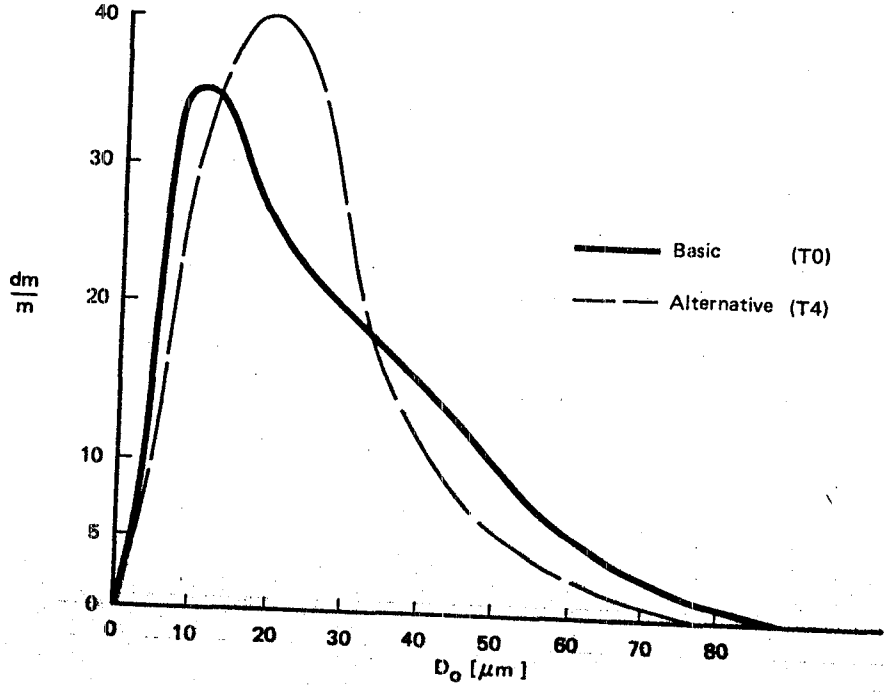

Figure 4.6 Droplet Distribution Functions at the Inlet (Injection) to the Chamber for Test Cases T0 - T4.

Table 4.3 Droplet Distribution Function For Basic Test Case TO and Test Case T4.

TO - TEST CASE		T4 - TEST CASE	
D_o	P	D_o	P
μm	-	μm	-
5	20	5	10
10	35	10	30
20	25	20	40
40	15	35	15
60	5	50	5

Influence of Injection Nonuniformity

The injector nonuniformity, in general, would require specification of the following:

a) location of partially or fully blocked fuel holes,
b) location of partially or fully blocked oxygen holes, and
c) percentages of blockages.

During the present study, only one test case (T5) of the injection nonuniformity has been considered for the computations.

It has been assumed that 25% of the fuel holes have been blocked. The blocked holes are located symmetrically near the chamber axis so the calculation domain stays unchanged as in the basic case TO.

Figure 4.7 presents the injector hole arrangement, fuel holes blockage and (y-θ) grid distribution at the injector plane. The blocked fuel entry area comprises 24.3% of the nominal fuel entry area. The fuel mass flow rate through open holes has increased so as the total flow rate is maintained to be the same as in basic test case TO.

4.5 RESULTS OF BASE TEST CASE

Presentation of the Results

Figure 4.8 presents typical velocity and pressure contours on an axial (XY) - plane of the combustor. Figures 4.9 and 4.10 show contours of absolute temperature (in ^{o}K) and contours of vaporized fuel concentrations in all four (X-Y) planes

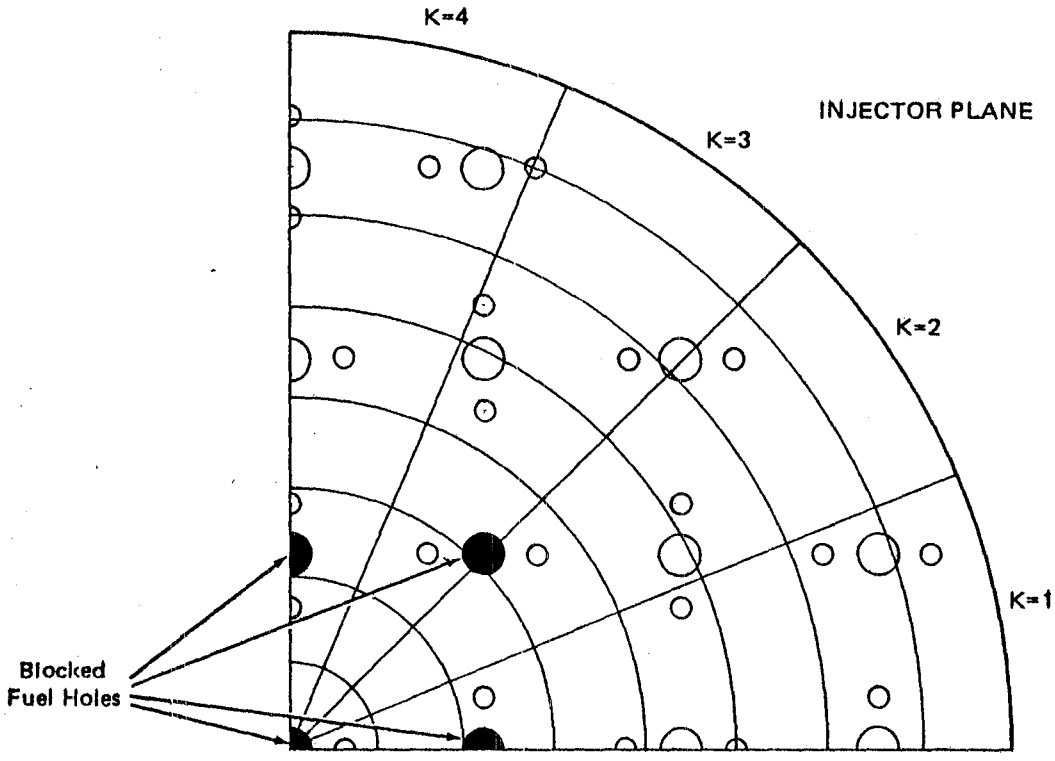

Figure 4.7 Injector Plane with Blocked Fuel Holes Near the Axis of the Chamber (Test Case T6).

Total No. of Holes in 90^{0} Sector: $9\frac{1}{4}$
Blocked No. of Holes : $2\frac{1}{4}$
% Blockage : 24.3%

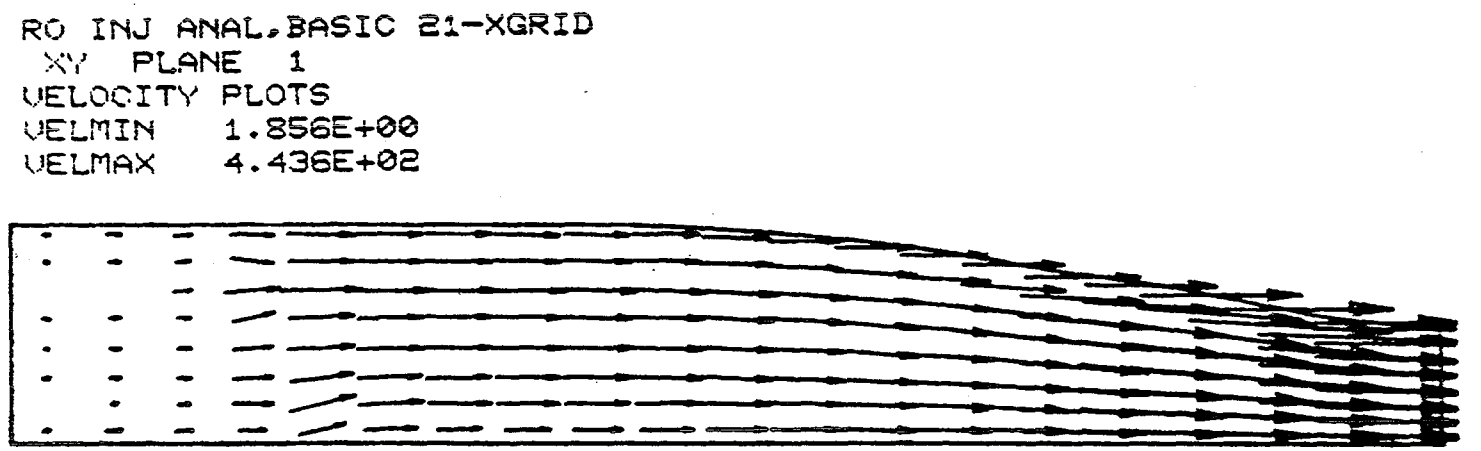

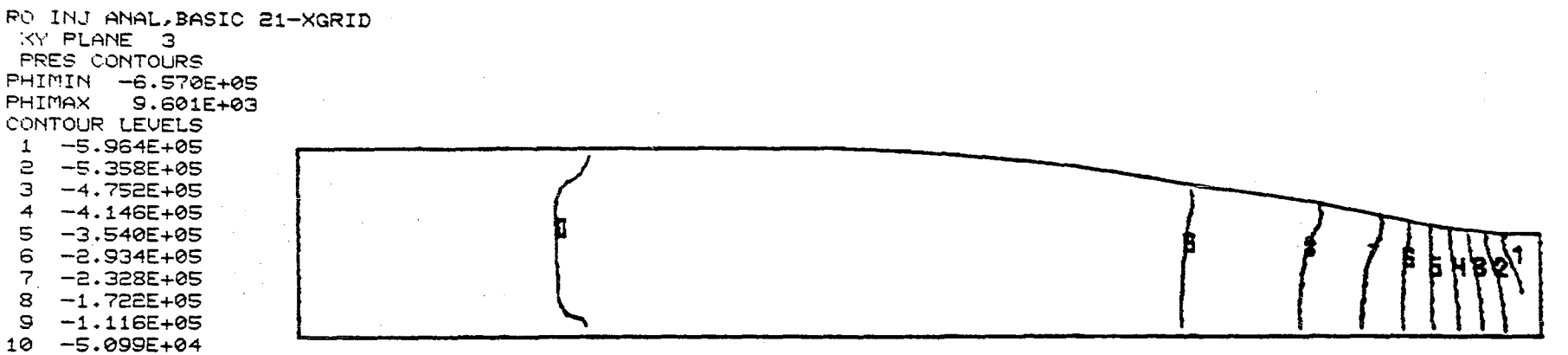

Figure 4.8 Velocity Vectors and Pressure Contours on an Axial Plane (XY) of the Combustor. (Basic Test Case T1).

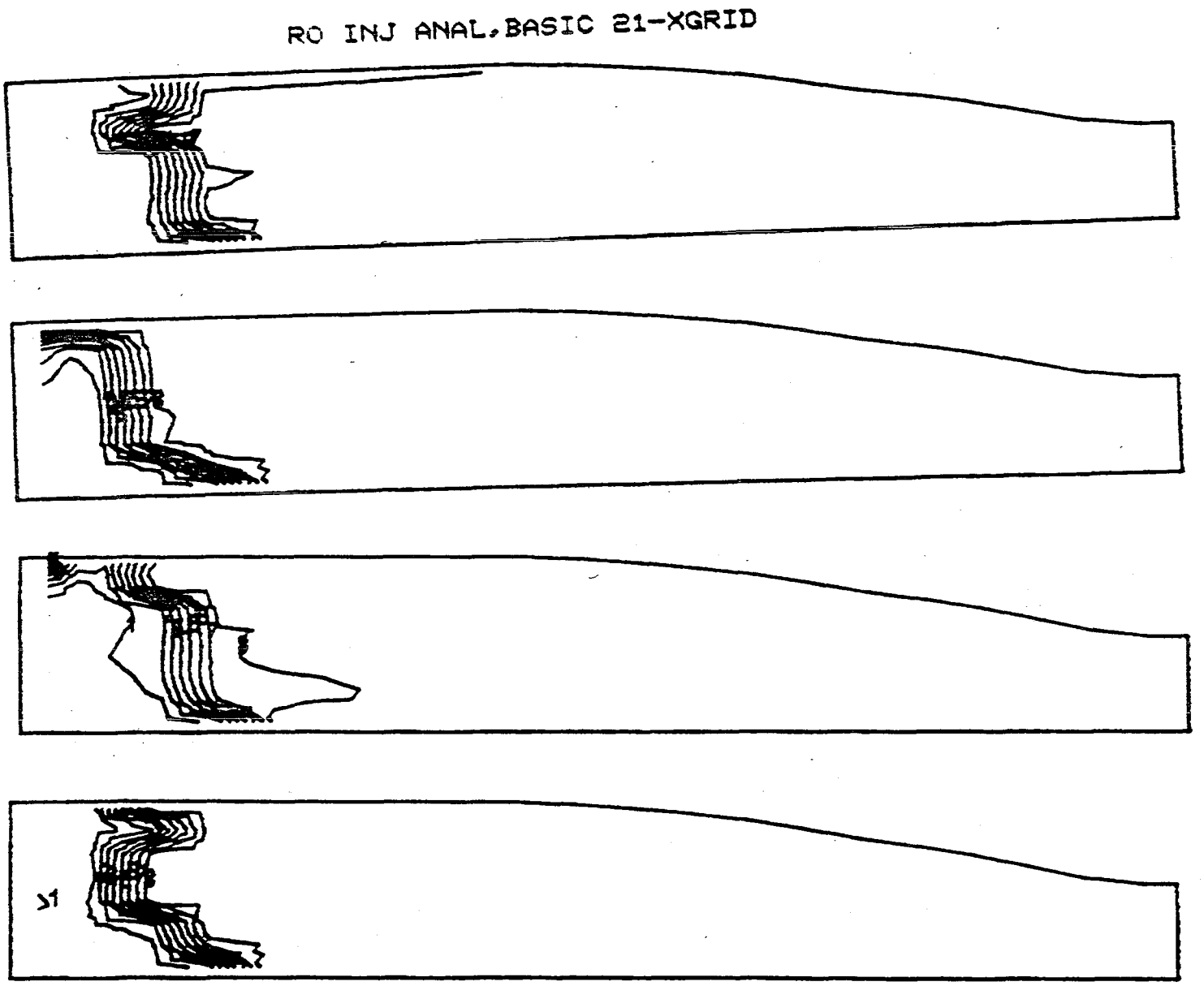

Figure 4.9 Temperature Contors in Axial (XY) Planes; Basic Test Case (T1).

XY PLANE 1
FUEL CONTOURS
PHIMIN 3.650E-07
PHIMAX 3.268E-01
CONTOUR LEVELS
1 3.632E-02
2 7.263E-02
3 1.090E-01
4 1.453E-01
5 1.816E-01
6 2.179E-01
7 2.542E-01
8 2.905E-01

XY PLANE 2
FUEL CONTOURS
PHIMIN 7.712E-08
PHIMAX 4.333E-01
CONTOUR LEVELS
1 4.815E-02
2 9.630E-02
3 1.444E-01
4 1.926E-01
5 2.407E-01
6 2.889E-01
7 3.370E-01
8 3.852E-01

XY PLANE 3
FUEL CONTOURS
PHIMIN 4.956E-08
PHIMAX 5.496E-01
CONTOUR LEVELS
1 6.106E-02
2 1.221E-01
3 1.832E-01
4 2.442E-01
5 3.053E-01
6 3.664E-01
7 4.274E-01
8 4.885E-01

XY PLANE 4
FUEL CONTOURS
PHIMIN 8.417E-08
PHIMAX 3.121E-01
CONTOUR LEVELS
1 3.468E-02
2 6.935E-02
3 1.040E-01
4 1.387E-01
5 1.734E-01
6 2.081E-01
7 2.427E-01
8 2.774E-01

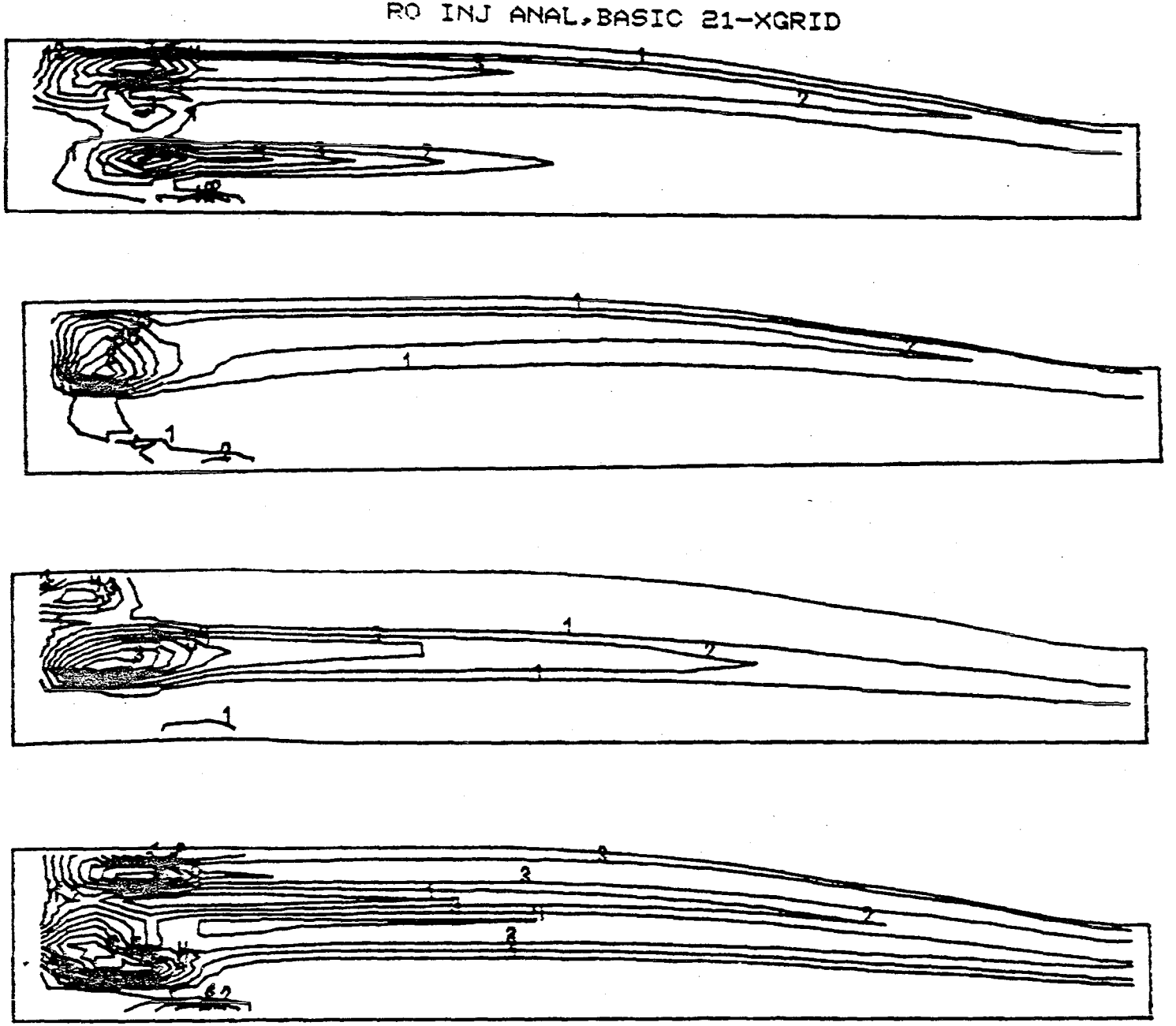

Figure 4.10 Contours of Gaseous Fuel Mass Fraction in XY Planes. (Basic Case T1).

of the combustor. Figure 4.11 presents fuel concentrations at three selected cross-sections of the combustor. Figure 4.12 shows the distribution of the convective heat transfer coefficient on one (X-Z) plane along the combustor wall (developed cylindrical surface). Figure 4.13 presents the heat transfer coefficients variation along the cylindrical wall for each θ - plane. Some of the results of the basic test case TO, such as total gaseous fuel flow rate, liquid spray rate, etc, are presented and discussed in the section describing parametric evaluation.

Discussion of the Results

The flow field represented by the velocity vecotor and pressure contours is typical of nozzle flows. Largest pressure gradient exists near the combustion throat, and the lowest pressure is also located in the same region.

In the front of the combustor, the gas velocities are relatively low. At a distance approximately equal to the chamber radius, a large increase in velocities takes place. At that distance the flame fronts of the individual triplet injectors are joined and large temperature gradients occur (see figure 4.9).

Figure 4.9 indicates that the flame front is nonuniform in both circumferential and axial directions. Temperature rise takes place in shorter axial distance at mid-radii than at small radii (i.e. near the axis). Note that at 2nd and 3rd XY - plane near the chamber wall there is a recirculation region carring hot combustion products towards the injection plane.

The largest fuel concentration gradients exist in the front part of the chamber where droplets enter hot combustion zone and intensive evaporation takes place. The smallest droplets evaporate in a short distance after entering the reaction zone creating a region of significant interphase mass transfer. The largest droplets penetrate further into the chamber and create a zone of reacting vapor fuel along the trajectory. Figure 4.14 presents qualitative comparison between the experimental results (photograph of single triplet flame [1] and calculated gaseous fuel concentration profiles at K = 2 plane. In both diagrams (Figure 4.14), an enlongated flame shape can be seen. Note that the photograph represents only a "hot luminous" zone where unburned hydrocarbon creates a luminous zone. No conclusion can be drawn regarding high temperature zone from this photograph. Figures 4.10 and 4.11 present the gaseous fuel mass fraction

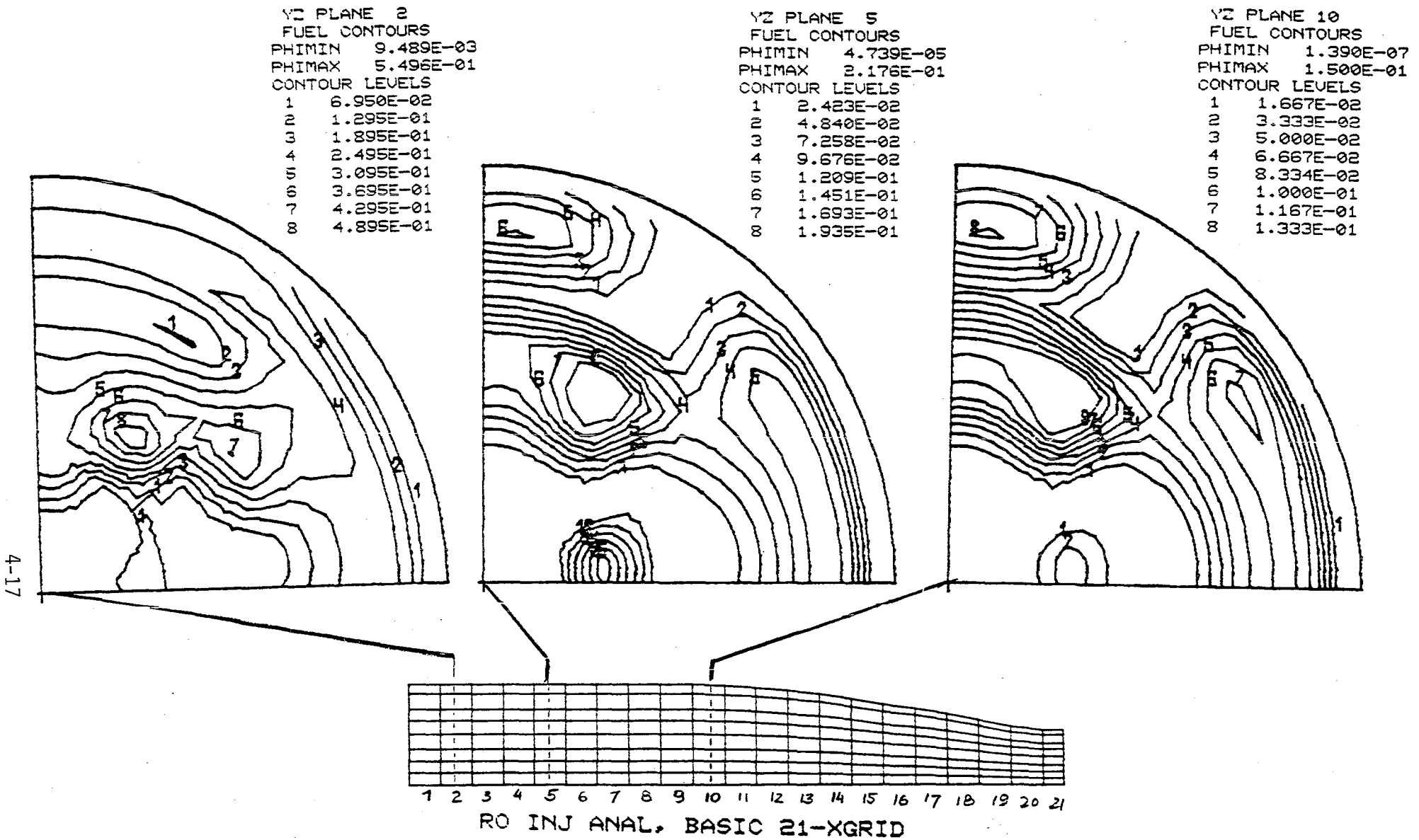

Figure 4.11 Contours of Gaseous Fuel Mass Fraction in YZ-Planes.
(Basic Case T1).

```
RO INJ ANAL. BASIC 21-XGRID
 XZ PLANE  8
 GAMN CONTOURS
PHIMIN    5.862E+01
PHIMAX    3.762E+03
CONTOUR LEVELS
 1    4.702E+02
 2    8.817E+02
 3    1.293E+03
 4    1.705E+03
 5    2.116E+03
 6    2.528E+03
 7    2.939E+03
 8    3.351E+03
```

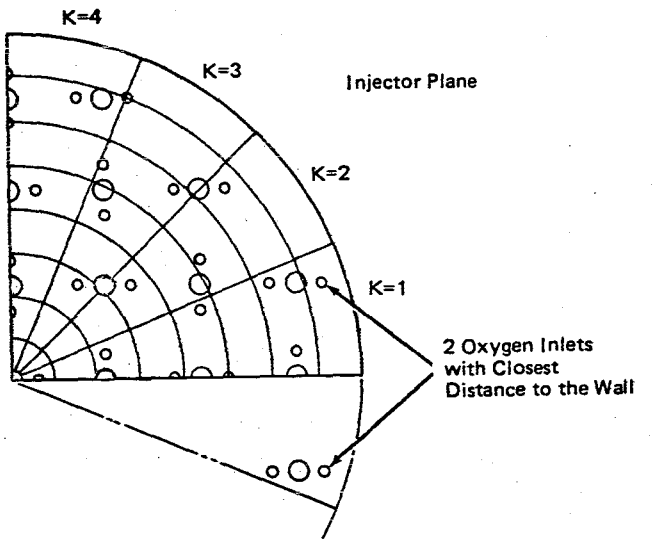

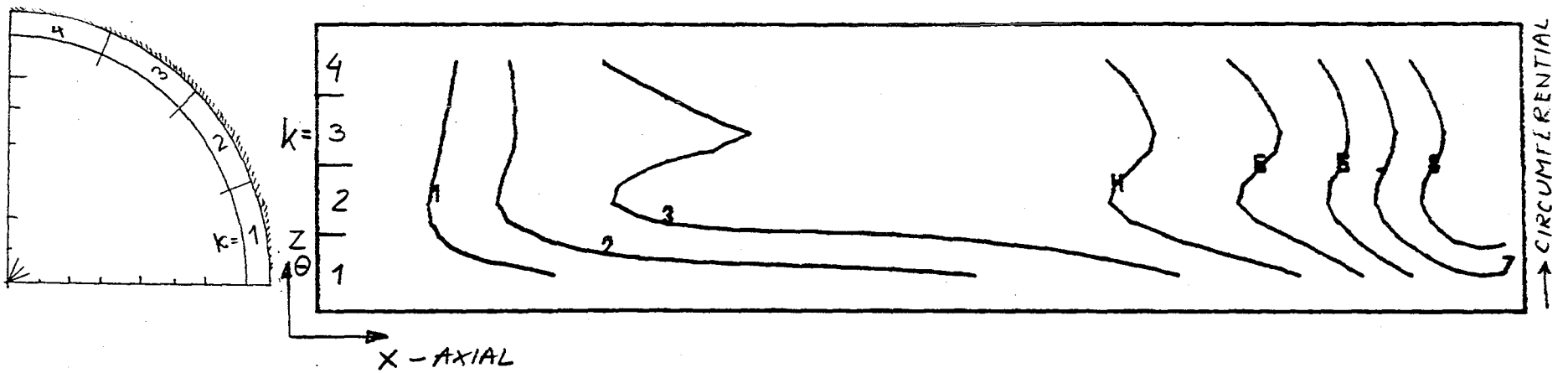

Figure 4.12 Heat Transfer Coefficient on the Cylindrical Wall (Development of X-Z Plane). Case T1

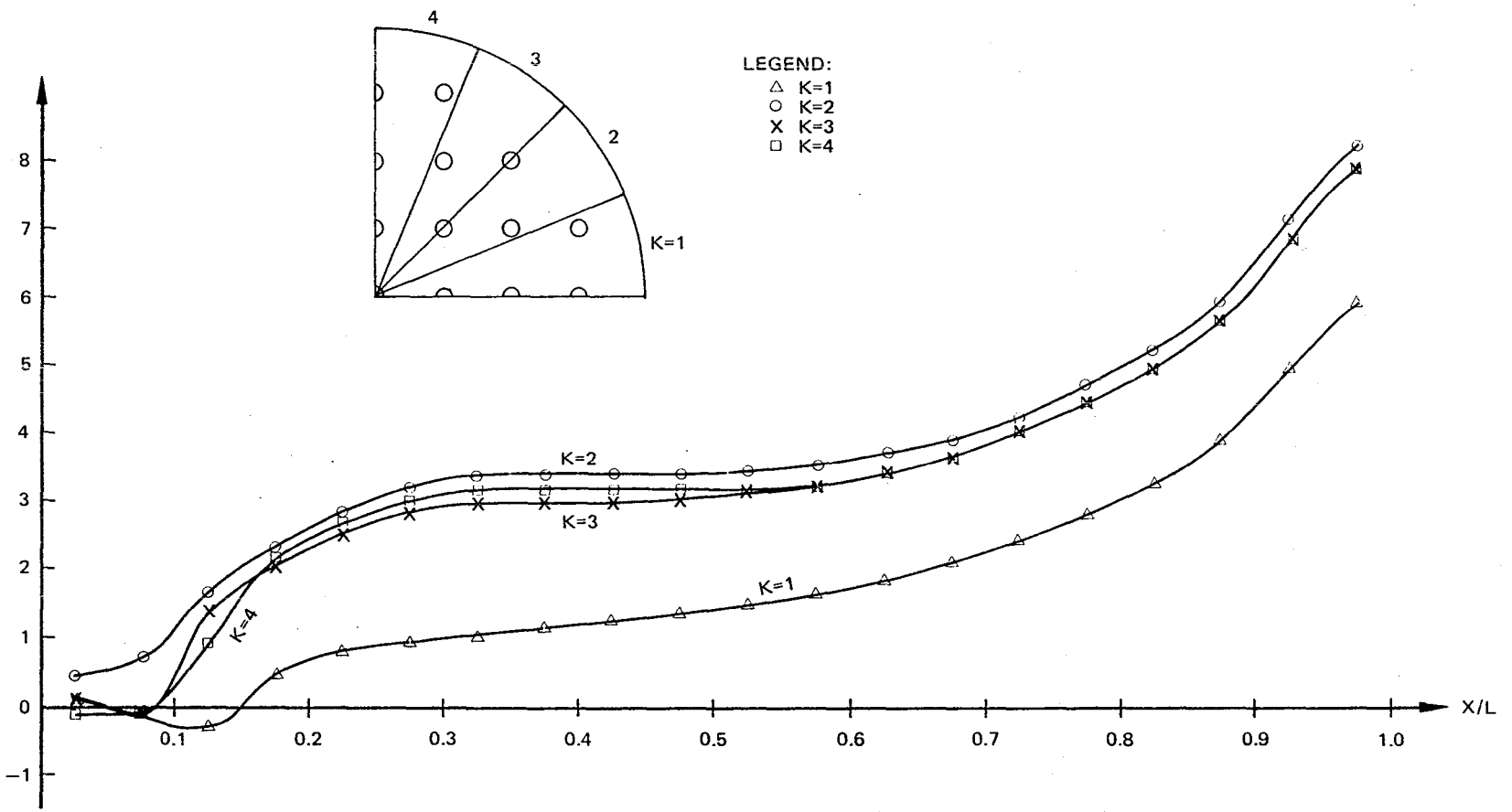

Figure 4.13 Distribution of convedtive heat fluxes along the cylindrical wall.

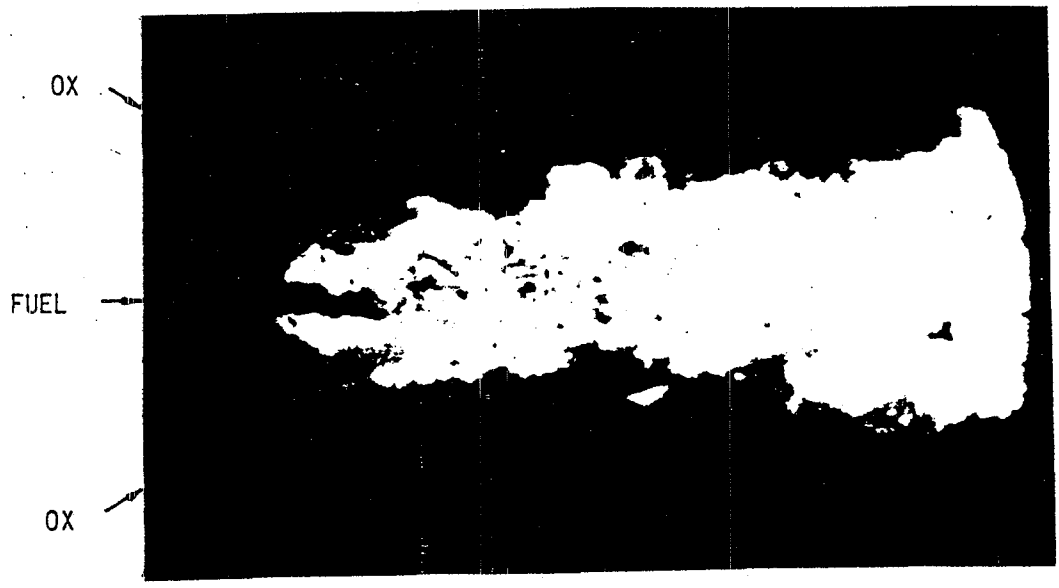

HIGH-SPEED PHOTOGRAPH OF OFO TRIPLET
CARBON FORMATION PHENOMENA, TEST 116

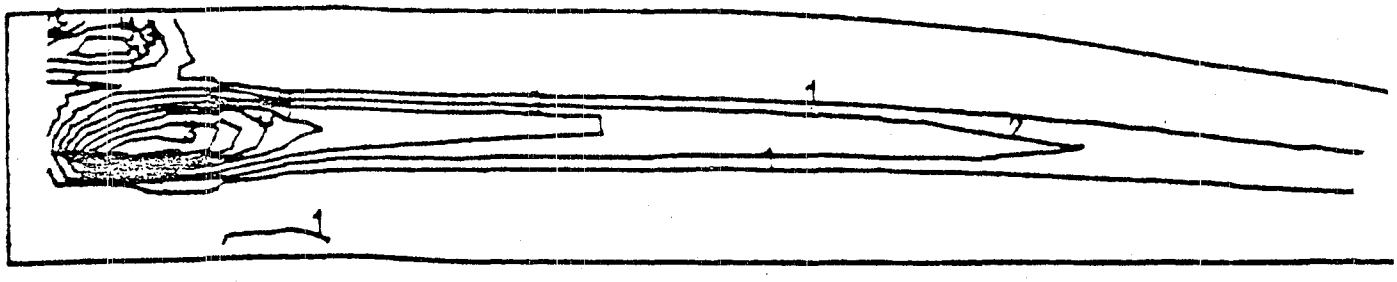

4.14 Comparison between predicted fuel mass function contours and experital flame photograph.

contours at different cross-sections of the combustor. Long wakes of the unburned vapor fuel are generated along the liquid jet trajectories (see figure 4.10). In Figure 4.11, the streams of unburned vapor fuel are represented by concentric semicircles.

Distribution of heat transfer coefficients Γ at the cylindrical wall is shown in Figure 4.12 (contour map) and in Figure 4.13 (distribution curves). From Figure 4.13, it is seen that the heat transfer coefficient is increasing with the distance, with the maximum being near the throat region. Similar observation has been reported in experiments. Note that Γ is quite nonuniform in the circumferential direction, especially in the upstream part of the chamber. The heat transfer curves at k = 2, 3, and 4 are quite similar. At k = 1, however, heat transfer coefficients are significantly smaller (see also Figure 4.12).

The outline of the grid and injection hole arrangement, shown in Figure 4.12, reveals that as compared with k = 2, 3, and 4 in the k = 1 plane, oxygen holes are at the shortest distance from the wall. This results in lower velocity and temperature (cooling effect) and lower heat transfer coefficient Γ.

The cooling effect may have been overpredicted due to grid coarseness at the large radii. Additionally, the influence of the oxygen jet is "averaged" (or smothered) over the entire grid volume. For better resolution, calculations with finer grid or alternative injection specification would be required.

4.6 RESULTS OF PARAMETRIC STUDIES

TEST T1 and T2: Influence of Diffusion Coefficient $\mathcal{D}$ in Evaporation Formula

The evaporation rate dD/dt is proportional to the diffusion coefficient $\mathcal{D}$ (see Equation 4.1). Assumed variants in the diffusion coefficient, viz:

T1 : $\rho\mathcal{D} = 3.0 \times 10^{-4}$ kg/ms

T0 : $\rho\mathcal{D} = 1.5 \times 10^{-4}$ kg/ms

T2 : $\rho\mathcal{D} = 0.75 \times 10^{-4}$ kg.ms

is approximately equal to the limits of uncertainty for this factor.

Figure 4.15 presents the axial variations of liquid fuel flow rate calculated for test cases T0, T1, and T2. The results show that:

a) larger $\mathcal{D}$ creates higher evaporation rates and shorter penetration of liquid fuel jets;

b) in case T1, liquid is totally evaporated within 3/4 of the chamber length;

c) in the other two cases, only droplets with the largest initial diameter D_o can be found at the throat. The liquid fuel flow rates at the exit are:

for T1 : $\dot{m}_{Liq} = 0.$, (i.e. 0% of $\dot{m}_{Liq.\ inj}$);

for T0 : $\dot{m}_{Liq} = 3.10^{-4}$, (i.e. 0.01% of $\dot{m}_{Liq.\ inj}$);

for T2 : $\dot{m}_{Liq} = 4.10^{-3}$, (i.e. 0.7% of $\dot{m}_{Liq.\ inj}$).

Detailed flow patterns indicate no major differences between the flow field and heat transfer in all three cases.

Test T3: Influence of the Fuel Reaction Rate Constant P_{FU}

Figure 4.16 presents the axial variations of gaseous fuel flow rate for two different fuel reaction rate constants; viz:

Case T0 with $P_{FU} = 10^{10}$ kg/m^{3}s ; and

Case T3 with $P_{FU} = 10^{12}$ kg/m^{3}s.

In the case of larger P_{FU} (Case T3) vapor fuel flow rates in the front part of the chamber are singificantly smaller that those in the basic case T0. From temperature contours (Figures 4.9 and 4.17) it can be seen that in the case of larger P_{FU}, the flame front is located closer to the injector plane. This seems physically plausible.

Test T4: Infulence of Alternative Droplet Distribution Function

By changing the droplet distribution, there are no significant changes in the calculated flow field and heat transfer characteristics. In Test T4, flame front is slightly closer to the injector plane. Inspection of the droplet distribution functions (Figure 4.6) reveals that in Test Case T4 there is a smaller amount of the finest drops (0-10μm) and therefore less vapor fuel will be evaporated in the front part of the combustor. This probably creates mixture conditions in Case T4 closer to the stoichiometric than that in base case T0.

Test T5: Influence of Injector Nonuniformity (Blocked Fuel Holes Near Axis)

Figure 4.7 presents injector plane with four blocked fuel holes in the 90^o sector. Blocked fuel entry area is 24.3% of the nominal fuel entry area. As

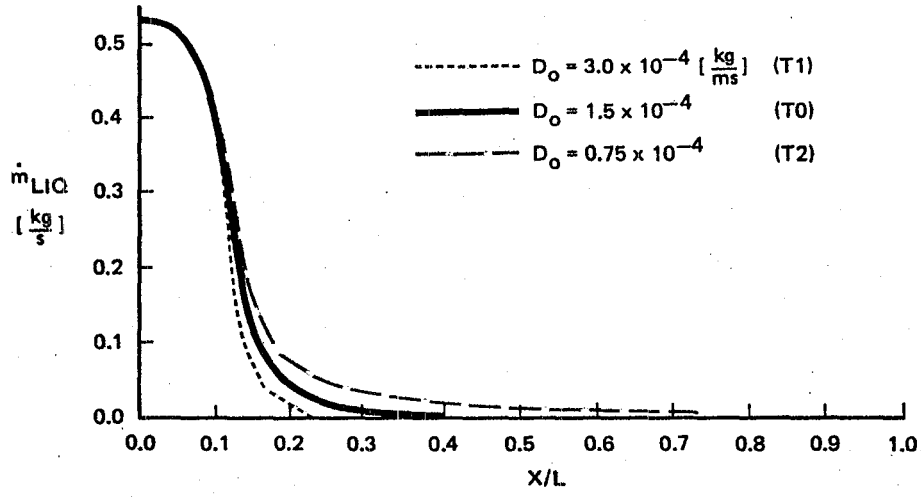

4.15 Axial Variation of Liquid Fuel Flow Rate (for 45^0 Sector of the Chamber); for (Tests TO, T1, and T2).

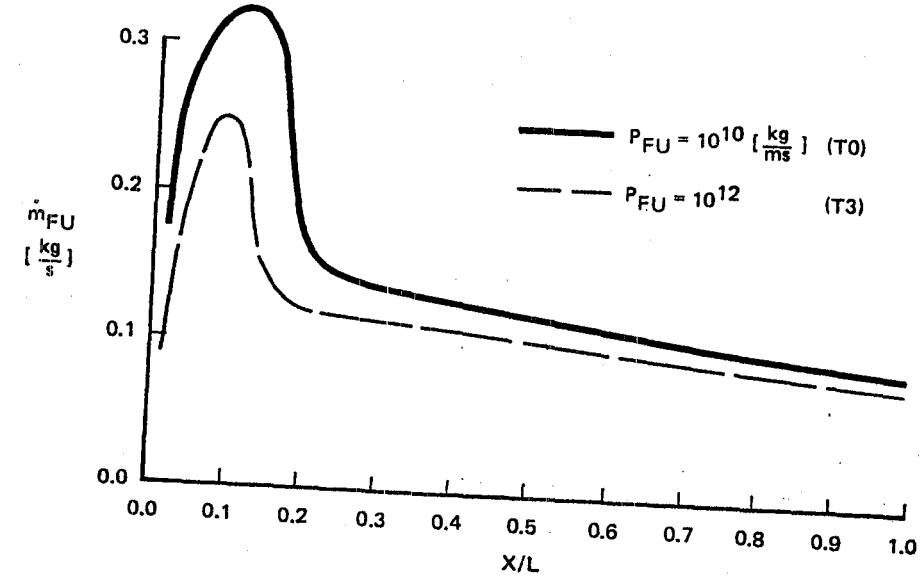

4.16 Axial variation of Gaseous Fuel Flow Rate (for 45^0 Sector of the Chamber); for (Tests TO and T3).

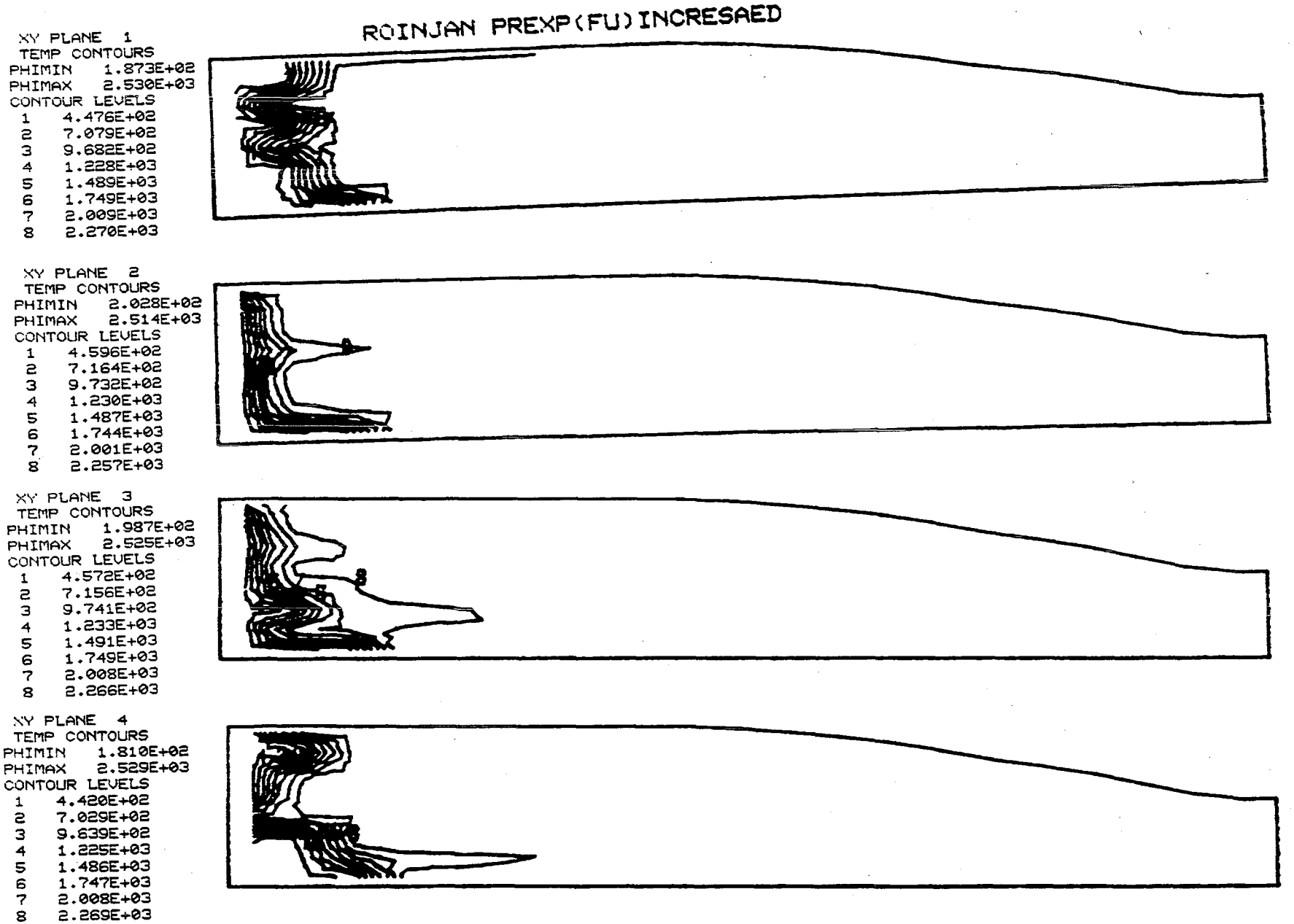

Figure 4.17 Fuel Mass Fraction Contours Test Case T4-Higher Fuel Reaction Rate Constant.

ROINJAN, BLOCKED 25% FUEL HOLES

XY PLANE 1
TEMP CONTOURS
PHIMIN 1.715E+02
PHIMAX 2.523E+03
CONTOUR LEVELS
1 4.328E+02
2 6.940E+02
3 9.552E+02
4 1.216E+03
5 1.478E+03
6 1.739E+03
7 2.000E+03
8 2.261E+03

XY PLANE 2
TEMP CONTOURS
PHIMIN 1.783E+02
PHIMAX 2.513E+03
CONTOUR LEVELS
1 4.377E+02
2 6.971E+02
3 9.565E+02
4 1.216E+03
5 1.475E+03
6 1.735E+03
7 1.994E+03
8 2.254E+03

XY PLANE 3
TEMP CONTOURS
PHIMIN 1.765E+02
PHIMAX 2.528E+03
CONTOUR LEVELS
1 4.378E+02
2 6.991E+02
3 9.603E+02
4 1.222E+03
5 1.483E+03
6 1.744E+03
7 2.005E+03
8 2.267E+03

XY PLANE 4
TEMP CONTOURS
PHIMIN 1.689E+02
PHIMAX 2.517E+03
CONTOUR LEVELS
1 4.298E+02
2 6.907E+02
3 9.516E+02
4 1.212E+03
5 1.473E+03
6 1.734E+03
7 1.995E+03
8 2.256E+03

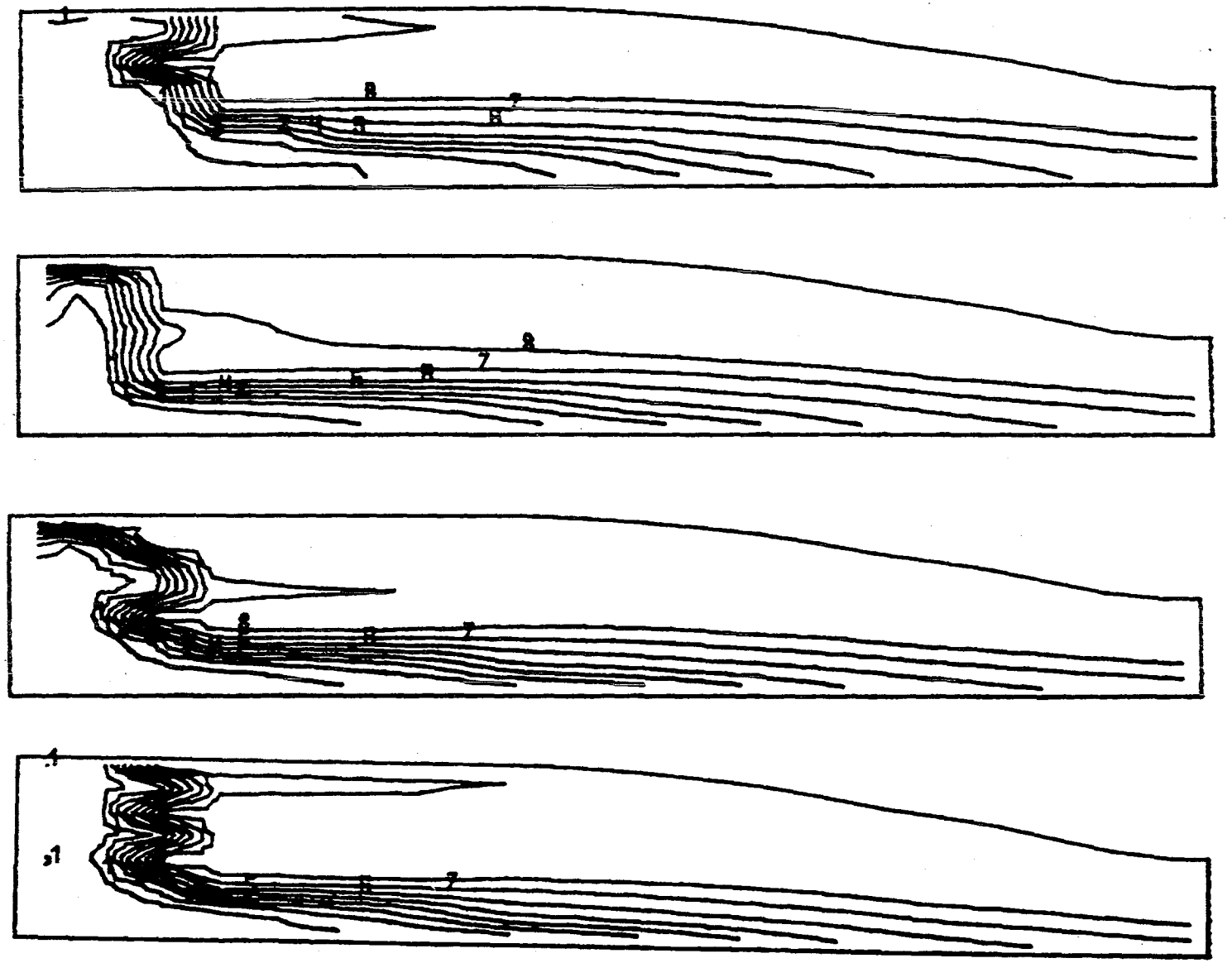

Figure 4.18 Temperature Contours in XY-Planes. Test Case T5- Near Axis Blockage of 25% of the Fuel Entry.

RINJAN BLOCED 25% FUEL HOLES
XZ PLANE 8
GAMN CONTOURS
PHIMIN 5.515E+01
PHIMAX 3.786E+03
CONTOUR LEVELS

1	4.697E+02
2	8.842E+02
3	1.299E+03
4	1.713E+03
5	2.128E+03
6	2.542E+03
7	2.957E+03
8	3.371E+03

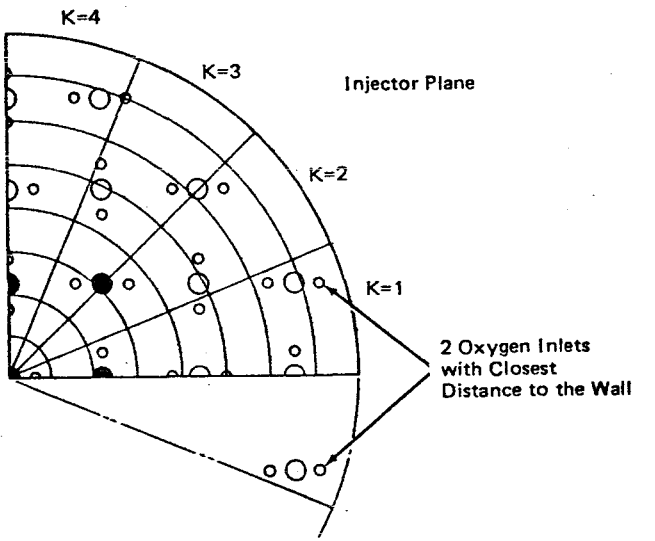

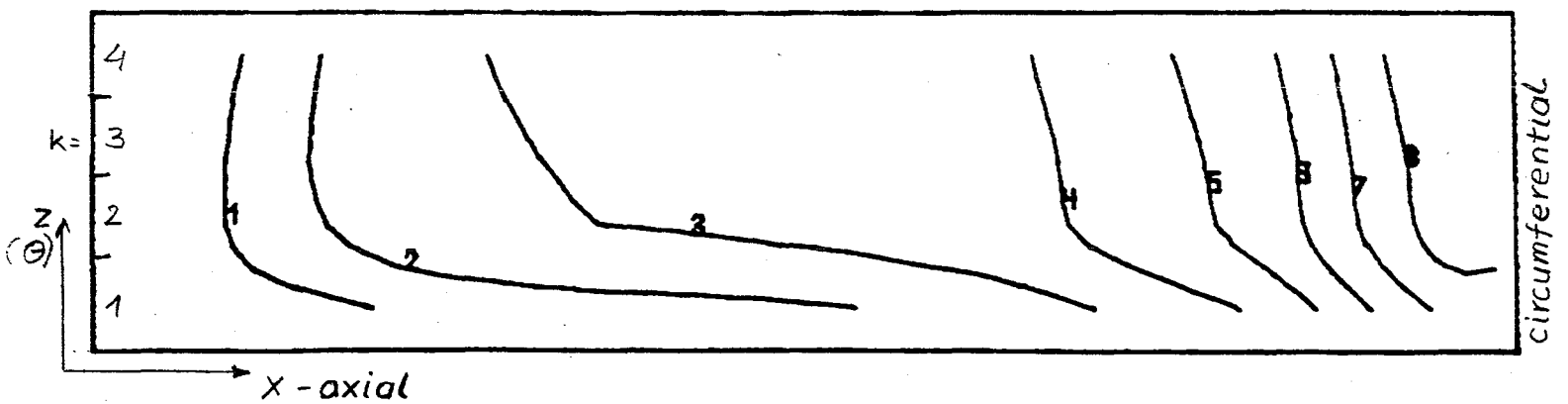

Figure 4.19 Heat Transfer Coefficient on the Cylindical Wall Test Case T6-Blocked 25% of the Fuel Entry.

compared to Cases T1 to T4, this test case (T5) shows much more singificant differences in the heat transfer and combustion within the chamber. Figure 4.18 presents the temperature contours (^{o}K) in four axial plans. The central, oxygen rich core is significantly cooler than the annular, fuel rich, zone. Steep gradients in the radial direction in the middle of the combustor represent the enlongated flame front.

Comparison of Figure 4.12 and 4.19 indicates that convective heat transfer coefficients at the combustor wall are nearly the same for the basic case T0 and blocked fuel entry case T5. This is due to the "blanketing" of the cylindrical wall by the hot reactive streams of operating fuel spray jets. An equivalent blockage near the combustor wall, rather than near the axis, is likely to have a much larger influence on the "wall" heat transfer coefficients. Further parametric studies, were not included in the current work scope, and are recommended for future.

SECTION 5
MODEL IMPROVEMENTS AND RESEARCH NEEDS

The applications reported in Sections 3 and 4 of this report have demonstrated the basic capability of simulating three-dimensional, two-phase flows with evaporation and combustion. The use of Langrangian technique for liquid fuel drops has provided necessary flexibility of predicting effects of small changes in injector plate geometry and/or flow conditions. Results of parametric studies have shown that the numerical model responds to changes in physical parameters in a plausible manner, and thus it can be utilized for the identification of sensitive parameters.

Several improvements and studies can and should be made for the code to be a valuable tool in design and performance analysis of rocket engines. The improvements are desirable for both mathematical models of physical processes built into the code as well as for numerical methods and solution algorithm employed. The code also requires verification and sensitivity study for both single and two-phase flows with and without mass transfer and combustion. The following three subsections describe recommendations for (a) physical model improvements; (b) numerical model improvements and (c) code validation and verification studies.

5.1 IMPROVEMENTS IN MATHEMATICAL MODELS OF PHYSICAL PROCESSES

There are several possible improvements in simulating the spray flow, evaporation and combustion processes implemented in current version of the code. Further refinements can be made in simulating the injector and spray atomization. This section briefly describes basic ideas of selected possible improvements.

Spray Atomization in Triplet Injectors

The unlike impinging elements accomplish mixing and atomization by direct impingement of fuel and oxidizer jets. Atomization takes place in the immediate vicinity of the impingement point. The effect of oxygen jet impingement on the central fuel stream scatters the fuel stream in the direction normal to the injection plane (Figure 5.1).

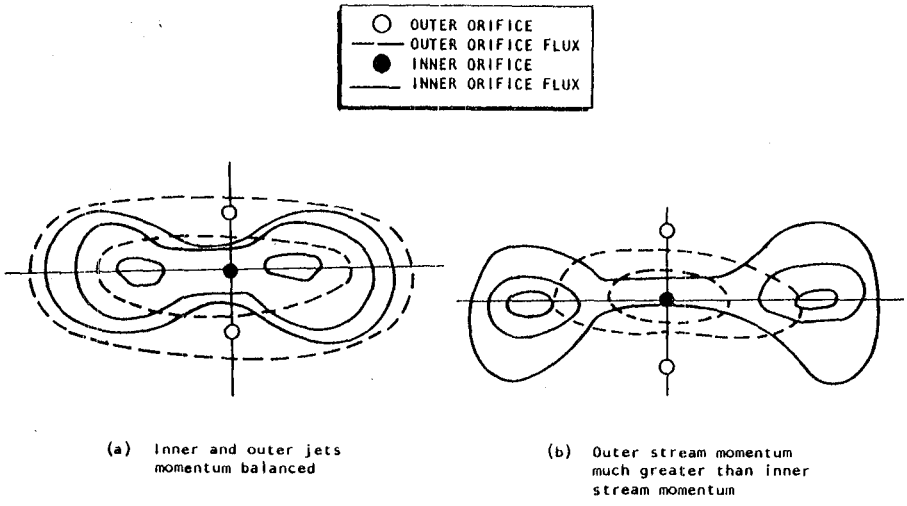

Figure 5.1 Triplet Injector Spray Mass Distribution

Experimental data exists (see Review in [3]) for specifying a range of droplet beams at the atomization point. Such information should be utilized in future studies and incorporated in if necessary in the code for regular use in analysis of injector anomalies.

Turbulent Droplet Diffusion

In the present version of the code, turbulent droplet diffusion has been neglected. This must be improved for future studies. The task of including turbulent particle diffusion into the model requires investigations of various possible approaches. One diffulty is that the fluid properties are constant within a cell, while the particles are tracked through a cell in a series of time steps smaller than the cell dimensions. Thus the particles at several time step positions within a cell see only one set of mean flow properties.

There are two basic approximate techniques for simulating the turbulent droplet diffusion.

a) random walk method (Dukowicz [4]) ; and
b) diffusive drift method of Jurewicz [5] and Stock [6].

In both techniques, an isotropic turbulence is assumed. The second technique seems to be more adequate for "fully coupled" calculations of spray combustion modeling, and is recommended for inclusion in REFLAN3D-Spray code.

Accurate Evaluation of Thermodynamic and Transport Properties

In the present version of the code, most of the liquid fuel properties (C_{pliq}, T_{sat}, ρ_{liq}, etc) have been assumed to be constant. More accurate representation would require sepcification of their functional dependence on local pressure and temperature.

The gaseous species specific heat formula coefficients (5-order polynomial) are valid for the "high temperature range" between 500-3000^{o}k. For the low-temperature liquid propellants, two sets of specific heat constants are desired.

5.2 IMPROVEMENTS IN NUMERICAL METHOD AND SOLUTION ALGORITHM

The computational process of the coupled Eulerian-Lagrangian analysis is highly nonlinear. In the present calculations, no special relaxation or linerization of interphase mass, momentum and energy transfer source terms has been undertaken. Calculations with (11 x 8 x 4) and (21 x 8 x 4) grid caused no numerical instabilities. However, trial runs with finer grids in the circumferential direction (21 x 8 x 8) showed slow convergence and oscillatory behavior. These difficulties must be investigated and remedied before the code can be regarded suitable for studies of injector anomalies.

Relaxation Practices

Investigations of the relaxation practices and linearization methods are desired. For the two-phase flow with mass transfer, possible relaxation practices include:

a) relaxation of the interphase mass transfer rate ;

b) relaxation of the average liquid property ϕ_{liq} in the transfer rate expression;

c) relaxation of velocities and enthalpies; and

d) combination of a, b, and c.

Accuracy Improvements

The accuracy of the three dimensional calculations in the Eulerian frame can be improved by refining the grid in the region of interest and/or by using higher order differencing methods.

The usefulness of the first practice is often limited by the computer storage, especially for the reactive flow calculations where twelve or more differential equations must be solved.

The second approach is higher order finite differencing and has attracted more attention in the recent publications [7,8,9]. One of the most promising methods of the accuracy improvement has been developed by the authors [10,11]. The new method called "Multiflux Conservative Differencing" (MCD), has been successfully applied in a 2-dimensional calculation. Results obtained with the coarse grids 10 x 10 and 20 x 20 compare very well with results on 50 x 50 or finer grids obtained with the other (e.g. upwind differencing) methods. It is recommended that: (a) MCD be incorporated in REFLAN3D-Spray Code, and (b) comparative studies be performed to evaluate the improvements due to MCD.

The second part of the computational algorithm (Lagrangian part) is relatively new in comparison with the Eulerian part and the computational experience is still very limited. Some basic studies in the area of Eulerian-Lagrangian approach would greatly enhance the computational fluid dynamics. New solution schemes for the homogenous and heterogenous combustion and fluid flow calculations could be explored.

For the rocket engine calculations, the first improvement should probably be made in the calculations of the interphase mass source. In the present version of the code, the source terms are calculated at the grid cells through which the particles are passing (see Figure 5.2a).

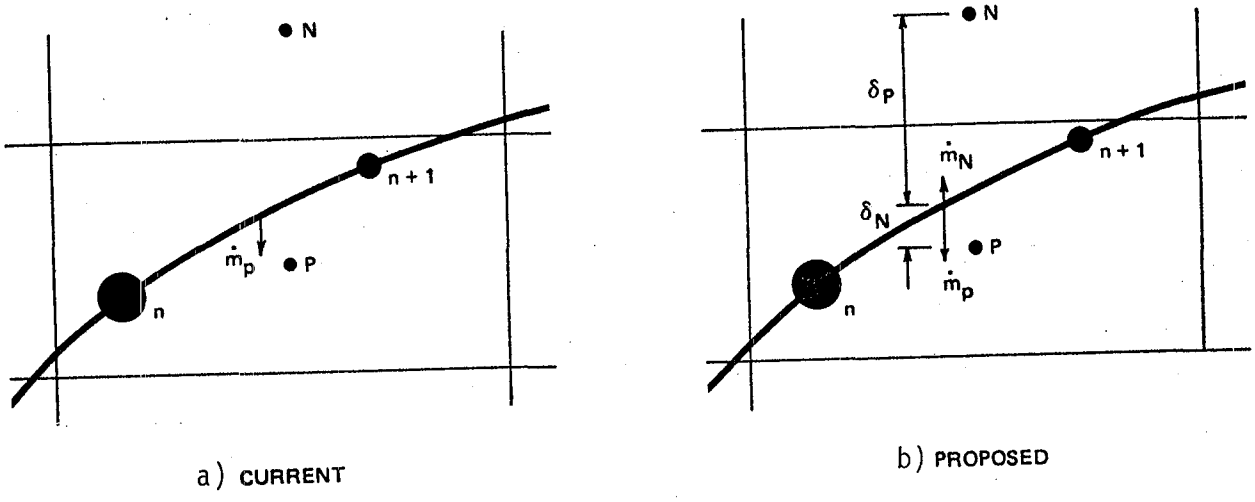

Figure 5.2 Lagrangian Interphase Source Term Calculations for Eulerian Transport Equations.

Therefore, the mass release is "lumped" in the source at point "P" with no source for point N. In reality, however, the droplet trajectory represents an average droplet path and one could expect to have the mass transfer to the N cell as well. The practice in Figure 5.2b presents an alternate approach for the source term calculations around the average particle path. The mass transfer from the liquid to the gaseous phase will be distributed to both N and P points based on

a) distance weighting factors or,

b) volume weighting factors.

With this practice, implementation of the droplet turbulent diffusion models would also be more realistic and economical. Simple test cases on a 2-dimensional grid are recommended as the first step.

Improvements in the Nonorthogonal Grid System

The nonorthogonal grid system and associated velocity components in the present version of the code are shown in figure 5.3a. The orthogonal velocity components, u and v are used on the nonorthogonal grid. Within this practice it has been assumed that the u_p velocity is driven by the $(p_p - p_w)$ pressure gradient. This assumption is valid only if the velocity components are aligned with the grid lines, or the degree of departure from this condition is small (say $\leq 30^o$). A new practice is proposed in which the grid lines and velocity resolutes (nonorthogonal) are used figure (5.3b). Most of the derivations for preliminary testing have been done under CHAM's in-house development project. Its implementation and numerical test in REFLAN3D-SPRAY are recommended to enhance the code capability and accuracy.

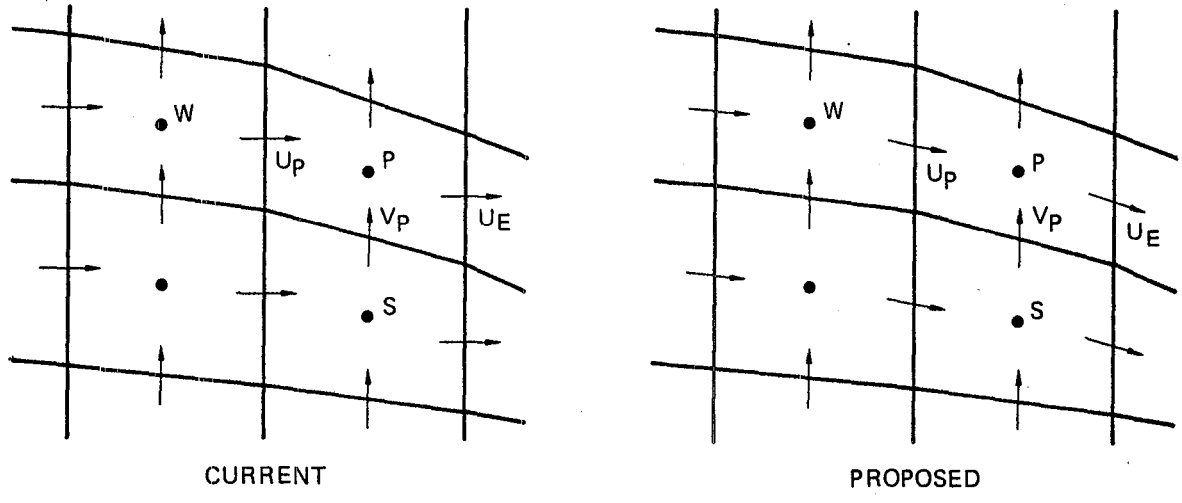

Figure 5.3 A Nonorthogonal Grid Systems

Modification of the Code Structure

In the present version of the REFLAN3D Code, COMMON statements are used to transfer the variables between subroutines themselves.

A more economical method of passing data to a subprogram is through the argument list in the CALL statement. This practice is more economical (small storage allocation) and offers greater flexibility by "dynamic storage reservation" option. This practice is also preferred in recently specified "NASA Standard Requirements for Digital Computer Programs"

The modification does not require any changes in the bulk of the coding, and is recommended for REFLAN3D-SPRAY code.

Improvements in Solution Algorithm

The current solution algorithm employs a modified version of the SIMPLE procedure [12] for calculating the hydrodynamic field (u-v-w-p). Figure 5-4 presents the flow chart of the iterative scheme employed. Note that after solving the pressure correction equation, velocities are corrected by using approximate velocity-pressure coefficients based on truncated momentum equations. Therefore, the u, v, and w do not satisfy the full momentum equations with body forces, large shear stress and interphase momentum transfer. An alternative scheme which can be useful for flow with high shear stresses and/or with intensive interphase momentum transfer is shown in Figure 5.5. The scheme differs from the SIMPLE algorithm in that after the correction of p, u, v, and w, a second correction is performed based on the Poisson equation for pressure, obtained from the full (not truncated) momentum equations. Velocities are corrected using these secondary pressure corrections and the subiterative loop returns to the "continuity conserving" pressure correction equation. It is recommended that in the next stage of study, a few variations of the proposed scheme be tested and the most economical one employed for retention as a permanent feature of REFLAN3D-SPRAY Code.

5.3 VALIDATION AND VERIFICATION STUDY

The calculations of the three-dimensional two-phase flow in rocket engine combustion chambers undertaken in the present project represent the first attempt to model 3-D combustion by the Eulerian-Lagrangian algorithm.

Additional validation and verification tests of the present model are required and recommended. The computational studies should be performed for:

- tests for improvements in physical model and numerical algorithm (as described in Sections 5.1 and 5.2);
- wider range of physical parameters;
- prediction of single triplet injector flow and combustion (Experimental results of the relevant case are available in NASA CR 1169006. The geometry of the combustion chamber and the photograph of the triplet jet flame are shown in Figure 5.6);
- Injector nonuniformity study for several hole arrangements and injection hole blockages.

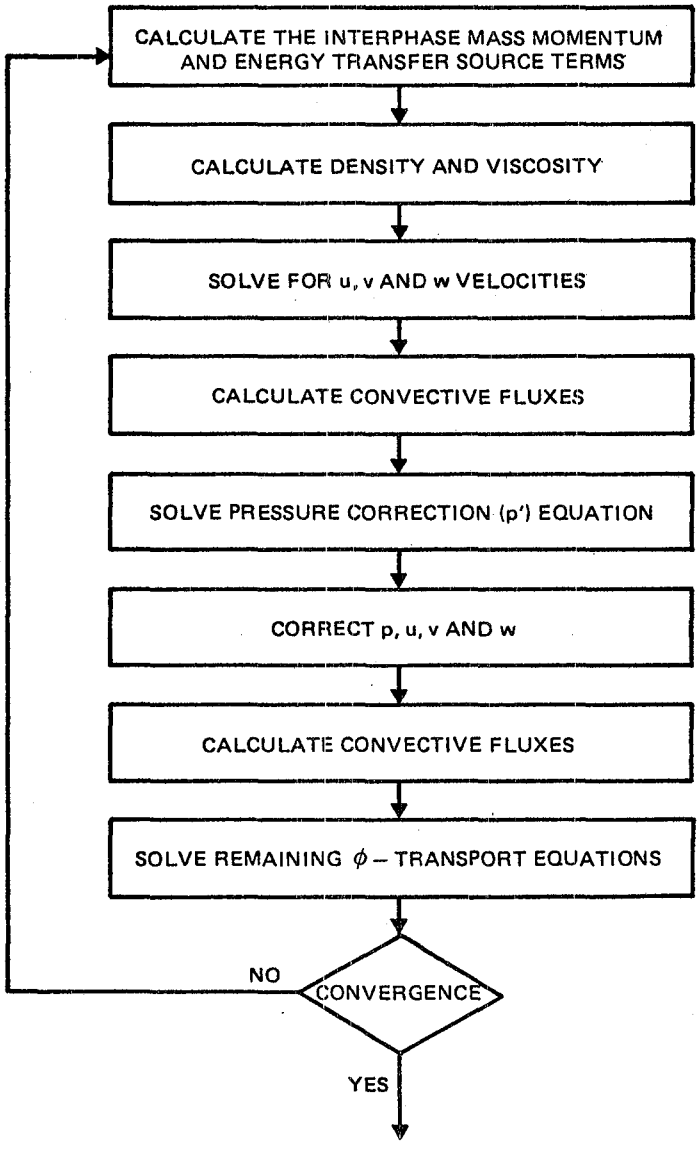

Figure 5.4 Flow Chart of Current Solution Algorithm

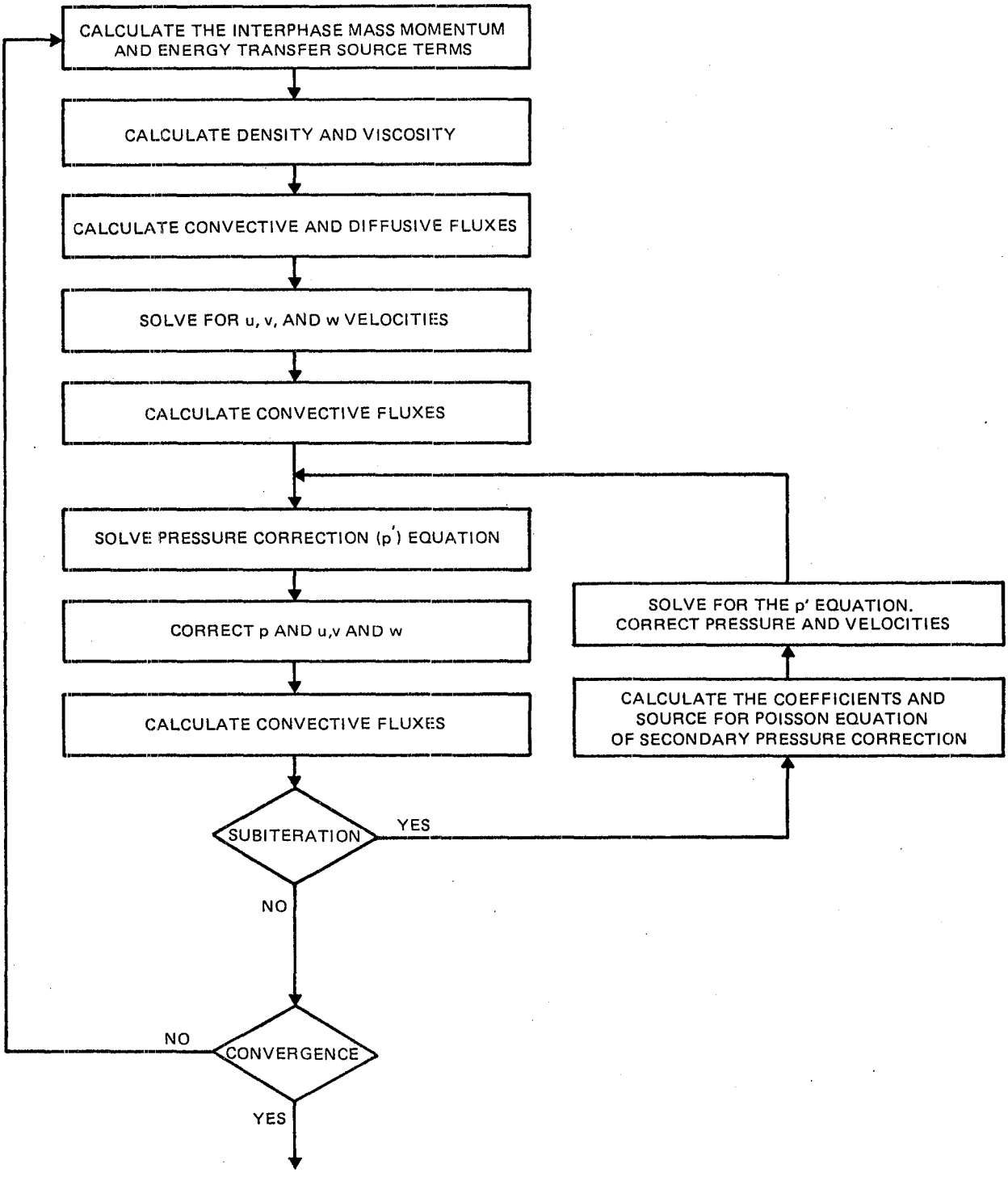

Figure 5.5 Flow Chart of Proposed Double Pressure Correction Algorithm.

OFO TRIPLET INJECTOR COLD-FLOW SPRAY PATTERN

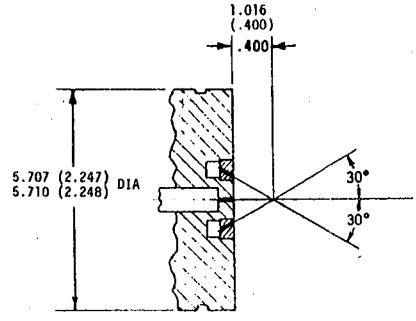

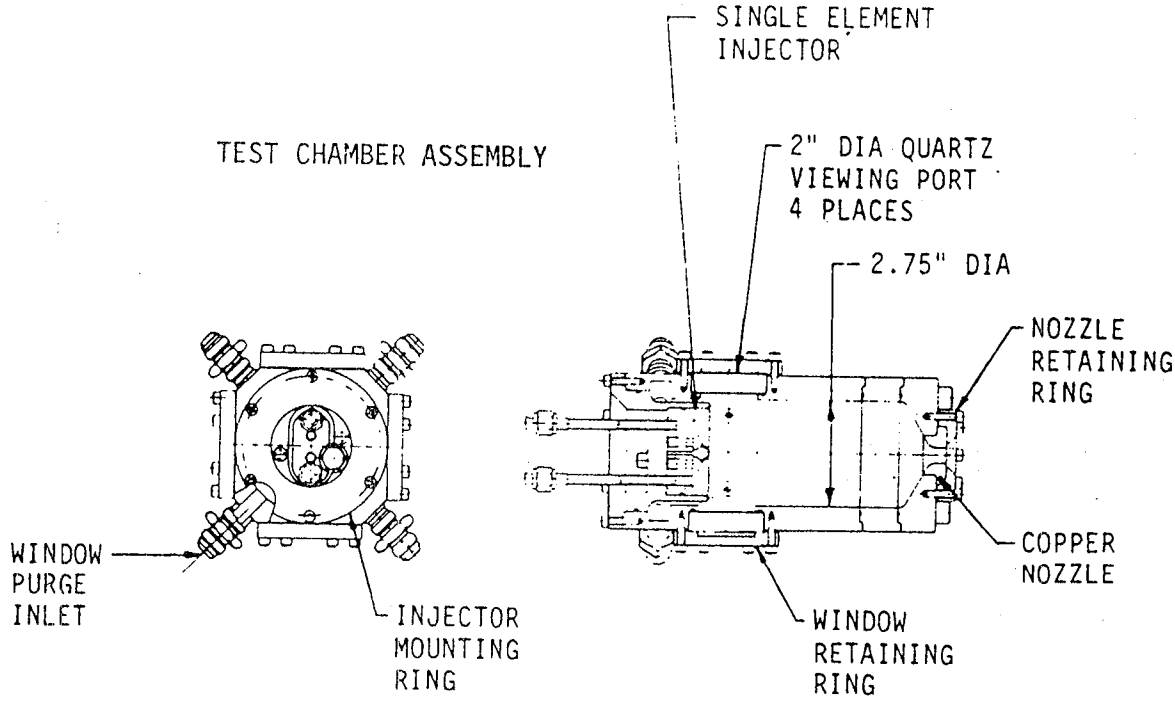

Figure 5.6 Experimental Test Chamber Geometry and OFO Triplet Injection Spray Pattern (Reference 1).

SECTION 6

REFERENCES

1. J. Fang "LOX/Hydrocarbon Fuel Carbon Formation and Mixing Data analysis", NASA CR 169006, by Aerojet Liquid Rocket Co, November 1983.

2. G. M. Faeth "Current Status of Droplet and Liquid Combustion" Progress in Energy and Combustion Science, Vol 3, 1977.

3. G.S. Gill and W. H. Nurick "Liquid Rocket Engine Injectors" NASA SP-8089, March 1976.

4. J. K. Dukowicz "A Particle- Fluid Numerical Model For Liquid Sprays" Journal of Comp. Phys. v35, (1980), pp 229-253

5. J.T. Jurewicz and D. E. Stock, "A Numerical Model for Turbulent Diffusion in Gas Particle Flows", Paper 76-S/FE-33, Winter Annual Meeting, NY 1976

6. G. Arnason and D. E. Stock "Dispersion of Particles in Turbulent Pipe Flow" in "Gas Solid Flow" ASME FED-vol 10, ed by J. T. Jurewicz 1983.

7. B.P. Leonard, "A Stable and Accurate Convective Modeling Procedure Based on Quadratic Upstream Interpolation," Comp. Meth. App. Mech. Eng., Vol. 12 (1979), 59.

8. C. J. Chen, J. Naseri-Nashat, and P. Li, "Finate Analytic Method," Iowa Inst. of Hydraulic Res., University of Iowa, Rep. E-CJC-1-80, 1980.

9. R. W. Claus, G. M. Neely, S. A. Syed, and A. D. Gosman, "Reducing Numerical Diffusion for Incompressible Flow Calculations", preprint copy to be published as a NASA TM, 1984.

10. A. J. Przekwas, A. K. Singhal, and L. T. Tam, "A Multi-Flux Conservative Differencing Scheme to Reduce Numerical Diffusion in Fluid Flow Calculations," submitted for publication in Computer Methods in Applied Mechanics and Engineering.

11. A. J. Przekwas and L. T. Tam "A Multiflux Conservative Differencing Method for Fluid Flow and Heat Transfer Calculations" to be presented at ASME Winter Annual Meeting, New Orleans, December 1984.

12. S. V. Patankar "Numerical Heat Transfer and Fluid Flow" Hemisphere Publ. Corp., Washington, 1980.

APPENDIX A

INTERPRETATION OF RESULTS AND THE COMPUTER OUTPUT

The computational results discussed in this report are presented in the form of tables of computer output and graphical plots of velocity vectors and contour maps of the dependent variables. This appendix describes geometry, grid distribution notation and interpretation of graphical and tabulated results obtained from the REFLAN3D code.

A.1 GEOMETRY AND COMPUTATIONAL GRID

A sample geometry for elliptic flow calculations is presented in figure A.1. In this particular case a symmetry plane is assumed and only the 180^{o} sector of the flow region is considered as a calculation domain.

The fluid enters the cylindrical channel through the front plane which is partially blocked (Figure A.1), and leaves the channel through the fully opened exit plane.

The selected grid distribution for this geometry is shown in Figures A.2a and A.2b respectively for two cross-sections viz:

a) XY - axial plane - aligned with the main stream direction, and

b) YZ - cross-section plane - perpendicular to the main stream direction.

The coordinate directions are selected as:

X - axial direction,

Y - radial direction, and

Z - circumferential direction, (in radians for polar coordinates).

The boundries of the calculation domain are identified as:

West Boundary - located at X = 0,

East Boundary - located at X = X_{max}

South Boundary- located at Y = 0

North Boundary- located at Y = Y_{max}

Low Boundary - located at Z = 0

High Boundary - located at Z = Z_{max}

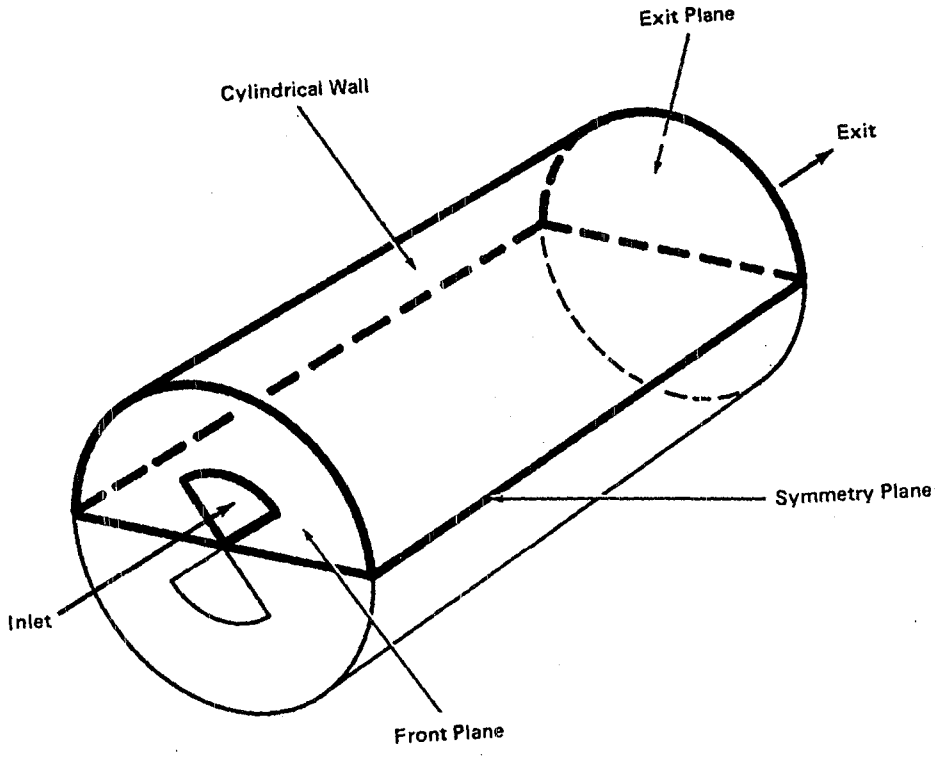

Figure A.1 Geometry for test Flow Calculations.

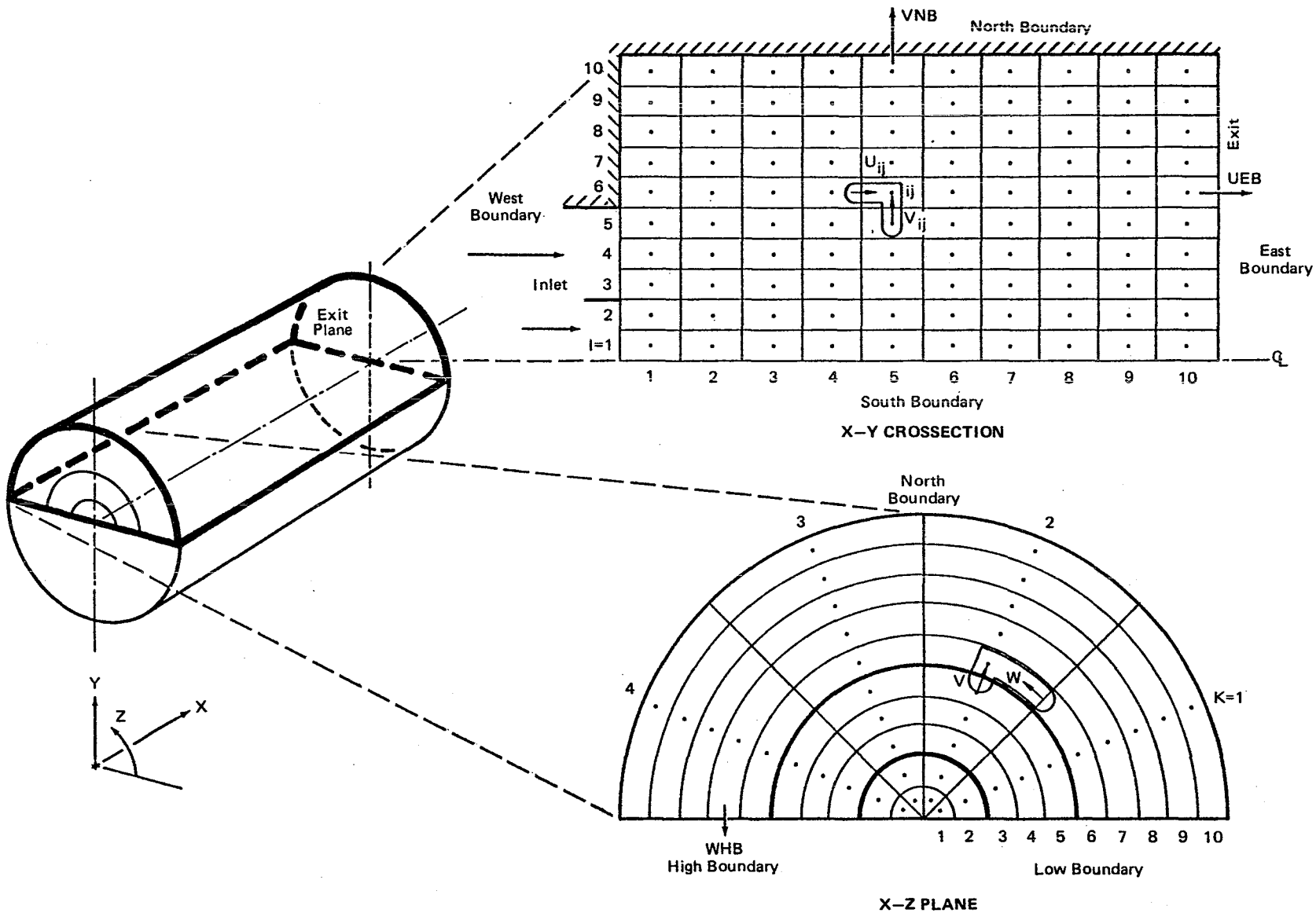

Figure A.2 Coordinate Direction and Grid Distribution in Two Planes: XY- axial plane; and YX cross-sectional plane.

Figure A.2 also presents staggered grid arrangement and the storage location of velocity components. Note that "backward boomerang" is used for storing all three velocity components viz: U-axial, V-radial and W-circumferential. Seperate arrays are allocated for velocities at the last X-face (UEB), last y-face (VNB) and last z-face (WHB). All scalar variables (p,T,k,ε,m_{fu} . . .) are stored in the middle of the grid cell.

A.2 INTERPRETATION OF THE PRINTOUT

Figure A.3 presents the typical printout of the axial velocity components, and appropriate diagrams for the output interpretation.

All variables (including velocity) are printed in the form of tables; each table for a particular axial plane (Z = Const) numbered K=1, K=2, etc. For velocity components additional arrays for:

- east boundary axial velocity UEB,
- north boundary radial velocity VNB, and
- high boundary circumferential velocity WHB are printed too.

Velocities are calculated and printed at appropriate cell faces of the control volume. Scalar quantities are printed at the grid centers. All variables are printed in SI-units i.e.

k	- kinetic energy of turbulence	m^2/s^2
ε	- dissipation rate	m^2/s^3
h	- total enthalpy	J/kg
T	- absolute temperature	^oK
f	- mixture fractions	-
m_{fu}	- fuel mass fraction	-
p	- pressure (N/m^2) relative to the reference point.	
μ	- effective viscosity	kg/ms

A.3 INTERPRETATION OF THE GRAPHICAL PLOTS

Graphical representations of the calculation results include:

- velocity vectors in XY, YZ or XZ plane
- isoline contours of scalar variables in XY, YZ or XZ plane.

The velocity vectors $\overline{U}$, are calculated and plotted at the grid centers based on the linear interpolation from the velocity components located at the grid cell faces (see Figure A.4).

Figure A.3 Example of the Interpretation for the Axial Velocity Printout.

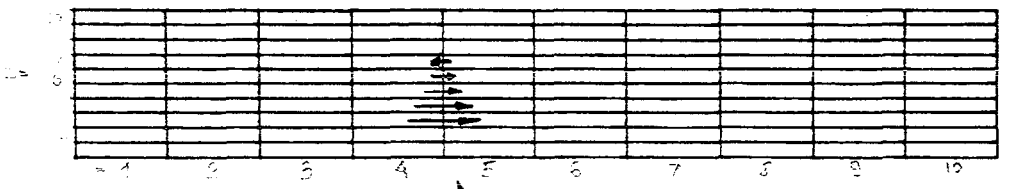

U-VELOCITY

*** K = 1 ***

J	I= 1	2	3	4	5	6	7	8	9	10
10	0,00E+00	-4,53E-01	-7,94E-01	-8,83E-01	-7,66E-01	-5,60E-01	-3,51E-01	-1,76E-01	-3,64E-02	9,27E-02
9	0,00E+00	-1,76E+00	-2,56E+00	-2,62E+00	-2,17E+00	-1,47E+00	-7,85E-01	-1,97E-01	2,86E-01	7,47E-01
8	0,00E+00	-2,39E+00	-3,05E+00	-2,84E+00	-2,11E+00	-1,10E+00	-2,90E-01	4,54E-01	1,05E+00	1,64E+00
7	0,00E+00	-2,43E+00	-2,67E+00	-1,96E+00	-9,07E-01	1,59E-01	9,66E-01	1,63E+00	2,19E+00	2,75E+00
6	0,00E+00	-1,92E+00	-1,67E+00	-3,51E-01	1,08E+00	2,03E+00	2,70E+00	3,20E+00	3,62E+00	4,01E+00
5	0,00E+00	-8,68E-01	-9,63E-02	1,74E+00	3,26E+00	4,14E+00	4,66E+00	4,99E+00	5,21E+00	5,36E+00
4	0,00E+00	7,45E-01	2,21E+00	4,00E+00	5,39E+00	6,15E+00	6,54E+00	6,70E+00	6,74E+00	6,65E+00
3	0,00E+00	3,14E+00	5,08E+00	6,48E+00	7,36E+00	7,86E+00	8,08E+00	8,11E+00	7,99E+00	7,72E+00
2	0,00E+00	5,97E+00	7,69E+00	8,46E+00	8,90E+00	9,12E+00	9,17E+00	9,07E+00	8,85E+00	8,45E+00
1	0,00E+00	8,72E+00	9,49E+00	9,71E+00	9,81E+00	9,85E+00	9,75E+00	9,57E+00	9,27E+00	8,81E+00

*** K = 2 ***

J	I= 1	2	3	4	5	6	7	8	9	10
10	0,00E+00	-5,07E-01	-5,27E-01	-4,46E-01	-3,99E-01	-3,55E-01	-2,59E-01	-1,59E-01	-5,08E-02	5,37E-02
9	0,00E+00	-9,84E-01	-5,84E-01	-4,05E-01	-5,12E-01	-4,49E-01	-2,57E-01	-8,01E-03	2,47E-01	5,54E-01
8	0,00E+00	1,84E-01	1,43E+00	1,34E+00	9,45E-01	7,19E-01	7,21E-01	8,01E-01	1,07E+00	1,35E+00
7	0,00E+00	5,59E+00	9,13E+00	4,72E+00	3,88E+00	3,10E+00	2,71E+00	2,50E+00	2,45E+00	2,49E+00
6	0,00E+00	1,05E+01	1,02E+01	9,15E+00	7,85E+00	6,59E+00	5,58E+00	4,85E+00	4,36E+00	3,97E+00
5	2,00E+01	1,69E+01	1,51E+01	1,34E+01	1,18E+01	1,02E+01	8,77E+00	7,57E+00	6,60E+00	5,71E+00
4	2,00E+01	1,81E+01	1,68E+01	1,52E+01	1,37E+01	1,22E+01	1,08E+01	9,51E+00	8,42E+00	7,27E+00
3	2,00E+01	1,78E+01	1,63E+01	1,49E+01	1,35E+01	1,24E+01	1,13E+01	1,02E+01	9,51E+00	8,26E+00
2	1,00E+01	1,29E+01	1,30E+01	1,25E+01	1,19E+01	1,13E+01	1,07E+01	1,01E+01	9,49E+00	8,71E+00
1	1,00E+01	9,92E+00	1,04E+01	1,04E+01	1,03E+01	1,02E+01	1,00E+01	9,73E+00	9,37E+00	8,84E+00

*** K = 3 ***

J	I= 1	2	3	4	5	6	7	8	9	10
10	0,00E+00	-5,07E-01	-5,27E-01	-4,46E-01	-3,99E-01	-3,55E-01	-2,59E-01	-1,59E-01	-5,08E-02	5,37E-02
9	0,00E+00	-9,84E-01	-5,84E-01	-4,05E-01	-5,12E-01	-4,49E-01	-2,57E-01	-8,01E-03	2,47E-01	5,54E-01
8	0,00E+00	1,84E-01	1,43E+00	1,34E+00	9,45E-01	7,19E-01	7,21E-01	8,01E-01	1,07E+00	1,35E+00
7	0,00E+00	5,59E+00	9,13E+00	4,72E+00	3,88E+00	3,10E+00	2,71E+00	2,50E+00	2,45E+00	2,49E+00
6	0,00E+00	1,05E+01	1,02E+01	9,15E+00	7,85E+00	6,59E+00	5,58E+00	4,85E+00	4,36E+00	3,97E+00
5	2,00E+01	1,69E+01	1,51E+01	1,34E+01	1,18E+01	1,02E+01	8,77E+00	7,57E+00	6,60E+00	5,71E+00
4	2,00E+01	1,81E+01	1,68E+01	1,52E+01	1,37E+01	1,22E+01	1,08E+01	9,51E+00	8,42E+00	7,27E+00
3	2,00E+01	1,78E+01	1,63E+01	1,49E+01	1,35E+01	1,24E+01	1,13E+01	1,02E+01	9,51E+00	8,26E+00
2	1,00E+01	1,29E+01	1,30E+01	1,25E+01	1,19E+01	1,13E+01	1,07E+01	1,01E+01	9,49E+00	8,71E+00
1	1,00E+01	9,92E+00	1,04E+01	1,04E+01	1,03E+01	1,02E+01	1,00E+01	9,73E+00	9,37E+00	8,84E+00

*** K = 4 ***

J	I= 1	2	3	4	5	6	7	8	9	10
10	0,00E+00	-4,53E-01	-7,94E-01	-8,83E-01	-7,66E-01	-5,60E-01	-3,51E-01	-1,76E-01	-3,64E-02	9,27E-02
9	0,00E+00	-1,76E+00	-2,56E+00	-2,62E+00	-2,17E+00	-1,47E+00	-7,85E-01	-1,97E-01	2,86E-01	7,47E-01
8	0,00E+00	-2,39E+00	-3,05E+00	-2,84E+00	-2,11E+00	-1,10E+00	-2,90E-01	4,54E-01	1,05E+00	1,64E+00
7	0,00E+00	-2,43E+00	-2,67E+00	-1,96E+00	-9,07E-01	1,59E-01	9,66E-01	1,63E+00	2,19E+00	2,75E+00
6	0,00E+00	-1,92E+00	-1,67E+00	-3,51E-01	1,08E+00	2,03E+00	2,70E+00	3,20E+00	3,62E+00	4,01E+00
5	0,00E+00	-8,68E-01	-9,63E-02	1,74E+00	3,26E+00	4,14E+00	4,66E+00	4,99E+00	5,21E+00	5,36E+00
4	0,00E+00	7,45E-01	2,21E+00	4,00E+00	5,39E+00	6,15E+00	6,54E+00	6,70E+00	6,74E+00	6,65E+00
3	0,00E+00	3,14E+00	5,08E+00	6,48E+00	7,36E+00	7,86E+00	8,08E+00	8,11E+00	7,99E+00	7,72E+00
2	0,00E+00	5,97E+00	7,69E+00	8,46E+00	8,90E+00	9,12E+00	9,17E+00	9,07E+00	8,85E+00	8,45E+00
1	0,00E+00	8,72E+00	9,49E+00	9,71E+00	9,81E+00	9,85E+00	9,75E+00	9,57E+00	9,27E+00	8,81E+00

**** CHECK2 PRINT OF UEB I1= 1 IL=10 J1= 1 JL= 4

J	I= 1	2	3	4	5	6	7	8	9	10
4	8,43E+00	8,11E+00	7,44E+00	6,46E+00	5,30E+00	4,10E+00	2,99E+00	2,03E+00	1,21E+00	4,65E-01
3	8,37E+00	8,15E+00	7,62E+00	6,63E+00	5,21E+00	3,69E+00	2,43E+00	1,48E+00	7,83E-01	2,51E-01
2	8,37E+00	8,15E+00	7,62E+00	6,63E+00	5,21E+00	3,69E+00	2,43E+00	1,48E+00	7,83E-01	2,51E-01
1	8,43E+00	8,11E+00	7,44E+00	6,46E+00	5,30E+00	4,10E+00	2,99E+00	2,03E+00	1,21E+00	4,65E-01

WALL

INLET

EXIT

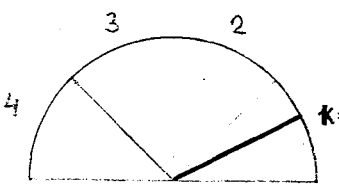

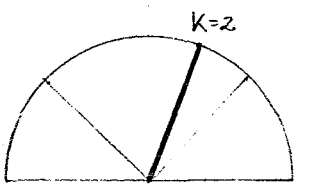

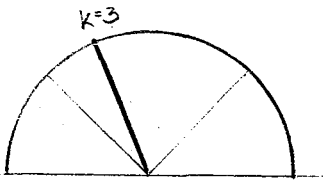

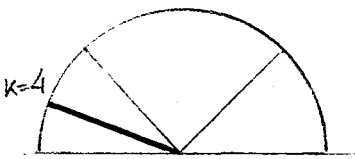

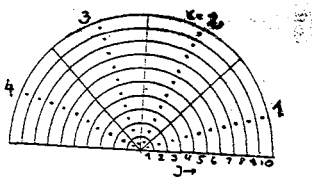

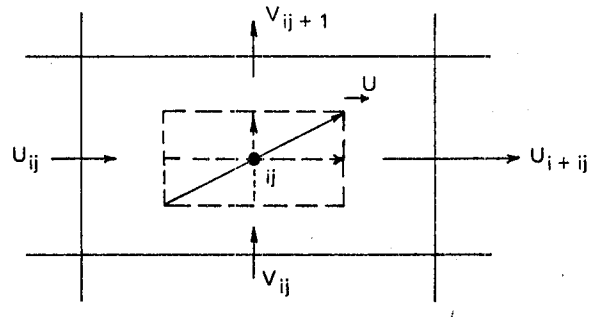

Figure A.4: Calculation on Velocity Vectors.

The vector $\vec{U}$ length is taken as:

$$\left|\vec{U}\right| = \sqrt{\left(\frac{u_{ij} + u_{i+1j}}{2}\right) + \left(\frac{v_{ij} + v_{ij+1}}{2}\right)}$$

Figure A.5 presents a typical distribution of velocity vectors for the first XY plane with an overlayed grid line system and contours of the scalar quantity (temperature) on the second XY plane.

Additional information for velocity vectors includes printout of minimum (VELMIN) and maximum (VELMAX) velocity vectors at that plane.

The legend for the contours of scalar property ϕ includes:

- plane orientation eg: XY Plane 2;
- name of the contoured quanity: TEMP;
- minimum and maximum value of ϕ within that plane (PHIMAX and PHIMIN); and
- contour numbers and appropriate contour levels.

Figure A.5 Example of the Graphical Results Interpretation

```
 XY  PLANE  1
VELOCITY PLOTS
VELMIN    4.056E-01
VELMAX    2.260E+01
```

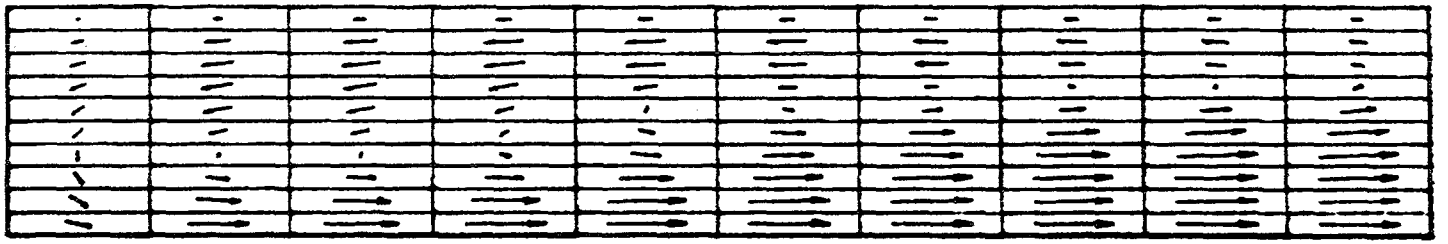

```
XY PLANE  2
TEMP CONTOURS
PHIMAX     PHIMIN
  4.9519E+02  3.0457E+02
CONTOUR LEVELS ARE
 1   3.2190E+02
 2   3.3923E+02
 3   3.5656E+02
 4   3.7389E+02
 5   3.9122E+02
 6   4.0855E+02
 7   4.2587E+02
 8   4.4320E+02
 9   4.6053E+02
10   4.7786E+02
```

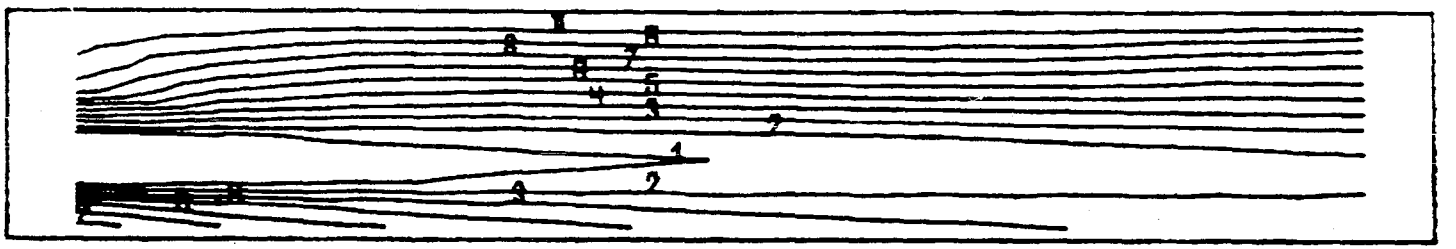

End of Document